Archives of Computational Methods in Engineering
https://doi.org/10.1007/s11831-024-10197-1

RESEARCH

Residual-Based Stabilized Reduced-Order Models of the Transient Convection–Diffusion–Reaction Equation Obtained Through Discrete and Continuous Projection

Eric Parish[1] · Masayuki Yano[2] · Irina Tezaur[3] · Traian Iliescu[4]

Received: 4 August 2024 / Accepted: 9 October 2024

Abstract
Galerkin and Petrov–Galerkin projection-based reduced-order models (ROMs) of transient partial differential equations are typically obtained by performing a dimension reduction and projection process that is defined at either the spatially continuous or spatially discrete level. In both cases, it is common to add stabilization to the resulting ROM to increase the stability and accuracy of the method; the addition of stabilization is particularly common for convection-dominated systems when the ROM is under-resolved. While continuous and discrete approaches can be equivalent in certain settings, a plethora of different techniques have emerged for each approach. However, to the best of our knowledge, a thorough comparison of these techniques is currently missing. In this work, we take a first, foundational step and provide an in-depth review of seven commonly used residual-based ROM stabilization strategies within the setting of finite element method (FEM) discretizations using the convection-dominated convection–diffusion–reaction (CDR) equation, an established testbed for stabilization methods. We present the formulations in a unified setting, highlight connections between the strategies, and numerically assess the strategies. In the spatially continuous case, we examine the Galerkin, streamline upwind Petrov–Galerkin (SUPG), Galerkin/least-squares (GLS), and adjoint (ADJ) stabilization methods. For the GLS and ADJ methods, we examine formulations constructed from both the "discretize-then-stabilize" technique and the space–time technique. In the spatially discrete case, we examine the Galerkin, least-squares Petrov–Galerkin (LSPG), and adjoint Petrov–Galerkin (APG) methods. We summarize existing analyses for these methods and provide numerical experiments, comparing competing methods for the first time in the literature and assessing the impact of stabilization parameters and time step sizes. Our numerical experiments demonstrate that residual-based stabilized methods developed via continuous and discrete processes yield substantial improvements over standard Galerkin methods when the underlying FEM model is under-resolved. We find that SUPG, space–time GLS, and space–time ADJ are the best continuous stabilization techniques considered. For discrete ROMs, we find that APG is more accurate than LSPG at the expense of a smaller region of stability with respect to the stabilization parameter. The combination of an APG ROM constructed on top of a SUPG FEM is the overall best performing method. The review, discussion, and numerical inter-comparison of the seven stabilizations strategies using the CDR equations serves as a stepping stone toward a comprehensive investigation and further development of stabilization methods for more challenging problems.

1 Introduction

Despite advances in high-performance computing, numerically solving parameterized partial differential equations (PDEs) remains computationally expensive for systems displaying a wide range of spatio-temporal scales. This high cost can be prohibitive, particularly for many-query problems (e.g., optimization, uncertainty quantification) in which case many evaluations of the forward model are required. A variety of techniques have thus been developed to generate approximations to many PDEs of interest at a reduced computational cost [17, 67, 113, 115, 124]. Galerkin and

✉ Eric Parish
ejparis@sandia.gov

[1] Computational Data Science, Sandia National Laboratories, Livermore, CA 94550, USA

[2] Institute for Aerospace Studies, University of Toronto, Toronto, ON M3H 5T6, Canada

[3] Quantitative Modeling & Software Engineering, Sandia National Laboratories, Livermore, CA 94550, USA

[4] Department of Mathematics, Virginia Tech, Blacksburg, VA 24061, USA

Published online: 21 November 2024

Petrov–Galerkin (PG)-type reduced-order models are one such promising technique and are the focus of the present work. We will refer to the latter class of methods as PG ROMs. Broadly speaking, PG ROMs operate by (1) restricting the state to belong to a low-dimensional trial space, and (2) computing an approximation to the weak form of the PDE given the low-dimensional trial space and an additional test space; this step can be analogously viewed as restricting the residual to be orthogonal to the test space. To enhance the stability and accuracy of the ROM, the test space often differs from the trial space (i.e., a Petrov–Galerkin scheme) and/or additional stabilization terms are added to the governing equations.

Over the past decades, PG ROMs have been implemented in numerous codes with varying discretization techniques to provide model reduction capabilities for a variety of problems. This diverse set of applications has led, by necessity, to varying ROM formulations that are suited to different applications of interest. In particular, two distinct types of ROMs have emerged: PG ROMs that define a trial space and Petrov–Galerkin projection scheme at the spatially-*continuous* level, and PG ROMs that define a trial space and Petrov–Galerkin projection scheme at the spatially-*discrete* level. In this work, we refer to these approaches as *continuous ROMs* and *discrete ROMs*, respectively.[1]

In continuous ROMs, the state variables are approximated at the spatially-continuous level in a low-dimensional function space, and generalized coordinates associated with the state representation are then obtained by computing an approximate solution to the weak form of the PDE by employing low-dimensional trial and test function spaces. Continuous ROMs are most often employed within the context of weighted residual methods (e.g., finite element methods, spectral methods), and examples of continuous ROMs can be found in [11, 12, 18, 27, 79, 125, 136, 138, 139, 163, 165, 166, 169, 177] (and many other works). We do note that several pieces of work have examined extensions to finite volume methods [108, 156]. Discrete ROMs, on the other hand, are typically described at the dynamical system level and work directly with the spatially-discrete system emerging after discretization of the differential operators present in the PDE[2]. Discrete ROMs approximate the *discretized* state variables within a low-dimensional Euclidean vector space, and the generalized coordinates associated with the state representation are then obtained by defining a (Petrov–)Galerkin scheme using a discrete (e.g., Euclidean) inner product and the discrete residual. Discrete ROMs have received significant attention for model reduction of finite difference and finite volume discretizations as well as for model reduction of large-scale application codes where underlying information about the discretization (e.g., mass matrices) are difficult or impossible to access. Examples of discrete ROMs can be found in [1, 24–26, 29, 31, 32, 37, 99–101, 172].

We note that, in certain settings (e.g., finite elements), it is straightforward to obtain the discrete form of the ROM equations obtained via continuous projection. As a result, provided proper selection of inner products at the discrete level, it is well-known that there is direct equivalence between continuous and discrete ROMs [122, 167]. Thus, some discrete ROM formulations are equivalent to their continuous ROM counterparts. We emphasize, however, that the same duality does not exist for all discretizations. As a result, for the most part, discrete and continuous ROMs have each developed independently, each branch proposing strategies that do not find a straightforward counterpart in the other branch. To our knowledge, comparisons of the continuous and discrete ROMs are relatively scarce (see, however, [85] for a notable exception). It is one of the main goals of this paper to (i) discuss and investigate representative continuous and discrete ROMs in the context of stabilization, and (ii) outline the similarities and differences among those stabilizations.

Just like standard discretization techniques, both continuous ROMs and discrete ROMs oftentimes require stabilization to maintain stability and accuracy; it is well-known that Galerkin projection, in which the trial space is the same as the test space, often lacks robustness in the presence of sharp, under-resolved gradients. One appealing and widely employed class of stabization techniques is known as *residual-based stabilization*. In this class of approaches, an additional residual-based term is added to the weak form of the PDE. Certain types of residual-based stabilization approaches can be written as Petrov–Galerkin schemes and some can correspond to residual minimization statements (e.g., least-squares Petrov–Galerkin). While residual-based stabilization techniques have been developed for both continuous ROMs and discrete ROMs, the approaches do not overlap due to the fundamentally different setting of the ROM formulations. Thus,

[1] We note that, in the transient case considered herein, reduced-order models are typically formulated by reducing the spatial dimension of the model and leveraging standard time-marching schemes for temporal discretization. We restrict our attention to this setting, but note that several pieces of work have examined the construction of space–time ROMs [15, 37, 42, 119, 163, 177], in which case the same thematic similarities of discrete vs. continuous are present.

[2] For transient PDEs, discrete ROMs can be formulated at either the ordinary *differential* equation (ODE) level (i.e., after spatial discretization) or the ordinary *difference* equation (OΔE level) (i.e., after spatial and temporal discretization); Ref. [29] examines commutativity of the time-discretization step for Galerkin and least-squares Petrov Galerkin ROM formulations.

while there is a duality between continuous ROMs and discrete ROMs in, e.g., finite elements, the same cannot necessarily be said about *stabilized* continuous ROMs and discrete ROMs. As a result, a plethora of different stabilization schemes are deployed across the two settings. For discrete ROMs, stabilized ROM formulations include, but are not limited to: least-squares formulations from LeGresley, Alonso, Bui-Tanh, Willcox, and Ghattas [24–26, 99–101]; the "least-squares Petrov–Galerkin (LSPG)" and "Gauss–Newton with Approximated Tensors (GNAT)" approaches of Carlberg, Farhat, and others [28–30, 32]; the "Adjoint Petrov–Galerkin" approach explored by Parish, Wentland, and Duraisamy [121, 172]; and the "model-form preserving least-squares with variable transformation" approach of Huang et al. [71]. For continuous ROMs, stabilization strategies include, but are certainly not limited to: "streamline upwind Petrov-Galerkin (SUPG)" approaches of Bergmann and Iollo [18], Rozza and Pacciarini [118], Iliescu and John [52], Azaiez, Chacon Rebollo, and Rubino [8], and Novo and John [82]; "variational multiscale" approaches developed by Bergmann and Iollo [18], Iliescu, Wang, and Mou [78, 79, 114], Codina and Baiges [10], and Rozza and Stabile [157]; "eddy viscosity" approaches of Iliescu and Wang [170] and Noack [117]; "minimal subspace rotation" methods of Balajewicz, Tezaur and Dowell [11, 12]; energy- and entropy-stable formulations of Rowley, Kalashnikova and Barone, and Serre et al. based on carefully-constructed inner products [85–88, 138, 148]; "filter based regularizations" developed by Iliescu and Wells [171], Ballarin, and Strazzullo [147, 158], and Quaini, Girfoglio, and Rozza [53, 54]; energy- and entropy-stable methods of Yano [178] and Chen [34] that build on stability of the underlying discontinuous-Galerkin and finite-volume methods based on upwinded fluxes; and "local projection stabilization" of Rubino and Novo [116, 141].

A side-by-side review and assessment of stabilization schemes developed for continuous ROMs and discrete ROMs does not exist in the literature. Such a review is needed to assess the overlap, advantages, disadvantages, and comparative performance of the various strategies. While a comparison between such a wide range of methods is daunting, particularly because the methods are often developed for different spatial and temporal discretizations (e.g., finite element and finite volume, and explicit and implicit time stepping) with different end-goals in mind, and may perform better in some scenarios (e.g., for moderate and high Reynolds numbers), a side-by-side comparison of the different approaches could be tremendously useful for practitioners. Furthermore, there is an interplay between stabilization schemes that are added to the full-order model (FOM) and those added to the ROM that is not well explored. For example, should an LSPG ROM be constructed for a stabilized finite element method (FEM)? This interplay can interact with the ROM stabilization and further motivates a detailed examination of the various methods.

As *a first, foundational step* in a wider comparison of ROM stabilizations, this work provides a review of seven commonly used residual-based stabilization techniques developed for both continuous and discrete ROMs in a unified setting and assesses their performance to help fill this gap. To ensure a fair comparison, we use the same spatial discretization, i.e., the FEM, for all the stabilizations. As a test problem for our numerical investigation, we choose the *convection–diffusion–reaction (CDR)* equation. One reason for choosing the CDR equation is that it is *widely used as a testbed* for the development of stabilized methods for classical discretizations, e.g., the finite element and finite difference methods (see the research monograph [135], which summarizes numerous stabilization methods and assesses their performance for the CDR equation). We emphasize that, although the CDR equation is linear, it exemplifies stability challenges that are relevant for convection-dominated flow problems, such as the Navier–Stokes equations (NSE). For example, for the CDR equation in the *convection-dominated regime* (i.e., when the diffusion coefficient is significantly smaller than the magnitude of the convection field) and the *under-resolved regime* (i.e., when the number of degrees of freedom is not large enough to capture the complex dynamics), standard Galerkin ROMs can yield inaccurate results, generally in the form of spurious numerical oscillations. Thus, in the convection-dominated and under-resolved regimes of the CDR equations, ROMs generally require stabilization. Another reason for choosing the CDR equation as a test problem for our numerical investigation is that it allows us to *isolate the impact* of the stabilization schemes from other discretization choices, e.g., velocity-pressure coupling [67], hyperreduction [67], discretization of the nonlinearity [80], dimensional consistency and scalar vs. vector POD [120, 137, 138].

In this paper, we outline the development of seven continuous and discrete ROMs, establish commonalities between these approaches, and present several numerical examples assessing their performance. Lastly, we examine the sensitivity of the various stabilization approaches with respect to their stabilization parameters and the time step size. We note that this sensitivity is well-known to impact accuracy and robustness of classical numerical discretizations. In this paper, we show that this is the case for ROMs, too.

The novel contributions of the present work are as follows.

1. We give the *first* side-by-side presentation of several common residual-based-stabilized ROMs developed through discrete and continuous projection.

2. We build on Refs. [85, 88] to *introduce a taxonomy* for these various reduced-order modeling approaches. As will be seen in this manuscript, a "Galerkin" approach may entail different ROMs to different communities.
3. We provide *the first* summary of existing analyses for the various ROMs considered.
4. We present the *first* numerical comparison of discretely stabilized ROMs to continuously stabilized ROMs, including ranking 16 different stabilized ROM formulations in terms of the $L^2(\Omega)$ and $\mathcal{H}^1(\Omega)$ error for various basis dimensions in two CDR problem.
5. We present the *first* study of the Galerkin/least-squares and adjoint stabilization methods applied to projection-based ROMs.
6. We provide a comprehensive study on the *impact of the stabilization parameter*, τ, and *time step*, Δt, for all stabilized ROMs considered. This is the *first* such study that has been undertaken for the SUPG, GLS, and ADJ stabilization ROM methods.

The layout of this manuscript is as follows. In Sect. 2, we provide a brief review of stabilization techniques in Petrov–Galerkin-based model reduction. In Sect. 3, we outline the CDR equation, the Galerkin FEM, and stabilized FEM formulations for this equation. In Sects. 4 and 5, we outline ROMs constructed through continuous and discrete projection, respectively. Alternate ROM stabilization approaches that do not fall into either of these two categories are summarized in Appendix 1. Section 6 summarizes the available theoretical support for the various methods. Section 7 presents numerical experiments, and Sect. 8 provides conclusions.

2 Summary of Residual-Based Stabilization in Petrov–Galerkin Model Reduction

The Galerkin method, where the trial and test space coincide, is the standard approach for constructing a ROM. Galerkin projection yields optimal results in a given energy norm for symmetric coercive systems.[3] It is well-known, however, that for convection-dominated systems Galerkin projection often lacks robustness in the presence of sharp, under-resolved gradients. As a result, a wide variety of stabilization techniques have been developed to increase the ROM stability and accuracy for both continuous and discrete ROMs. While this work focuses on residual-based stabilization techniques, we briefly mention other approaches that include, but are not limited to: stabilizing inner products that guarantee a non-increasing energy [14, 87, 88, 138, 148] or non-decreasing entropy [34, 86]; stabilizing subspace rotations that account for truncated modes *a priori* [11, 12]; eigenvalue reassignment methods that calculate a stabilizing correction to a given linear [89] or nonlinear [133] ROM that is found to be unstable after it is constructed; structure preserving methods that guarantee that the ROM satisfy physical constraints [16, 31, 33, 35, 47, 59, 97]; spatial filtering-based stabilization methods [62, 77, 90, 158, 171] that filter out unphysical high-frequency content; *inf-sup* stabilization methods that enforce the *inf-sup* condition in the incompressible Stokes and Navier–Stokes equations [18, 27, 45]; and closure modeling approaches [3, 18, 145, 168–170] that add additional "closure" terms to the ROM so-as to account for the impact of truncated modes. A more in depth review of these methods in provided in Appendix 1 for the interested reader.

In the present work, we focus our review on what are referred to as "residual-based" stabilization techniques. Within the finite element community, various residual-based techniques have been proposed in an effort to develop robust numerical methods for non-symmetric, non-coercive, and under-resolved problems. These methods, which include stabilized finite elements [22, 23, 49, 75] (e.g., SUPG, Galerkin/least-squares (GLS)) and variational multiscale methods [74],[4] are typically formulated by adding terms involving a sum of element-wise integrals to the Galerkin method. These terms typically comprise the product of a test function (that does not belong to the trial space) with the residual of the governing equations, and thus the stabilized formulations can be written as Petrov–Galerkin projections.

These "residual-based" methods have proven to be quite successful, yielding, for example, robust solutions for the convection–diffusion equation, incompressible Navier–Stokes equations, and compressible Navier–Stokes equations [23, 50, 72, 75, 84, 160]. We note that, in the context of VMS methods, a body of work additionally exists that examines the addition of phenomenologically-inspired terms to the weighted residual form (e.g., eddy viscosity methods); we do not consider these approaches here and restrict our attention to residual-based methods. The extension of residual-based approaches to ROMs obtained via continuous projection is straightforward as they operate in a similar variational setting. As a result, various works have examined the formulation of stabilized ROMs via classical finite element stabilization techniques [4, 9, 18, 52, 94, 118, 136, 154, 155].

Another class of stabilized model reduction methods that is important to highlight is continuous minimum-residual

[3] Throughout this work, we define a coercive system as a system whose bilinear form $a(\cdot,\cdot)$ satisfies the condition $a(v,v) \geq \alpha \|v\|_\star^2$ for all v in a function space V endowed with the norm $\|\cdot\|_\star$. The condition is referred to as "strong coercivity" in some literature.

[4] It is noted that these methods are not mutually orthogonal, for example VMS methods can recover several stabilized methods.

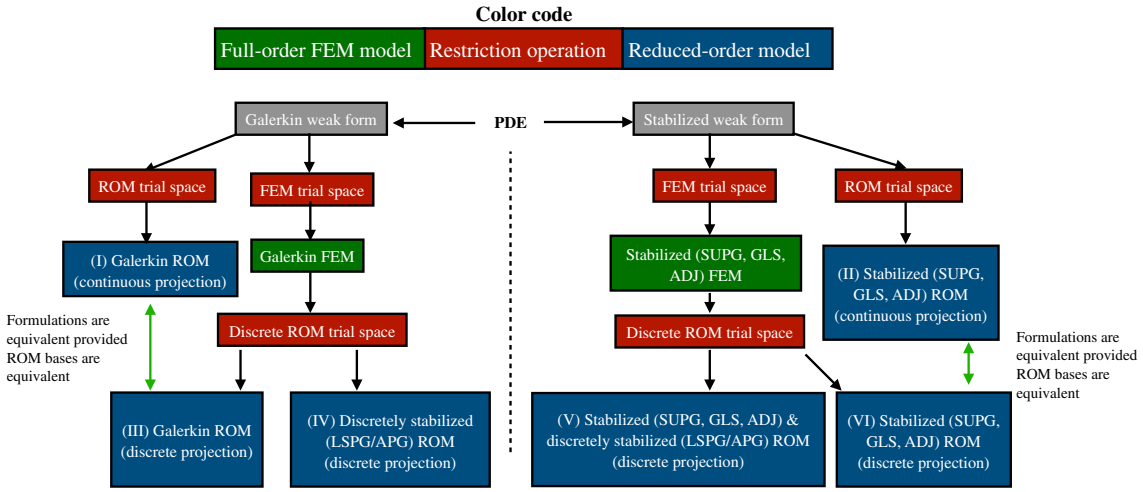

Fig. 1 Schematic of the various processes for constructing reduced-order models. Blocks in green comprise full-order models, blocks in red comprise restriction (projection) processes, and blocks in blue comprise reduced-order models

methods (or least-squares methods) [109, 136]. These methods compute solutions within the trial space that minimize the residual of the governing PDE in the least-squares sense. Minimum-residual methods can be interpreted as Petrov–Galerkin methods, where the (parameter-dependent) test space is defined to be the one that maximizes the inf-sup stability constant, and hence the method is guaranteed to be stable. We also note a related double greedy algorithm [44], which constructs a fixed test space for a Petrov–Galerkin formulation that approximately maximizes the *inf-sup* constant for all parameter values in a greedy fashion. While minimum-residual methods are robust and display commonalities with discrete stabilization approaches, we do not consider them here.

The extension of classic stabilization techniques to discrete ROMs is less straightforward. This is a consequence of the fact that discrete ROMs start from the spatially discrete level, and, as such, do not generally operate in the same variational setting as their continuous counterparts. As a result, various stabilization techniques have been developed for discrete ROMs. One class of particularly popular stabilization techniques are discrete residual minimization approaches [24–26, 28–30, 32, 99–101]. These approaches compute a solution within the trial space that minimizes the discrete FOM residual. In the time-varying case, which we consider here, this residual minimization process is typically formulated by sequentially minimizing the time-discrete residual arising at each time instance on a discrete time grid.[5] This formulation is commonly referred to as the least-squares Petrov–Galerkin (LSPG) approach [29, 32], and can be written as a Petrov–Galerkin projection of the FOM OΔE (i.e., the FOM ODE after temporal discretization). In finite element language, LSPG most closely resembles a discrete least squares principle. We refer to Grimberg et al. [58] for an overview of LSPG within the context of stabilization. The adjoint–Petrov Galerkin (APG) method [121] is an additional discrete model reduction approach that falls into the class of residual-based methods. In APG, the variational multiscale method is applied at the discrete level to decompose the Euclidean state-space into coarse and fine-scale components. The impact of the fine scales on the coarse scales is then accounted for by virtue of a residual-based stabilization term that is derived from the Mori–Zwanzig formalism [38]. APG differs from FEM stabilization techniques in that the residual is defined at the level of the FOM ODE (i.e., after spatial discretization).

Figure 1 provides a schematic of the various ROM approaches just discussed within the context of finite element discretizations. Continuous ROMs (methods I and II in Fig. 1) rely on the definition of a weak form and a ROM trial space, while discrete ROMs (methods III, IV, V, and VI in Fig. 1) rely on the definition of a "full-order" FEM system and a discrete ROM trial space. As noted earlier, in certain settings (e.g., FEM), continuous and discrete ROMs can be equivalent [122, 167] (green arrows in Fig. 1), but this same duality does not exist, e.g., for for finite volume methods. As a result, the development and study of ROM methodologies has effectively forked into bodies of work that start at the spatially continuous level, and bodies of work that start at the spatially discrete level. This fact is not well-documented in the community. To the best of the authors' knowledge it is most clearly outlined in Refs. [85, 88].

[5] We note that recent work has examined windowed least-squares minimization [119] and space–time residual minimization [37]. These approaches have better stability properties than LSPG, but here we restrict our focus to the standard LSPG approach, for simplicity.

3 Finite Element Discretizations for the Convection–Diffusion–Reaction Equation

We consider the demonstrative example of the CDR equation. We emphasize that the concepts presented here generalize to other systems, including nonlinear equations; the CDR equation serves as a useful benchmark, as described in the preceding sections. The CDR equation is given by

$$\begin{aligned} &\tfrac{\partial u_*}{\partial t} - \epsilon\Delta u_* + \mathbf{b}\cdot\nabla u_* + \sigma u_* = f && \text{in } (0,T]\times\Omega,\\ &u_*(0,\boldsymbol{x}) = u_0(\boldsymbol{x}), && \boldsymbol{x}\in\Omega,\\ &u_*(t,\boldsymbol{x}) = 0, && \boldsymbol{x}\in\Gamma, t\in(0,T], \end{aligned} \tag{1}$$

where $u_* : [0,T]\times\overline{\Omega}\to\mathbb{R}$ is the state implicitly defined as the solution to Eq. (1), $\Omega\subset\mathbb{R}^d$ is the physical domain, $\overline{\Omega}$ is its closure, Γ is the domain boundary, $T\in\mathbb{R}_{>0}$ is the final time, $\epsilon\in\mathbb{R}_{>0}$ is the diffusion coefficient, $\mathbf{b}\in\mathbb{R}^d$ are the convection coefficients, $\sigma\in\mathbb{R}_{\geq 0}$ is the reaction coefficient, $u_0 : \Omega\to\mathbb{R}$ is the initial condition, and $f\in L^2(\Omega)$ is a forcing term. In what follows, we use the notation $u_*(t)\equiv u_*(t,\cdot) : \Omega\to\mathbb{R}$. We consider homogeneous Dirichlet boundary conditions, for simplicity. We refer to [127] for more details on the CDR equation and its mathematical setting.

We consider the standard weighted residual formulation of (1) in space, which reads as follows: find $u\in C^1((0,T];L^2(\Omega))\cap L^2((0,T];\mathcal{H}^1_0(\Omega))$ such that $\forall t\in(0,T]$

$$\begin{aligned} &m\big(\mathsf{v}, u_t(t)\big) + m(\epsilon\nabla\mathsf{v},\nabla u(t)) + m(\mathsf{v},\mathbf{b}\cdot\nabla u(t))\\ &+ m(\mathsf{v},\sigma u(t)) = m(\mathsf{v},f), \qquad \forall\mathsf{v}\in\mathcal{H}^1_0(\Omega), \end{aligned} \tag{2}$$

and satisfies the initial condition $u(0)=u_0\in L^2(\Omega)$, where $m : (v,w)\mapsto\int_\Omega v(\boldsymbol{x})w(\boldsymbol{x})d\boldsymbol{x}$ is the $L^2(\Omega)$ inner product, and $\mathcal{H}^1_0(\Omega)$ is the standard Sobolev space of functions that have square-integrable weak first derivatives and vanish on Γ in a weak sense. The problem (2) is well-posed; see, e.g., [127]. For notational simplicity, we introduce the bilinear form

$$\mathcal{B}_{\mathrm{G}} : (\mathsf{v},\mathsf{u})\mapsto m(\epsilon\nabla\mathsf{v},\nabla\mathsf{u}) + m(\mathsf{v},\mathbf{b}\cdot\nabla\mathsf{u}) + m(\mathsf{v},\sigma\mathsf{u}).$$

To transcribe (2) into a discrete problem, we need to introduce spatial and temporal discretizations. In this work, we consider, for simplicity and without loss of generality, the implicit Euler method for temporal discretization and a FEM for the spatial discretization; the concepts presented here can be extended to other time stepping schemes. We introduce without loss of generality a uniform partition of the time domain $[0,T]$ into N_t+1 time instances $t^n = n\Delta t$, $n=0,\dots,N_t$, with $\Delta t = T/N_t$. Application of the implicit Euler method yields the series of strong form stationary PDEs for $\mathsf{u}^n_*\big(\approx u_*(t^n)\big)$, $n=1,\dots,N_t$,

$$\frac{\mathsf{u}^n_* - \mathsf{u}^{n-1}_*}{\Delta t} - \epsilon\Delta\mathsf{u}^n_* + \mathbf{b}\cdot\nabla\mathsf{u}^n_* + \sigma\mathsf{u}^n_* = f \tag{3}$$

with $\mathsf{u}^0_* = u_0$ and $\mathsf{u}^n_* = 0$ on Γ, $n=1,\dots,N_t$. The weak form then yields the associated series of stationary problems: find $\mathsf{u}^n(\approx\mathsf{u}^n_*)\in\mathcal{H}^1_0(\Omega)$, $n=1,\dots,N_t$, such that

$$m\left(\mathsf{v},\frac{\mathsf{u}^n-\mathsf{u}^{n-1}}{\Delta t}\right) + \mathcal{B}_{\mathrm{G}}(\mathsf{v},\mathsf{u}^n) = m(\mathsf{v},f), \qquad \forall\mathsf{v}\in\mathcal{H}^1_0(\Omega), \tag{4}$$

with initial condition $\mathsf{u}^0 = u_0$.

For spatial discretization, let $\mathcal{V}_{\mathrm{h}}\subset\mathcal{H}^1_0(\Omega)$ and $\mathcal{W}_{\mathrm{h}}\subset\mathcal{H}^1_0(\Omega)$ denote conforming trial and test spaces, respectively, obtained via a finite element discretization of Ω into N_{el} non-overlapping elements Ω_k, $k=1,\dots,N_{\mathrm{el}}$. The spatially discrete counterpart of (4) reads: find $\mathsf{u}^n_{\mathrm{h}}\in\mathcal{V}_{\mathrm{h}}$, $n=1,\dots,N_t$, such that

$$m\left(\mathsf{v},\frac{\mathsf{u}^n_{\mathrm{h}}-\mathsf{u}^{n-1}_{\mathrm{h}}}{\Delta t}\right) + \mathcal{B}_{\mathrm{G}}(\mathsf{v},\mathsf{u}^n_{\mathrm{h}}) = m(\mathsf{v},f), \qquad \forall\mathsf{v}\in\mathcal{W}_{\mathrm{h}}, \tag{5}$$

with (approximate) initial condition $\mathsf{u}^n_{\mathrm{h}} = u_{0,h}$, where $u_{0,h}$ is, e.g., the $L^2(\Omega)$ projection of u_0 onto $\mathcal{V}_{\mathrm{h}}$.

3.1 Galerkin Approach

The standard Galerkin approach is obtained by setting $\mathcal{W}_{\mathrm{h}} = \mathcal{V}_{\mathrm{h}}$ in (5). We introduce the basis $\{\mathsf{v}_i\}_{i=1}^N$ for $\mathcal{V}_{\mathrm{h}}$, which yields the following FOM basis vector $\forall\boldsymbol{x}\in\Omega$:

$$\mathsf{v}(\boldsymbol{x}) \equiv \begin{bmatrix}\mathsf{v}_1(\boldsymbol{x}) & \cdots & \mathsf{v}_N(\boldsymbol{x})\end{bmatrix}. \tag{6}$$

The time-discrete state at time-instance t^n is described with these basis functions as $\mathsf{u}^n_{\mathrm{h}}(\boldsymbol{x}) = \mathsf{v}(\boldsymbol{x})\mathbf{a}^n_{\mathrm{h}}$, where $\mathbf{a}^n_{\mathrm{h}}\in\mathbb{R}^N$, $n=0,\dots,N_t$. We refer to $\mathbf{a}^n_{\mathrm{h}}$ as the FEM coefficients. The Galerkin method yields the OΔE system to be solved for $\mathbf{a}^n_{\mathrm{h}}$, $n=1,\dots,N_t$,

$$\mathbf{r}_{\mathrm{G}}(\mathbf{a}^n_{\mathrm{h}};\mathbf{a}^{n-1}_{\mathrm{h}}) = \mathbf{0}, \tag{7}$$

where

$$\mathbf{r}_{\mathrm{G}} : (\mathbf{w};\mathbf{z})\mapsto\mathbf{M}\left[\frac{\mathbf{w}-\mathbf{z}}{\Delta t}\right] + \mathbf{B}\mathbf{w} - \mathbf{f}.$$

In the above, $\mathbf{M}\in\mathbb{S}^N$ with $\mathbf{M}_{ij}\equiv m\big(\mathsf{v}_i,\mathsf{v}_j\big)$ is the FEM mass matrix, $\mathbf{B}\in\mathbb{R}^{N\times N}$ with $\mathbf{B}_{ij}\equiv\mathcal{B}_{\mathrm{G}}(\mathsf{v}_i,\mathsf{v}_j)$ is a dynamics matrix resulting from the bilinear form, and $\mathbf{f}\in\mathbb{R}^N$ with $\mathbf{f}_i\equiv m\big(\mathsf{v}_i,f\big)$ is the discrete forcing; we denote the space of $N\times N$ symmetric positive definite matrices by $\mathbb{S}^N$. We refer to (7) as the Galerkin FOM OΔE.

Remark 3.1 Obtaining the discrete problem (7) requires evaluating the inner products in the system (5). In general, evaluating these inner products requires introducing a quadrature

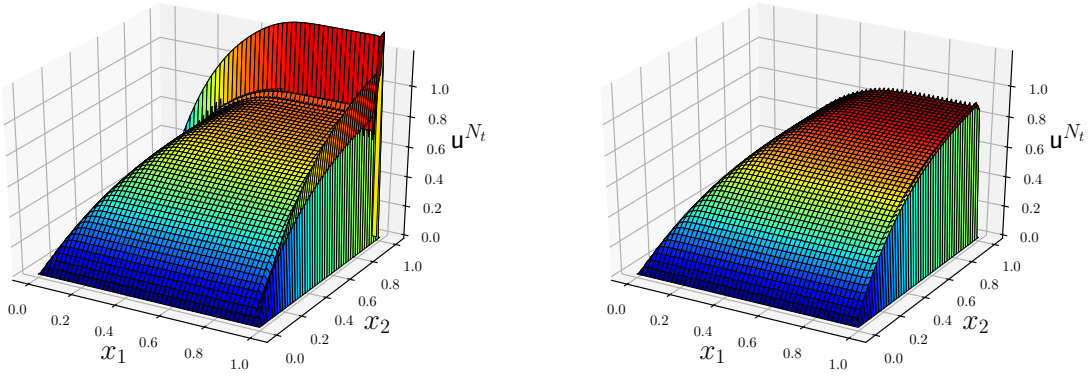

(a) Galerkin FEM (b) SUPG FEM

Fig. 2 Finite element solutions to the CDR equation, with the setup described in Sect. 7.2, at $t = 5$

rule. We note that for linear problems (and problems displaying polynomial nonlinearities) with piecewise polynomial forcing operators, the inner products can be evaluated exactly with an appropriate quadrature rule, e.g., Gaussian quadrature.

3.2 Residual-Based Stabilization

The Galerkin approach is known to perform well for symmetric positive definite systems, in which case the Galerkin method comprises a minimization principle in a system-specific energy norm. In the presence of sharp, under-resolved gradients, however, it is well-known that the Galerkin approach can lack robustness. In the present context, this poor performance is most pronounced for large grid Peclet numbers (i.e., $\mathrm{Pe}_\mathrm{h} := ||\mathbf{b}||_2 h/\epsilon \gg 1$, where h is a measure of the element size and $||\cdot||_2$ is the Euclidian norm). We note that large grid Peclet numbers occur, e.g., for coarse meshes (i.e., in the under-resolved regime), small diffusion coefficients, or a combination of both. In this regime, the skew-symmetric convection operator dominates the symmetric diffusion operator. Figure 2 demonstrates this by showing finite element solutions to the CDR equation obtained using the Galerkin FEM as well as a stabilized FEM. The Galerkin approach is seen to yield large oscillations near the boundary of the computational domain, while the stabilized approach suppresses these oscillations and yields accurate solutions.[6]

To improve the performance of the numerical method in such regimes, it is common to introduce stabilization to smooth the numerical solution. Various stabilization techniques exist, including flux limiters, artificial viscosity, etc. In the finite element community, *residual-based stabilization* is a popular stabilization technique. Residual-based FEMs, which include the likes of the SUPG [22, 23, 73], GLS [75], and adjoint [49, 50, 74] (ADJ) (also known as unusual or subgrid-scale) stabilization methods, are typically formulated by adding terms involving a sum of element-wise integrals to the Galerkin method. These terms usually comprise the product of a test function with the residual of the governing equations. These approaches have been successful in providing robust methodologies for a variety of systems, including the CDR, incompressible Navier–Stokes, and compressible Navier–Stokes equations [23, 50, 72, 75, 84, 135, 160].

For transient systems, like the CDR equation described in this work, stabilized methods are typically employed in one of two ways.

- *Space–time discretizations.* Space–time finite elements are employed in both time and space. The temporal dimension is then viewed as an additional spatial dimension, and standard stabilization approaches can be applied. This is the approach that was first employed for stabilized and variational multiscale methods of unsteady problems [76, 149].
- *Discretize-then-stabilize.* The PDE is first discretized in time, and then a stabilized method is applied to the time-discrete, spatially-continuous system. This approach is popular as it can be more computationally efficient than space–time discretizations and is compatible with numerous time marching schemes [41].

In this work, we explore both approaches.

A stabilized form of (4) can be written generally as: find $\mathsf{u}^n \in \mathcal{V}_\mathrm{h}$, $n = 1, \ldots, N_t$, such that

[6] We note that one negative consequence of stabilized methods is that the convergence rates for the methods are often lower than the unstabilized FEM.

$$m\left(\mathsf{v}, \frac{\mathsf{u}^n - \mathsf{u}^{n-1}}{\Delta t}\right) + \mathcal{B}_{\mathrm{G}}(\mathsf{v}, \mathsf{u}^n) + m_{\mathrm{el}}\left(\mathcal{Q}\mathsf{v}, \tau\mathcal{R}\left(\mathsf{u}^n, \mathsf{u}^{n-1}\right)\right) = m(\mathsf{v}, f), \qquad \forall \mathsf{v} \in \mathcal{V}_{\mathrm{h}}, \tag{8}$$

where $m_{\mathrm{el}} : (u, v) \mapsto \sum_{K=1}^{N_{\mathrm{el}}} \int_{\Omega_k} u(\boldsymbol{x}) v(\boldsymbol{x}) d\boldsymbol{x}$ denotes the sum of element-wise $L^2(\Omega)$ inner products, $\tau : \Omega \to \mathbb{R}$ is a grid-dependent stabilization parameter, $\mathcal{R} : \left(\mathsf{u}^n, \mathsf{u}^{n-1}\right) \to \frac{\mathsf{u}^n - \mathsf{u}^{n-1}}{\Delta t} + \mathcal{L}\mathsf{u}^n - f$ is the strong form residual operator, $\mathcal{L} : \mathsf{u}^n \mapsto -\epsilon\Delta\mathsf{u}^n + \mathbf{b} \cdot \nabla\mathsf{u}^n + \sigma\mathsf{u}^n$, and $\mathcal{Q}$ is a linear stabilization operator that is scheme dependent. Note that $\left[\mathcal{L}\mathsf{u}^n + \frac{\mathsf{u}^n - \mathsf{u}^{n-1}}{\Delta t} - f\right]$ yields the strong form of the time-discrete residual. For notational simplicity, we denote the bilinear form associated with the stabilized formulations as

$$\mathcal{B}_{\mathrm{S}} : (\mathsf{v}, \mathsf{u}) \mapsto \mathcal{B}_{\mathrm{G}}(\mathsf{v}, \mathsf{u}) + m_{\mathrm{el}}\left(\mathcal{Q}\mathsf{v}, \tau\left(\mathcal{L}\mathsf{u} + \frac{\mathsf{u}}{\Delta t}\right)\right).$$

Remark 3.2 We note that the stabilized form (8) is consistent with respect to the continuous equations (1) semi-discretized in time using an implicit Euler scheme. That is, if one substitutes in the exact solution, $\mathsf{u}^n \leftarrow \mathsf{u}^n_*$, the additional stabilization terms in (8) vanish. We discuss consistency in more detail in Sect. 6.1.

Some of the most popular types of stabilization methods are SUPG [22, 73], GLS [75], and ADJ [66]. If a discretize-then-stabilize approach is taken, the operator $\mathcal{Q}$ takes the form

$$\mathcal{Q}_{\mathrm{DS-SUPG}} : \mathsf{v} \mapsto \frac{1}{2}\left(\mathcal{L}\mathsf{v} - \mathcal{L}^*\mathsf{v}\right) := \mathbf{b} \cdot \nabla\mathsf{v}, \tag{9}$$

$$\mathcal{Q}_{\mathrm{DS-GLS}} : \mathsf{v} \mapsto \frac{\mathsf{v}}{\Delta t} + \mathcal{L}\mathsf{v} := \frac{\mathsf{v}}{\Delta t} - \epsilon\Delta\mathsf{v} + \mathbf{b} \cdot \nabla\mathsf{v} + \sigma\mathsf{v}, \tag{10}$$

$$\mathcal{Q}_{\mathrm{DS-ADJ}} : \mathsf{v} \mapsto -\frac{\mathsf{v}}{\Delta t} - \mathcal{L}^*\mathsf{v} := -\frac{\mathsf{v}}{\Delta t} + \epsilon\Delta\mathsf{v} + \mathbf{b} \cdot \nabla\mathsf{v} - \sigma\mathsf{v}, \tag{11}$$

where the subscript "DS" denotes "discretize-then-stablize", and $\mathcal{L}^* : \mathsf{v} \mapsto -\epsilon\Delta\mathsf{v} - \mathbf{b} \cdot \nabla\mathsf{v} + \sigma\mathsf{v}$ denotes the adjoint of $\mathcal{L}$. For the space–time approach, we note that the implicit Euler method is equivalent to a space–time method with $p = 0$ discontinuous Galerkin (DG) finite elements in time, and in this setting the space–time stabilization approach results in the operator $\mathcal{Q}$ taking the form

$$\mathcal{Q}_{\mathrm{ST-SUPG}} \equiv \mathcal{Q}_{\mathrm{DS-SUPG}}, \tag{12}$$

$$\mathcal{Q}_{\mathrm{ST-GLS}} : \mathsf{v} \mapsto \mathcal{L}\mathsf{v} := -\epsilon\Delta\mathsf{v} + \mathbf{b} \cdot \nabla\mathsf{v} + \sigma\mathsf{v}, \tag{13}$$

$$\mathcal{Q}_{\mathrm{ST-ADJ}} : \mathsf{v} \mapsto -\mathcal{L}^*\mathsf{v} := \epsilon\Delta\mathsf{v} + \mathbf{b} \cdot \nabla\mathsf{v} - \sigma\mathsf{v}, \tag{14}$$

where the subscript "ST" denotes space–time.

Remark 3.3 We emphasize that, in this work, for space–time stabilization methods with the implicit Euler method, we employ the full residual operator $\mathcal{R}$ in the right slot of the stabilization term as in (8). In Refs. [39, 75], the authors do not include the $\left(\mathsf{u}^n - \mathsf{u}^{n-1}\right)/\Delta t$ term for $p = 0$ DG. We include this term for consistency at the time-discrete level. In our numerical experiments, we observed this term to make very little difference.

Employing a finite element discretization in space and leveraging the basis vector (6) yields the stabilized OΔE system to be solved for $\mathbf{a}^n_{\mathrm{h}}$, $n = 1, \ldots, N_t$,

$$\mathbf{r}_{\mathrm{S}}(\mathbf{a}^n_{\mathrm{h}}; \mathbf{a}^{n-1}_{\mathrm{h}}) = \mathbf{0}. \tag{15}$$

The discrete residual of the stabilized discretization is given by

$$\mathbf{r}_{\mathrm{S}} : (\mathbf{w}; \mathbf{z}) \mapsto \mathbf{r}_{\mathrm{G}}(\mathbf{w}; \mathbf{z}) + \mathbf{Q}\mathbf{w} - \mathbf{f}_{\mathrm{S}} - \mathbf{M}_{\mathrm{S}}\frac{\mathbf{z}}{\Delta t},$$

with $\mathbf{Q}_{ij} = m_{\mathrm{el}}\left(\mathcal{Q}\mathsf{v}_i, \tau\left(\mathcal{L}\mathsf{v}_j + \frac{\mathsf{v}_j}{\Delta t}\right)\right)$, $\mathbf{f}_{\mathrm{S}_i} = m_{\mathrm{el}}\left(\mathcal{Q}\mathsf{v}_i, \tau f\right)$, and $\mathbf{M}_{\mathrm{S}_{ij}} = m_{\mathrm{el}}\left(\mathcal{Q}\mathsf{v}_i, \tau\mathsf{v}_j\right)$.

3.3 Selection and Scaling of the Stabilization Parameter, τ

The stabilized form (8) requires specification of the stabilization parameter τ. The *a priori* selection of suitable stabilization parameters has been a topic of much research; see, for example, [41, 66, 70] and references therein. Traditionally, the stabilization constants are obtained through asymptotic scaling arguments [70], and depend on, e.g., the grid size, the diffusion coefficient and, for transient problems, the time step.

While existing definitions and scalings of the stabilization constant are well established and have been used successfully in a myriad of applications (see, e.g., the review in [135]), there are some outstanding challenges. Relevant to the current work is that classical definitions of the stabilization parameters are subject to several issues when deployed on transient problems. First and foremost, in addition to depending on the spatial grid resolution, classical definitions of τ depend on the time step. These definitions become poorly behaved in both the low time step *and* steady-state regimes. As an example, one common definition of τ is [70]

$$\tau = \left(\frac{4}{\Delta t^2} + \mathbf{b} \cdot \mathbf{G}\mathbf{b} + C\epsilon^2\mathbf{G} : \mathbf{G}\right)^{-1/2}, \tag{16}$$

where $G_{ij} = \frac{\partial\zeta_k}{\partial x_i}\frac{\partial\zeta_k}{\partial x_j}$ and $C \in \mathbb{R}^+$ is a positive constant. Here, $\frac{\partial\zeta}{\partial\boldsymbol{x}}$ is the inverse Jacobian of the element mapping between

the parametric and physical domains, i.e., the grid metrics, and we note that in one dimension $G \propto \frac{1}{h^2}$, where h is the element size. This type of definition enables, e.g., $\mathcal{O}(h^2)$ scaling in the low Peclet number limit which helps maintain optimal convergence rates. As highlighted in Ref. [70], the definition (16) is not robust in the small time step limit. As $\Delta t \to 0$, the $4/\Delta t^2$ term dominates and the formulation reverts to a Galerkin method, which is known to lack robustness. We highlight that a very similar issue exists for the LSPG approach discussed later in this manuscript.

For all numerical experiments considered in the work, we present results for numerous values of τ and as such do not restrict ourselves to a particular definition, but rather explore the sensitivity of the various methods to this parameter.

3.4 Sensitivity to the Time Step, Δt

In addition to depending on the stabilization parameter τ, it is well-known that stabilized formulations depend on the time step Δt. Stability analyses have demonstrated, for example, that stabilized formulations may become unstable at low CFL numbers [20]. This sensitivity to the time step can be understood intuitively for GLS and ADJ stabilization, where changing the time step size changes the nature of the stabilization operator $\mathcal{Q}$. Thus, changing the time step modifies both the error incurred due to temporal discretization *and* the properties of the stabilized scheme. As will be seen later in the manuscript, the LSPG approach suffers from similar issues. Thus, in our numerical examples, we perform a thorough investigation of the sensitivity of the results with respect to the time step, Δt.

4 Continuous Projection Reduced-Order Models

We now develop ROMs of the CDR system via continuous projection. Continuous ROMs generate approximate solutions $\mathsf{u}_\mathrm{r}^n (\approx \mathsf{u}^n)$ within a low-dimensional spatial trial space $\mathsf{u}_\mathrm{r}^n \in \mathcal{V}_\mathrm{r} \subset \mathcal{V}_\mathrm{h} \subset \mathcal{H}_0^1(\Omega)$, and have been studied in a number of references including [11, 12, 14, 52, 79, 85, 88, 138, 169, 170]. Various techniques exist for constructing this trial space, and here we consider proper orthogonal decomposition (POD) [19]. To construct the trial space through POD, we assume access to an ensemble of snapshots at time instances t^n, $n = 0, \dots, N_t$.[7] We collect these snapshots into the matrix

$$\mathbf{S}_{\mathsf{u}_\mathrm{h}} = \begin{bmatrix} \mathsf{u}^0 & \cdots & \mathsf{u}^{N_t} \end{bmatrix}.$$

The POD method seeks to find an $\mathcal{X}$-orthonormal basis of rank $R \ll N$ (where N is the size of the FOM from which the reduced basis is built) that minimizes the projection error

$$\underset{\{\phi_i\}_{i=1}^R, \phi_i \in \mathcal{V}_\mathrm{h}}{\text{minimize}} \sum_{n=0}^{N_t} \left\| \mathsf{u}^n - \sum_{j=1}^{R} m\big(\mathsf{u}^n, \phi_j\big)_{\mathcal{X}} \phi_j \right\|_{\mathcal{X}}^2, \tag{17}$$

where $\phi_j : \Omega \to \mathbb{R}$, $j = 1, \dots, R$, are ROM basis functions and $\mathcal{X}$ denotes inner product type (e.g., $\mathcal{H}^1(\Omega)$, $L^2(\Omega)$, weighted $L^2(\Omega)$ [14]). The minimization problem (17) can be solved via the eigenvalue problem

$$\mathbf{K}_\mathsf{u} \mathbf{E}_\mathsf{u} = \mathbf{E}_\mathsf{u} \mathbf{\Lambda}_\mathsf{u},$$

where $[\mathbf{K}_\mathsf{u}]_{ij} = m\big([\mathbf{S}_{\mathsf{u}_\mathrm{h}}]_i, [\mathbf{S}_{\mathsf{u}_\mathrm{h}}]_j\big)_{\mathcal{X}} \in \mathbb{S}^{N_s \times N_s}$, and $\mathbf{E}_\mathsf{u}$ and $\mathbf{\Lambda}_\mathsf{u}$ are the matrices associated with the eigenvectors and eigenvalues, respectively. Assuming the snapshot matrix is full rank, it can be shown that the minimizer of the problem (17) is

$$\boldsymbol{\phi} = \mathbf{S}_{\mathsf{u}_\mathrm{h}} \mathbf{E}_\mathsf{u} \sqrt{\mathbf{\Lambda}_\mathsf{u}^{-1}}. \tag{18}$$

For each $\boldsymbol{x} \in \Omega$, we evaluate these basis functions at $\boldsymbol{x}$ and assemble the ROM basis vector $\boldsymbol{\phi}(\boldsymbol{x}) \equiv \begin{bmatrix} \phi_1(\boldsymbol{x}) & \cdots & \phi_R(\boldsymbol{x}) \end{bmatrix}$ with $\boldsymbol{\phi}(\boldsymbol{x}) \in \mathbb{R}^{1 \times R}$. We then set $\mathcal{V}_\mathrm{r} \equiv \mathrm{span}\{\phi_1, \dots, \phi_R\}$. We additionally note that, as $\mathcal{V}_\mathrm{r} \subset \mathcal{V}_\mathrm{h}$, it directly follows that the ROM basis vectors can be described with a linear combination of the FOM basis vectors, i.e., $\boldsymbol{\phi}(\boldsymbol{x}) = \mathsf{v}(\boldsymbol{x})\mathbf{C}$, where $\mathbf{C} \in \mathbb{R}^{N \times R}$ is a coefficient matrix.

4.1 Galerkin Reduced-Order Models

The Galerkin ROM achieved after time discretization is: find $\mathsf{u}_\mathrm{r}^n \in \mathcal{V}_\mathrm{r}$, $n = 1, \dots, N_t$, such that

$$\begin{aligned} &m\left(\phi, \frac{\mathsf{u}_\mathrm{r}^n - \mathsf{u}_\mathrm{r}^{n-1}}{\Delta t}\right) + m\big(\epsilon \nabla \phi, \nabla \mathsf{u}_\mathrm{r}^n\big) \\ &+ m\big(\phi, \mathbf{b} \cdot \nabla \mathsf{u}_\mathrm{r}^n\big) + m\big(\phi, \sigma \mathsf{u}_\mathrm{r}^n\big) = m(\phi, f), \qquad \forall \phi \in \mathcal{V}_\mathrm{r}. \end{aligned} \tag{19}$$

Leveraging the ROM basis vector $\boldsymbol{\phi}$, the Galerkin ROM can be cast as the sequence of OΔEs to be solved for $\hat{\mathbf{x}}^n$, $n = 1, \dots, N_t$,

$$\mathbf{r}_{\mathrm{G-r}}(\hat{\mathbf{x}}^n; \hat{\mathbf{x}}^{n-1}) = \mathbf{0}, \tag{20}$$

where $\hat{\mathbf{x}}^n \in \mathbb{R}^R$ are the ROM "generalized coordinates" such that the approximate state is defined as $\mathsf{u}_\mathrm{r}^n = \boldsymbol{\phi}\hat{\mathbf{x}}^n$, and the residual operator is given by

$$\mathbf{r}_{\mathrm{G-r}} : (\mathbf{w}; \mathbf{z}) \mapsto \mathbf{M}_\mathrm{r}\left[\frac{\mathbf{w} - \mathbf{z}}{\Delta t}\right] + \mathbf{B}_\mathrm{r}\mathbf{w} - \mathbf{f}_\mathrm{r},$$

[7] In practice, snapshots are often collected at only a subset of the time steps. Additionally, snapshots can be collected for a variety of parameter values, in the case of a parametrized PDE.

with $\mathbf{B}_\mathrm{r} \in \mathbb{R}^{R\times R}$, $\mathbf{B}_{\mathrm{r}_{ij}} \equiv \mathcal{B}_\mathrm{G}(\phi_i,\phi_j)$, $\mathbf{M}_\mathrm{r} \in \mathbb{R}^{R\times R}$, $\mathbf{M}_{\mathrm{r}_{ij}} \equiv m(\phi_i,\phi_j)$, and $\mathbf{f}_\mathrm{r} \in \mathbb{R}^R$, $\mathbf{f}_{\mathrm{r}_i} \equiv m(\phi_i,f)$. The Galerkin ROM formulation (19) corresponds to method I in Fig. 1.

4.2 Residual-Based Stabilized Reduced-Order Models

Analogously to the FEM case, the Galerkin ROM can lack robustness in the presence of sharp, under-resolved gradients. In the present context, such a situation may arise when the diffusion constant is small (relatively to $\mathbf{b}$) and not enough ROM basis vectors are employed to capture the behavior of the solution of interest. A stabilized ROM formulation can be written generally as: find $\mathsf{u}_\mathrm{r}^n \in \mathcal{V}_\mathrm{r}$, $n = 1,\dots,N_t$, such that

$$m\left(\phi, \frac{\mathsf{u}_\mathrm{r}^n - \mathsf{u}_\mathrm{r}^{n-1}}{\Delta t}\right) + m\left(\epsilon\nabla\phi, \nabla\mathsf{u}_\mathrm{r}^n\right) + m\left(\phi, \mathbf{b}\cdot\nabla\mathsf{u}_\mathrm{r}^n\right) + m\left(\phi, \sigma\mathsf{u}_\mathrm{r}^n\right) + m_\mathrm{el}\left(\mathcal{Q}\phi, \tau\mathcal{R}\left(\mathsf{u}_\mathrm{r}^n, \mathsf{u}_\mathrm{r}^{n-1}\right)\right) = m(\phi,f), \qquad \forall\phi \in \mathcal{V}_\mathrm{r} \tag{21}$$

where $\mathcal{Q}$ can be any of the forms given in Eqs. (9)–(14). We consider the SUPG, GLS_DS, ADJ_DS, GLS_ST, and ADJ_ST ROMs as defined by the operators in Eqs. (9)–(14). Leveraging the ROM basis vectors yields the stabilized OΔE system to be solved for $\hat{\mathbf{x}}^n$, $n = 1,\dots,N_t$,

$$\mathbf{r}_{\mathrm{S}-\mathrm{r}}(\hat{\mathbf{x}}^n;\hat{\mathbf{x}}^{n-1}) = \mathbf{0}. \tag{22}$$

The discrete residual of the stabilized discretization is given by

$$\mathbf{r}_{\mathrm{S}-\mathrm{r}} : (\mathbf{w};\mathbf{z}) \mapsto \mathbf{r}_{\mathrm{G}-\mathrm{r}}(\mathbf{w};\mathbf{z}) + \mathbf{Q}_\mathrm{r}\mathbf{w} - \mathbf{M}_{\mathrm{S}-\mathrm{r}}\frac{\mathbf{z}}{\Delta t} - \mathbf{f}_{\mathrm{S}-\mathrm{r}},$$

with $\mathbf{Q}_{\mathrm{r}ij} = m_\mathrm{el}\left(\mathcal{Q}\phi_i, \tau\left(\mathcal{L}\phi_j + \frac{\phi_j}{\Delta t}\right)\right) \in \mathbb{R}^{R\times R}$, $\mathbf{f}_{\mathrm{S}-\mathrm{r}\,i} = m_\mathrm{el}\left(\mathcal{Q}\phi_i, \tau f\right) \in \mathbb{R}^R$, and $\mathbf{M}_{\mathrm{S}-\mathrm{r}\,ij} = m_\mathrm{el}\left(\mathcal{Q}\phi_i, \tau\phi_j\right) \in \mathbb{R}^{R\times R}$. The stabilized ROM formulations (21) correspond to method II in Fig. 1.

In the literature, SUPG ROMs have been considered in [18, 52, 82, 94, 111, 118, 179, 180], amongst others. To the best of our knowledge, ROMs based on GLS_DS, ADJ_DS, GLS_ST, and ADJ_ST are novel.

4.3 Selection and Scaling of the Stabilization Parameter, τ

Like in the standard FEM, the stabilized ROM form (21) requires specification of the stabilization parameter τ. *A priori* selection of this parameter in the context of ROMs is not as well explored as in the standard FEM case. It remains unclear, for instance, if the stabilization parameter should take on a different value for the ROM as opposed to the full-order FEM discretization. While selecting a different value of τ for the ROM as the one used in the FOM would lead to a lack of consistency between the ROM and the FOM, it may nonetheless improve the stability and accuracy of the ROM. To the best of the authors knowledge, [52], which explores the selection of the stabilization parameter in the context of the SUPG approach, is the only present study that examines the selection of τ within the ROM context. Specifically, [52] employs the same strategy as that used in standard FEM: a SUPG-ROM error bound is first proved, and τ is chosen to minimize this bound. However, since the ROM space is a subspace of the FEM space, two types of inverse inequalities are used to prove the SUPG-ROM bound: a standard FEM inverse inequality, and a ROM inverse inequality [95]. These two inverse inequalities yield two SUPG-ROM error bounds, which in turn yield two τ scalings: a standard FEM scaling in which τ depends on the FEM mesh size, and a new ROM scaling in which τ depends on the ROM parameters (e.g., the ROM dimension, the POD basis functions, and the corresponding eigenvalues). We note that other approaches leveraging residual-based stabilization for ROMs (see, e.g., [118]) use standard definitions of τ inherited from the FEM community in which case τ depends on the FEM discretization (as opposed to the resolution of the ROM basis).

5 Discrete Projection Reduced-Order Models

ROMs developed through continuous projection operate in a weighted residual setting defined at the spatially-continuous level. ROMs developed through discrete projection, however, perform model reduction at either the level of the FOM ODE or FOM OΔE; Ref. [29] shows that these two approaches are equivalent for the Galerkin method. In this work, we restrict our discussion to discrete projection-based ROMs developed at the OΔE level.

Discrete projection ROMs approximate the degrees of freedom associated with the spatial discretization in a low-dimensional (vector) trial space, $\mathbf{a}_\mathrm{r}^n (\approx \mathbf{a}_\mathrm{h}^n) \in V_r \subseteq \mathbb{R}^N$, $n = 0,\dots,N_t$, where V_r is the discrete ROM trial subspace. We again employ POD to construct this space. Towards this end, on the vector space $\mathbb{R}^N$ we first define the $\mathbf{P}$-weighted inner product $m_d(\cdot,\cdot)_\mathbf{P} : (\mathbf{U},\mathbf{V}) \mapsto \mathbf{U}^T\mathbf{P}\mathbf{V}$, where $\mathbf{P} \in \mathbb{S}^N$ is a symmetric-positive definite weighting matrix. The associated $\mathbf{P}$-weighted norm is $\|\mathbf{x}\|_\mathbf{P}^2 = \mathbf{x}^T\mathbf{P}\mathbf{x}$. Next, we assume access to an ensemble of snapshots of the FEM coefficients at time instances t^n, $n = 0,\dots,N_t$. We then seek a $\mathbf{P}$-orthonormal basis of rank R that minimizes the projection error

$$\underset{\boldsymbol{\Psi}\in\mathbb{R}^{N\times R},\, \boldsymbol{\Psi}^T\mathbf{P}\boldsymbol{\Psi}=\mathbf{I}}{\text{minimize}} \sum_{n=0}^{N_t} \|\mathbf{a}_\mathrm{h}^n - \boldsymbol{\Psi}\boldsymbol{\Psi}^T\mathbf{P}\mathbf{a}_\mathrm{h}^n\|_\mathbf{P}^2. \tag{23}$$

The solution to the minimization problem (23) can be obtained via an eigenvalue problem or via the generalized singular value decomposition; we present the former here. We denote the snapshots of FEM coefficients as

$$\mathbf{S}_{\mathbf{a}_\mathrm{h}} \equiv \left[\mathbf{a}_\mathrm{h}^0 \ \cdots \ \mathbf{a}_\mathrm{h}^{N_t}\right] \in \mathbb{R}^{N\times N_t+1}.$$

We note that $\mathbf{S}_{\mathrm{u}_\mathrm{h}} = \mathsf{v}\mathbf{S}_{\mathbf{a}_\mathrm{h}}$. Defining the time correlation matrix as $\mathbf{K}_{\mathbf{a}_\mathrm{h}} = m_d\left(\mathbf{S}_{\mathbf{a}_\mathrm{h}}, \mathbf{S}_{\mathbf{a}_\mathrm{h}}\right)_\mathbf{P}$, we can leverage the eigenvalue problem

$$\mathbf{K}_{\mathbf{a}_\mathrm{h}}\mathbf{E}_{\mathbf{a}_\mathrm{h}} = \mathbf{E}_{\mathbf{a}_\mathrm{h}}\mathbf{\Lambda}_{\mathbf{a}_\mathrm{h}}$$

to obtain the POD bases. The solution to the minimization problem (23) can be shown to be

$$\mathbf{\Psi} = \mathbf{S}_{\mathbf{a}_\mathrm{h}}\mathbf{E}_{\mathbf{a}_\mathrm{h}}^R\sqrt{[\mathbf{\Lambda}_{\mathbf{a}_\mathrm{h}}^R]^{-1}},$$

where $\mathbf{E}_{\mathbf{a}_\mathrm{h}}^R$ and $\mathbf{\Lambda}_{\mathbf{a}_\mathrm{h}}^R$ comprise the first R columns of $\mathbf{E}_{\mathbf{a}_\mathrm{h}}$ and the first R columns and rows of $\mathbf{\Lambda}_{\mathbf{a}_\mathrm{h}}$, respectively.

Remark 5.1 Setting $\mathbf{P}_{ij} \leftarrow m\left(\mathsf{v}_i, \mathsf{v}_j\right)_\mathcal{X}$, we can express the correlation matrix as

$$\mathbf{K}_{\mathbf{a}_\mathrm{h}}t_{ij} = m\left([\mathbf{S}_{\mathrm{u}_\mathrm{h}}]_i, [\mathbf{S}_{\mathrm{u}_\mathrm{h}}]_j\right)_\mathcal{X},$$

which recovers the correlation matrix used in continuous projection ROMs. Further, as $\mathbf{S}_{\mathrm{u}_\mathrm{h}} = \mathsf{v}\mathbf{S}_{\mathbf{a}_\mathrm{h}}$, we can express Eq. (18) as $\boldsymbol{\phi}(x) = \mathsf{v}(x)\mathbf{S}_{\mathbf{a}_\mathrm{h}}\mathbf{E}_\mathrm{u}\sqrt{\mathbf{\Lambda}_\mathrm{u}^{-1}}$ and we see that

$$\boldsymbol{\phi}(\boldsymbol{x}) = \mathsf{v}(\boldsymbol{x})\mathbf{\Psi}.$$

We emphasize that this result is well-documented in the community, see, e.g., [122, 167].

5.1 Galerkin Reduced-Order Model

The Galerkin ROM developed through discrete projection is obtained by (i) making the substitution $\mathbf{a}_\mathrm{h}^n \leftarrow \mathbf{\Psi}\hat{\mathbf{x}}^n$, $n = 0, \ldots, N_t$, and (ii) restricting the residual of the FOM OΔE to be $\mathbf{W}$-orthogonal to the vector trial space V_r. Here $\hat{\mathbf{x}}^n \in \mathbb{R}^R$, $n = 0, \ldots, N_t$ are the ROM generalized coordinates and $\mathbf{W} \in \mathbb{S}^N$ is a weighting matrix inducing the inner product $m_d(\cdot,\cdot)_\mathbf{W} : (\mathbf{U}, \mathbf{V}) \mapsto \mathbf{U}^T\mathbf{W}\mathbf{V}$ with the associated $\mathbf{W}$-weighted norm $\|\mathbf{x}\|_\mathbf{W}^2 = \mathbf{x}^T\mathbf{W}\mathbf{x}$; $\mathbf{W}$ may or may not be the same as $\mathbf{P}$. It is critical to note that the Galerkin ROM developed via discrete projection can be developed for any FOM OΔE; e.g., the FOM OΔE could associate with the Galerkin FOM OΔE (7), *or* it could associate with the stabilized FOM OΔE (15).

We denote the residual of a generic FOM OΔE[8] as

$$\mathbf{r} : (\mathbf{w};\mathbf{z}) \mapsto \mathbf{r}(\mathbf{w};\mathbf{z}).$$

Examples of this residual are $\mathbf{r} = \mathbf{r}_\mathrm{G}$ for association with the Galerkin FOM OΔE (7) and $\mathbf{r} = \mathbf{r}_\mathrm{S}$ for association with the stabilized FOM OΔE (15). The Galerkin ROM obtained via discrete projection yields the OΔE system to be solved for $\hat{\mathbf{x}}^n$, $n = 1, \ldots, N_t$,

$$\mathbf{r}_{\mathrm{G-DROM}}(\hat{\mathbf{x}}^n;\hat{\mathbf{x}}^{n-1}) = \mathbf{0}, \tag{24}$$

where the residual of the discretely projected Galerkin ROM is given by

$$\mathbf{r}_{\mathrm{G-DROM}} : (\mathbf{w};\mathbf{z}) \mapsto m_d(\mathbf{\Psi}, \mathbf{r}(\mathbf{\Psi}\mathbf{w};\mathbf{\Psi}\mathbf{z}))_\mathbf{W}.$$

The discrete Galerkin ROM formulation (24) corresponds to methods III and VI in Fig. 1, depending on the underlying FEM model.

Remark 5.2 Setting $\mathbf{P}_{ij} \leftarrow m\left(\mathsf{v}_i, \mathsf{v}_j\right)_\mathcal{X}$ in optimization problem (23), and $\mathbf{W} \leftarrow \mathbf{I}$, $\mathbf{r} \leftarrow \mathbf{r}_\mathrm{G}$ in problem (24), the Galerkin ROM obtained via discrete projection (24) recovers the Galerkin ROM obtained via continuous projection (20).

Remark 5.3 Analogously to Remark 5.2, setting $\mathbf{P}_{ij} \leftarrow m\left(\mathsf{v}_i, \mathsf{v}_j\right)_\mathcal{X}$ in optimization problem (23), and $\mathbf{W} \leftarrow \mathbf{I}$, $\mathbf{r} \leftarrow \mathbf{r}_\mathrm{S}$ in problem (24), the Galerkin ROM obtained via discrete projection (24) recovers the stabilized ROM obtained via continuous projection (22).

5.2 Least-Squares Petrov–Galerkin Reduced-Order Model

Similar to the continuous Galerkin ROM, the discrete Galerkin ROM has been observed to yield inaccurate or unstable solutions in a variety of settings and thus various stabilization approaches have been developed for discrete ROMs. The LSPG approach comprises one particularly popular stabilization approach for discrete ROMs [24, 26, 29, 30]. LSPG operates by computing a sequence of solutions $\hat{\mathbf{x}}^n$, $n = 1, \ldots, N_t$, that satisfy the minimization problem

$$\hat{\mathbf{x}}^n = \underset{\hat{\mathbf{y}}\in\mathbb{R}^R}{\arg\min} \ ||\mathbf{r}(\mathbf{\Psi}\hat{\mathbf{y}};\mathbf{\Psi}\hat{\mathbf{x}}^{n-1})||_\mathbf{W}^2, \tag{25}$$

where $\mathbf{r}$ is again the residual of the FOM OΔE. The optimization problem (25) can be solved via the first-order optimality conditions, which yield the sequence of algebraic equations for $\hat{\mathbf{x}}^n, n = 1, \ldots, N_t$,

[8] For simplicity of presentation, we assume the FOM OΔE to depend only on the state at the current time instance and previous time instance, as would be the case with an implicit Euler temporal discretization.

$$m_d\left(\frac{\partial \mathbf{r}}{\partial \mathbf{y}}(\boldsymbol{\Psi}\hat{\mathbf{x}}^n)\boldsymbol{\Psi}, \mathbf{r}(\boldsymbol{\Psi}\hat{\mathbf{x}}^n;\boldsymbol{\Psi}\hat{\mathbf{x}}^{n-1})\right)_{\mathbf{W}} = \mathbf{0},$$

where $\frac{\partial \mathbf{r}}{\partial \mathbf{y}}$ is the Jacobian of the residual $\mathbf{r}(\cdot,\cdot)$ with respect to the first argument. In the case $\mathbf{r} \leftarrow \mathbf{r}_{\mathrm{G}}$, the optimality conditions become

$$m_d\left(\frac{\mathbf{M}\boldsymbol{\Psi}}{\Delta t} + \mathbf{B}\boldsymbol{\Psi}, \mathbf{r}_{\mathrm{G}}(\boldsymbol{\Psi}\hat{\mathbf{x}}^n;\boldsymbol{\Psi}\hat{\mathbf{x}}^{n-1})\right)_{\mathbf{W}} = \mathbf{0}.$$

We see that LSPG takes the form of a Petrov–Galerkin ROM and hence we classify it as a residual-based method. The LSPG ROM formulation (25) corresponds to methods IV and V in Fig. 1, depending on the underlying FEM.

Remark 5.4 (LSPG can correspond to a continuous minimization principle.) Setting $\mathbf{r} \leftarrow \mathbf{r}_{\mathrm{G}}$ and $\mathbf{W} \leftarrow \mathbf{M}^{-1}$ in optimization problem (25), LSPG corresponds to the continuous minimization principle for $\mathsf{u}_{\mathrm{r}}^n$, $n = 1, \ldots, N_t$,

$$\mathsf{u}_{\mathrm{r}}^n = \underset{\mathsf{u}\in\mathcal{V}_{\mathrm{r}}}{\arg\min} \int_{\Omega} \left(\mathsf{R}_{\mathrm{G}}^{\|}(\mathsf{u};\mathsf{u}_{\mathrm{r}}^{n-1})\right)^2 d\boldsymbol{x}, \tag{26}$$

where

$$\mathsf{R}_{\mathrm{G}}^{\|} : (\mathsf{w};\mathsf{z}) \mapsto \mathsf{v}\mathbf{M}^{-1} m\left(\mathsf{v}, \mathsf{R}_{\mathrm{cdr}}(\mathsf{w};\mathsf{z})\right)$$

and

$$\mathsf{R}_{\mathrm{cdr}} : (\mathsf{w};\mathsf{z}) \mapsto \frac{\mathsf{w}-\mathsf{z}}{\Delta t} - \nu\nabla^2\mathsf{w} + \mathbf{b}\cdot\nabla\mathsf{w} + \sigma\mathsf{w} - f.$$

LSPG computes the solution $\mathsf{u}_{\mathrm{r}}^n$ within the ROM trial space $\mathcal{V}_{\mathrm{r}}$ that minimizes the $L^2(\Omega)$-norm of the time-discrete, spatially continuous residual projected onto the finite element trial space $\mathcal{V}_{\mathrm{h}}$. The full derivation for this equivalence is presented in Appendix 2.

Remark 5.5 For the case $\mathbf{r} \leftarrow \mathbf{r}_{\mathrm{S}}$, it is not clear if LSPG corresponds to an underlying residual minimization principle defined at the continuous level.

5.2.1 Selection of the Time Step, Δt

While LSPG does not contain a stabilization parameter, its performance depends on the time step and time integration scheme [29]. This is due to the fact that changing the time step (i) modifies the error incurred due to temporal discretization and (ii) modifies the LSPG minimization problem (i.e., the time-discrete residual changes). As a result, LSPG yields best results at an intermediary time step [29]. LSPG lacks robustness for too small a time step (in the limit $\Delta t \to 0$ LSPG recovers the Galerkin approach [29]) and too large a time step. Minimal work has examined the *a priori* selection of an appropriate time step.

5.3 Adjoint Petrov–Galerkin reduced-Order Model

The final residual-based stabilization technique considered in this work is the APG method [121]. APG is a VMS-based approach for constructing discrete ROMs, and is derived from a time-continuous ODE setting. APG is derived via a multiscale decomposition of $\mathbb{R}^N$ into a coarse-scale, resolved trial space V_r and a fine-scale, unresolved trial space, V_r' such that $\mathbb{R}^N = V_r \oplus V_r'$. The impact of fine scales on the coarse-scale dynamics is then accounted for by virtue of the Mori–Zwanzig formalism and the variational multiscale method [121]. Setting $\mathbf{P} \leftarrow \mathbf{M}$ in (23), associating with the Galerkin FOM OΔE (7), and using the implicit Euler method for time-discretization, APG yields the sequence of OΔE's to be solved for $\hat{\mathbf{x}}^1, \ldots, \hat{\mathbf{x}}^{N_t}$,

$$\mathbf{r}_{\mathrm{APG}}(\hat{\mathbf{x}}^n;\hat{\mathbf{x}}^{n-1}) = \mathbf{0}. \tag{27}$$

The APG residual is given by

$$\mathbf{r}_{\mathrm{APG}} : (\mathbf{w};\mathbf{z}) \mapsto \left(\left(\mathbf{I} - \tau_{\mathrm{APG}}[\mathbb{A}']^T\left[\mathbf{B}\right]^T\right)\boldsymbol{\Psi}, \mathbf{r}_{\mathrm{G}}(\boldsymbol{\Psi}\mathbf{w};\boldsymbol{\Psi}\mathbf{z})\right)_{\mathbf{I}},$$

where $\mathbb{A}' = \mathbf{M}^{-1} - \boldsymbol{\Psi}\boldsymbol{\Psi}^T$, $\mathbb{A}' : \mathbb{R}^N \to V_r'$, and $\tau_{\mathrm{APG}} \in \mathbb{R}_{>0}$ is a stabilization parameter. The full derivation for APG is provided in Appendix 3.

Remark 5.6 The APG approach displays conceptual similarities with adjoint stabilization and the (quasi-static) orthogonal subscales (OSS) approach from the variational multiscale method [10, 40, 130]; see Ref. [121] for details. There is no clear **direct** equivalence between these approaches, however. This is a result of APG being formulated at the discrete level, while adjoint stabilization and orthogonal subscales are formulated at the continuous level.

Like LSPG, APG could also associate with a stabilized FOM. Some of the stabilized FEM formulations considered in this work, however, are developed at the time-discrete level (e.g., $\mathrm{ADJ}_{\mathrm{DS}}$ and $\mathrm{GLS}_{\mathrm{DS}}$). As APG is derived from a time-continuous setting, it is not straightforward to construct an APG ROM of all stabilized formulations, and we only consider the SUPG, $\mathrm{GLS}_{\mathrm{ST}}$, and $\mathrm{ADJ}_{\mathrm{ST}}$ FEM models. We note that this is due to the fact that the test functions in these formulations do not contain terms of the form $\frac{v}{\Delta t}$. The APG ROM associating with one of these stabilized FEM models is obtained by setting $\mathbf{P} \leftarrow \mathbf{M}$ in (23), associating with the stabilized FEM OΔE (7) with $\mathcal{Q} \leftarrow \mathcal{Q}_{\mathrm{DS-SUPG}}$, $\mathcal{Q}_{\mathrm{ST-GLS}}$, or $\mathcal{Q}_{\mathrm{ST-ADJ}}$, and using the implicit Euler method for time-discretization. This process yields the sequence of OΔE's to be solved for $\hat{\mathbf{x}}^1, \ldots, \hat{\mathbf{x}}^{N_t}$,

$$\mathbf{r}_{\mathrm{APG-S}}(\hat{\mathbf{x}}^n;\hat{\mathbf{x}}^{n-1}) = \mathbf{0}, \tag{28}$$

where

$$\mathbf{r}_{\mathrm{APG-S}} : (\mathbf{w};\mathbf{z}) \mapsto \left(\left(\mathbf{I} - \tau_{\mathrm{APG}}[\mathbb{A}']^T[\mathbf{B}+\mathbf{Q}]^T\right)\boldsymbol{\Psi}, \mathbf{r}_{\mathrm{S}}(\boldsymbol{\Psi}\mathbf{w};\boldsymbol{\Psi}\mathbf{z})\right)_{\mathbf{I}}.$$

The APG ROM formulation (27) corresponds to method IV Fig. 1, while the APG ROM formulation (28) corresponds to method V in Fig. 1.

5.4 Summary of Remarks for Discrete ROMs

A summary of the remarks provided in this section is as follows:

- **The discrete POD basis recovers the continuous POD basis**. The POD bases obtained through discrete projection recover the POD bases obtained through continuous projection under the conditions $\mathbf{P}_{ij} \leftarrow m\left(\mathsf{v}_i, \mathsf{v}_j\right)_{\mathcal{X}}$ in optimization problem (23).
- **The discrete Galerkin ROM recovers the continuous Galerkin ROM.** The discrete Galerkin ROM recovers the continuous Galerkin ROM under the conditions $\mathbf{W} \leftarrow \mathbf{I}$ in problem (24), $\mathbf{P}_{ij} \leftarrow m\left(\mathsf{v}_i, \mathsf{v}_j\right)_{\mathcal{X}}$ in optimization problem (23), and $\mathbf{r} \leftarrow \mathbf{r}_{\mathrm{G}}$ in problem (24).
- **The discrete Galerkin ROM recovers stabilized ROMs.** The discrete Galerkin ROM recovers the stabilized continuous ROM under the conditions $\mathbf{W} \leftarrow \mathbf{I}$ in problem (24), $\mathbf{P}_{ij} \leftarrow m\left(\mathsf{v}_i, \mathsf{v}_j\right)_{\mathcal{X}}$ in optimization problem (23), and $\mathbf{r} \leftarrow \mathbf{r}_{\mathrm{S}}$ in problem (24).
- **LSPG mimics a continuous $L^2(\Omega)$ minimization principle.** LSPG mimics a continuous $L^2(\Omega)$ minimization principle under the conditions $\mathbf{r} \leftarrow \mathbf{r}_{\mathrm{G}}$ and $\mathbf{W} \leftarrow \mathbf{M}^{-1}$ in optimization problem (25).
- **APG displays similarities to adjoint stabilization.** Similar to APG, ADJ can also be derived from the variational multiscale method. For transient systems ADJ results in a set of equations that are conceptually similar to APG, but without the appearance of an orthogonal projector. We note that FEM approaches for orthogonal subscales do exist, e.g., [10, 40, 130], and APG also displays similarities with these approaches.

6 Brief Survey of Numerical Analysis of Residual-Based ROM Stabilizations

In this section, we summarize the numerical analysis results that are currently available for the residual-based ROM stabilizations presented above. Specifically, we discuss the consistency, stability, and error bounds for these methods. We emphasize that this is just a brief summary of the existing results and reflects only our own view on the topic. Furthermore, we note that these definitions are not necessarily agreed upon.

6.1 Consistency

We start by considering consistency. For ROMs, two types of consistency can be considered, and for concreteness we use the following terminology:

- **Type 1: (Time-discrete) PDE consistency.** The ROM weak form holds when evaluated at the PDE solution, $\mathsf{u}_{\mathrm{r}}^n \leftarrow \mathsf{u}_*^n$, assuming $\mathsf{u}_*^n \in \mathcal{H}^2(\Omega)$. We note that Type 1 consistency is only relevant for continuous ROMs, as discrete ROMs have no notion of the underlying PDE. We also note that Type 1 consistency is the consistency concept used for classical numerical methods (e.g., FEM).
- **Type 2: FOM consistency:** The ROM weak form holds when evaluated at the FOM solution from which it is constructed. For continuous ROMs, this condition states that the weak form holds under the substitution $\mathsf{u}_{\mathrm{r}}^n \leftarrow \mathsf{u}_{\mathrm{h}}^n$. Analogously for discrete ROMs, the "discrete weak form" holds under the substitution $\mathbf{a}_{\mathrm{r}}^n \leftarrow \mathbf{a}_{\mathrm{h}}^n$.

Remark 6.1 (Model Consistency) A ROM is model consistent if the same stabilization method is used in the FOM and ROM. We note that, when the same parameters are used in the FOM and ROM (i.e., we have parameter FOM-ROM consistency [158]), model consistency is a special class of Type 2 consistency. In [118] (see also [52]), the authors have argued both numerically and theoretically (in particular, see Section 3.3 and Proposition 3.1 in [118]) that using the same type of stabilization (i.e., SUPG) in the FOM and ROM yields more accurate ROM results. More recently, model consistency for the evolve-filter-relax ROM [158] (which is a spatial filtering-based stabilization, such as those described in Appendix 1) was shown to increase the ROM accuracy.

6.1.1 Continuous Residual-Based ROM Stabilizations

Continuous Galerkin ROMs. The continuous Galerkin ROM is Type 1 and Type 2 consistent. Type 1 consistency follows directly from setting $\mathsf{v} = \phi$ in the weak form (4), where we have leveraged $\mathcal{V}_{\mathrm{r}} \subset \mathcal{H}_0^1(\Omega)$. Analogously, Type 2 consistency is shown from setting $\mathsf{v} = \phi$ in the weak form (5). We note that, assuming a consistent FOM, Type 2 consistency automatically implies Type 1 consistency. This allows for *a priori* convergence analyses of continuous Galerkin ROMs with respect to the FOM solution as well as the solution to the governing continuous PDEs, as discussed in Refs. [67, 87, 139]. We emphasize that, in order to maintain Type 2

consistency for a continuous Galerkin ROM, it is important to employ the same spatial and temporal discretization method in building the ROM as the one employed in building the FOM.

Continuous stabilized ROMs. Like continuous Galerkin ROMs, the SUPG, GLS_{DS}, and ADJ_{DS} stabilized ROMs (developed through both the discretize-then-stabilize and space–time formulations) are Type 1 and Type 2 consistent. These stabilized formulations display Type 1 consistency as the stabilization term vanishes when evaluated about the PDE solution; the term vanishes as the residual evaluates to zero for the PDE solution (assuming the solution is sufficiently regular). Type 2 consistency follows directly from setting $\mathsf{v} = \phi$ in the stabilized weak form (8), where we have leveraged $\mathcal{V}_{\text{r}} \subset \mathcal{V}_{\text{h}}$.

6.1.2 Discrete Residual-Based ROM Stabilizations

Discrete Galerkin ROMs. The discrete Galerkin ROM displays Type 2 consistency with the FEM model from which it is constructed. We show this by first setting $\mathbf{a}_{\text{h}}^n$, $n = 1, \dots, N_t$ to be the FOM solution obtained from the Galerkin FOM (7). Making the substitution $\mathbf{a}_{\text{r}}^n \leftarrow \mathbf{a}_{\text{h}}^n$, $n = 0, \dots, N_t$, it is straightforward to see that Eq. (24) is satisfied under the conditions $\mathbf{r} \leftarrow \mathbf{r}_{\text{G}}$ as $\mathbf{r}_{\text{G}}(\mathbf{a}_{\text{h}}^n, \mathbf{a}_{\text{h}}^{n-1}) = \mathbf{0}$, $n = 1, \dots, N_t$. Analogously, let $\mathbf{a}_{\text{h}}^n$, $n = 1, \dots, N_t$ be the FOM solution obtained from a stabilized FOM (15). Making the substitution $\mathbf{a}_{\text{r}}^n \leftarrow \mathbf{a}_{\text{h}}^n$, $n = 0, \dots, N_t$, it is again straightforward to see that (24) is satisfied under the conditions $\mathbf{r} \leftarrow \mathbf{r}_{\text{S}}$ as $\mathbf{r}_{\text{S}}(\mathbf{a}_{\text{h}}^n, \mathbf{a}_{\text{h}}^{n-1}) = \mathbf{0}$, $n = 1, \dots, N_t$.

Discrete Stabilized ROMs. Like the discrete Galerkin ROM, discrete stabilized ROMs display Type 2 consistency with the FEM model from which they are constructed. As both LSPG and APG can be written as a Petrov–Galerkin method, Type 2 consistency follows from the same arguments as the discrete Galerkin ROM.

Remark 6.2 The residual-based stabilizations examined here all display Type 2 consistency,[9] and all continuous ROMs display Type 1 consistency. We emphasize that, while all methods considered here are consistent within the setting described above, this does not hold for all stabilized methods. Stabilization approaches based on, for example, eddy viscosity approaches [78] typically *do not* display Type 1 consistency.

6.2 Stability

Stability properties of the ROM depend on the type of projection, and are a driving factor in the ROM development. Here, we highlight the stabilization properties of the various ROMs considered. For concreteness, we restrict our discussion to stability within the context of the CDR equation.

6.2.1 Continuous ROMs

For continuous ROMs, we define a stable formulation as one whose spatial bilinear form is *strongly coercive*. For continuous ROMs, coercivity is defined by

$$\mathcal{B}(\mathsf{u}, \mathsf{u}) \geq C \|\mathsf{u}\|_Y^2 \tag{29}$$

for some $C \in \mathbb{R}_{>0}$. In the above, $\mathcal{B}$ denotes a bilinear form, and $\|\cdot\|_Y^2$ denotes a norm associated with the formulation.

Remark 6.3 If the spatial bilinear form is strongly coercive, then the fully discrete bilinear form associated with an implicit Euler discretization in time is also strongly coercive.

Coercivity of the spatial bilinear form guarantees boundedness of the solution, i.e., for finite n and some $\beta > 0$,

$$\|\mathsf{u}^n\|_Y \leq \beta \|f^n\|_Y, \tag{30}$$

where f^n is the data at the nth time step.

Remark 6.4 Stability vs. accuracy. Before proceeding, we make the important point that a stable ROM does not necessarily imply an accurate ROM, and, often times, terminologies between instabilities and inaccuracies are mixed. As an example, for the CDR equation, the constants C and β in (29) and (30) depend on the diffusion parameter, ϵ. It can be shown that the continuous Galerkin ROM has $\beta \to \infty$ as $\epsilon \to 0$. Thus, for small ϵ values, the stability constant β can be very large. As a result, although the standard Galerkin ROM may be formally stable (in the sense of (30)), it can be extremely inaccurate and display spurious oscillations. These spurious oscillations are often viewed as instabilities. We emphasize that this is not just a theoretical issue. In practical ROM computations of convection-dominated systems (i.e., when ϵ is very small), the standard Galerkin ROM approximation—while mathematically stable—can indeed display large, spurious numerical oscillations (just as in the FEM setting [135]). Although these oscillations are often referred to as instabilities, we emphasize here that they are large, but bounded (by the large stability constant β).

With this in mind, we now outline stability properties of the various formulations in the sense of the definition (29).

- **Continuous Galerkin ROM.** Coercivity of the continuous Galerkin FEM model has been demonstrated in numerous contexts (see, for example, Ref. [159]), and it

[9] Formally, these methods are Type 2 consistent only if the same stabilization parameters and time steps are used in the FOM and ROM.

is straightforward to show that the continuous Galerkin FEM model is stable in the sense

$$\mathcal{B}_{\mathrm{G}}(\mathsf{u},\mathsf{u}) \geq C\|\mathsf{u}\|_{\mathrm{G}}^2, \tag{31}$$

where $\|\mathsf{u}\|_{\mathrm{G}}^2 = \sigma\|\mathsf{u}\|_{L^2(\Omega)}^2 + \epsilon\|\nabla\mathsf{u}\|_{L^2(\Omega)}^2$. We emphasize that this coercivity property guarantees boundedness of the solution. For instance, under a suitable time-step restriction, the Galerkin method with a θ-scheme for temporal discretization can be equipped with the stability bound

$$\|\mathsf{u}_{\mathrm{h}}^n\|_{L^2(\Omega)} \leq \|u_{0,h}\|_{L^2(\Omega)} + C\sqrt{\frac{t^n}{\epsilon}}\max_{t\in[0,T]}\|f(t)\|_{L^2(\Omega)}$$

for a constant C that depends only on Ω. See, e.g., Proposition 12.2.1 in [127]. In the limit of $\epsilon \to 0$, the stability statement (31) loses control over the gradient. Hence, the Galerkin method is *stable*, but not *robust* in the limit of $\epsilon \to 0$. The stability of the continuous Galerkin ROM follows along the same lines as that for the continuous Galerkin FEM model [95, Theorem 5].

- **Continuous SUPG ROM.** Coercivity of the SUPG FEM model has additionally been demonstrated in various contexts (see again Ref. [159, pg. 494], or Refs. [52, 83]). Coercivity of the SUPG FEM model depends on inverse estimates, and it is fairly straightforward to show that for some $\tau \in [0, \tau^*_{\mathrm{SUPG}}]$, where τ^*_{SUPG} is a grid and parameter dependent upper threshold on τ, the continuous SUPG FEM model is stable in the sense

$$\mathcal{B}_{\mathrm{S}}(\mathsf{u},\mathsf{u}) \geq C\|\mathsf{u}\|_{\mathrm{SUPG}}^2, \tag{32}$$

where $\|\mathsf{u}\|_{\mathrm{SUPG}}^2 = \sigma\|\mathsf{u}\|_{L^2(\Omega)}^2 + \epsilon\|\nabla\mathsf{u}\|_{L^2(\Omega)}^2 + \tau\sum_{k=1}^{N_{\mathrm{el}}}\|\mathbf{b}\cdot\nabla\mathsf{u}\|_{L^2(\Omega_k)}^2$. We note that, in the limit that $\epsilon \to 0$, the stability statement (32) maintains control over the gradient of the state in the streamline direction. Thus, the SUPG method is *stable* and *robust* in the limit of $\epsilon \to 0$. As a result, we do not expect the accuracy of the method to deteriorate for small ϵ. We additionally note that $\|\mathsf{u}\|_{\mathrm{SUPG}} \geq \|\mathsf{u}\|_{\mathrm{G}}$, so that SUPG is more dissipative than Galerkin. The stability of the continuous SUPG ROM follows along the same lines as that for the continuous SUPG FEM model (see, e.g., [52, Lemma 3.3]).
- **Continuous $\mathrm{GLS}_{\mathrm{DS}}$ ROM.** Stability of GLS is given in Ref. [75] in the steady case. Coercivity is straightforward to demonstrate as GLS adds a symmetric non-negative term to the bilinear form. As $\mathrm{GLS}_{\mathrm{DS}}$ is equivalent to the steady case but with a modified source term, the analysis in Ref. [75] is directly applicable and results in the stability statement

$$\mathcal{B}_{\mathrm{S}}(\mathsf{u},\mathsf{u}) \geq C\|\mathsf{u}\|_{\mathrm{GLS}}^2, \tag{33}$$

where $\|\mathsf{u}\|_{\mathrm{GLS}}^2 = \sigma\|\mathsf{u}\|_{L^2(\Omega)}^2 + \epsilon\|\nabla\mathsf{u}\|_{L^2(\Omega)}^2 + \tau\sum_{k=1}^{N_{\mathrm{el}}}\|\mathbf{b}\cdot\nabla\mathsf{u} + \left(\sigma + \frac{1}{\Delta t}\right)\mathsf{u} - \epsilon\Delta\mathsf{u}\|_{L^2(\Omega_k)}^2$. We note that $\mathrm{GLS}_{\mathrm{DS}}$ is stable for non-negative values of τ. Like SUPG, the stability statement (33) maintains control over the gradient of the state in the streamwise direction in the limit $\epsilon \to 0$. Thus, GLS is *stable* and *robust* in the limit of $\epsilon \to 0$. We additionally note that $\|\mathsf{u}\|_{\mathrm{GLS}}^2$ depends on the time step Δt. For very small time steps, the stability statement (33) deteriorates. It is worth noting that some definitions of the τ scale with Δt. The stability statement (33) is still not robust in this setting as all stabilization terms drop other than the $u/\Delta t$ contribution, which provides no additional control over the gradient of the state. The stability of the continuous $\mathrm{GLS}_{\mathrm{DS}}$ ROM follows along the same lines as that for the continuous $\mathrm{GLS}_{\mathrm{DS}}$ FEM model.
- **Continuous $\mathrm{ADJ}_{\mathrm{DS}}$ ROM.** Coercivity of the ADJ FEM model has been demonstrated for the steady convection diffusion reaction equation [48]. As $\mathrm{ADJ}_{\mathrm{DS}}$ is equivalent to the steady case but with a modified forcing term, the stability statement presented in Ref. [48] applies. The stability statement is given as: for $0 \leq \tau \leq \tau^*_{\mathrm{ADJ}}$,

$$\mathcal{B}_{\mathrm{S}}(\mathsf{u},\mathsf{u}) \geq C\|\mathsf{u}\|_{\mathrm{ADJ}}^2, \tag{34}$$

where $\|\mathsf{u}\|_{\mathrm{ADJ}}^2 = \sum_{k=1}^{N_{\mathrm{el}}}\left(\left(\sigma + \frac{1}{\Delta t}\right)\alpha_k\|\mathsf{u}\|_{L^2(\Omega_k)}^2 + \epsilon\alpha_k\|\nabla\mathsf{u}\|_{L^2(\Omega_k)}^2 + \tau\|\mathbf{b}\cdot\nabla\mathsf{u}\|_{L^2(\Omega_k)}^2\right)$ with α_k being a constant that depends on the mesh, parameters, and inverse estimates. We again observe more robust behavior in the limit of $\epsilon \to 0$ as well as a dependence on the time step Δt. We again expect poor behavior in the limit of $\Delta t \to 0$ as coercivity is dominated by the $\frac{1}{\Delta t}$ term. We further note the $\mathrm{ADJ}_{\mathrm{DS}}$ ROM is subject to the same issues as the $\mathrm{GLS}_{\mathrm{DS}}$ ROM for the case where the stabilization constant scales with Δt. The stability of the continuous $\mathrm{ADJ}_{\mathrm{DS}}$ ROM follows along the same lines as that for the continuous $\mathrm{ADJ}_{\mathrm{DS}}$ FEM model.
- **Continuous $\mathrm{GLS}_{\mathrm{ST}}$ ROM.** Coercivity of the $\mathrm{GLS}_{\mathrm{ST}}$ FEM model was demonstrated in one of the original references on GLS [75] by virtue of the formulation adding a symmetric term. We note that, here, we include the $\left(\mathsf{u}^n - \mathsf{u}^{n-1}\right)/\Delta t$ term in the definition of our residual to retain consistency for the $p = 0$ DG trial space, and as a result the analysis in [75] does not directly extend to the current case.[10] We also note that the space–time formulation was advocated in the original reference [75].
- **Continuous $\mathrm{ADJ}_{\mathrm{ST}}$ ROM.** Coercivity of the $\mathrm{ADJ}_{\mathrm{ST}}$ FEM model applied to the unsteady convection–diffusion–reaction equation has not been demonstrated to the best of our knowledge.

[10] We found that this term makes little difference in practice.

6.2.2 Discrete ROMs

We now consider stability of the various discrete ROMs discussed above. For the following analysis, we introduce the following notation for a generic discrete ROM as

$$\mathbf{E}\frac{\hat{\mathbf{x}}^n - \hat{\mathbf{x}}^{n-1}}{\Delta t} + \mathbf{G}\hat{\mathbf{x}}^n = \mathbf{f}^n,$$

where $\mathbf{E} \in \mathbb{R}^{R\times R}$ is a "mass matrix" (e.g., $\mathbf{E} = \boldsymbol{\Psi}^T\mathbf{M}\boldsymbol{\Psi}$ for the discrete Galerkin ROM of the Galerkin FEM), $\mathbf{G} \in \mathbb{R}^{R\times R}$ is a "dynamics" matrix, $\mathbf{f}^n \in \mathbb{R}^R$ is a forcing vector, and $\hat{\mathbf{x}}^n \in \mathbb{R}^R$ are the reduced coordinates. We define a stable discrete ROM as one whose "mass" matrix $\mathbf{E}$ is symmetric positive definite and whose dynamics matrix $\mathbf{G}$ is positive definite, i.e.,

$$\mathbf{v}^T\mathbf{G}\mathbf{v} > 0, \quad \forall \mathbf{v} \in \mathbb{R}^R \setminus \{\mathbf{0}\}. \tag{35}$$

We emphasize that this is analogous to coercivity in finite dimensional spaces since (35) ensures positive definiteness in any weighted ℓ^2 norm.

To proceed, it is first helpful to note that the continuous Galerkin FEM model (7) results in the system

$$\mathbf{M}\frac{\mathbf{a}_{\mathrm{h}}^n - \mathbf{a}_{\mathrm{h}}^{n-1}}{\Delta t} + (\mathbf{A} + \epsilon\mathbf{D} + \sigma\mathbf{M})\mathbf{a}_{\mathrm{h}}^n = \mathbf{f},$$

where $\mathbf{A} = m\left(\mathsf{v}_i, \mathbf{b}\cdot\nabla\mathsf{v}_j\right)$ is the convection matrix, $\mathbf{D} = m\left(\nabla\mathsf{v}_i, \nabla\mathsf{v}_j\right)$ the symmetric positive definite diffusion matrix, and $\mathbf{M} = m\left(\mathsf{v}_i, \mathsf{v}_j\right)$ the symmetric positive definite mass matrix. We note that $\mathbf{v}^T\mathbf{A}\mathbf{v} = 0$, $\mathbf{v}^T\mathbf{D}\mathbf{v} > 0$, and $\mathbf{v}^T\mathbf{M}\mathbf{v} > 0\ \forall \mathbf{v} \in \mathbb{R}^N\backslash\{\mathbf{0}\}$. For notational simplicity, we define $\mathbf{B} = \mathbf{A} + \epsilon\mathbf{D} + \sigma\mathbf{M}$.

- **Discrete Galerkin ROM with $\mathbf{W} = \mathbf{I}$**. As the discrete Galerkin ROM of the continuous Galerkin FEM model with $\mathbf{W} = \mathbf{I}$ is equivalent to the continuous Galerkin ROM, stability is implied. It is further straightforward to show that $\mathbf{v}^T\mathbf{B}\mathbf{v} > 0\ \forall \mathbf{v} \in \mathbb{R}^N\backslash\{\mathbf{0}\}$ at the discrete level directly. The Galerkin discrete ROM constructed from the Galerkin continuous ROM results in the dynamics matrix

  $$\mathbf{G}_{\mathrm{G}} = \boldsymbol{\Psi}^T(\mathbf{A} + \epsilon\mathbf{D} + \sigma\mathbf{M})\boldsymbol{\Psi}.$$

  It is straightforward to see that

  $$\mathbf{v}^T\mathbf{G}_{\mathrm{G}}\mathbf{v} = \epsilon\|\mathbf{v}\|^2_{\mathbf{D}_r} + \sigma\|\mathbf{v}\|^2_{\mathbf{M}_r} > 0,$$

  where $\mathbf{D}_r = \boldsymbol{\Psi}^T\mathbf{D}\boldsymbol{\Psi}$. We note the above is simply the discrete equivalent to the inequality (31). We additionally note that $\epsilon\|\mathbf{v}\|^2_{\mathbf{D}_r} + \sigma\|\mathbf{v}\|^2_{\mathbf{M}_r}$ is the discrete statement of a weighted $\mathcal{H}^1(\Omega)$ norm that approaches a σ-weighted discrete $L^2(\Omega)$ norm as $\epsilon \to 0$.

  It is less straightforward to demonstrate that $\mathbf{G}$ is positive definite for the discrete Galerkin ROM constructed from a stabilized FEM model. However, as the discrete Galerkin ROM dynamics recover the continuous Galerkin ROM dynamics under the condition $\mathbf{W} \leftarrow \mathbf{I}$, these ROMs can be expected to obey the same stability properties as their continuous counterparts.
- **Discrete LSPG ROMs**. To the best of our knowledge, no result exists in the literature demonstrating stability of a discrete LSPG ROM constructed from a Galerkin FEM FOM in the sense of (35). Stability analyses for LSPG have been carried out in other contexts; for instance, Ref. [71] demonstrates that, for LTI systems, LSPG with orthonormal bases results in an asymptotically stable ROM if the underlying FOM is asymptotically stable.[11]

  In the present context, one can show that a discrete LSPG ROM of the continuous Galerkin FEM model constructed in the inner product $\mathbf{W} \leftarrow \mathbf{M}^{-1}$ results in a mass matrix $\mathbf{E} = \boldsymbol{\Psi}^T\mathbf{M}\boldsymbol{\Psi}$ and a dynamics matrix

  $$\mathbf{G}_{\mathrm{LSPG}} = \boldsymbol{\Psi}^T\left[\mathbf{B} + \mathbf{B}^T\right]\boldsymbol{\Psi} + \Delta t\boldsymbol{\Psi}^T\mathbf{B}^T\mathbf{M}^{-1}\mathbf{B}\boldsymbol{\Psi}.$$

  Since $\mathbf{E} = \boldsymbol{\Psi}^T\mathbf{M}\boldsymbol{\Psi}$ is symmetric positive definite, the inequality $\mathbf{v}^T\mathbf{B}\mathbf{v} > 0\ \forall \mathbf{v} \in \mathbb{R}^N\backslash\{\mathbf{0}\}$ holds for the continuous Galerkin FEM, and $\mathbf{v}^T\mathbf{B}^T\mathbf{M}^{-1}\mathbf{B}\mathbf{v}^T > 0\ \forall \mathbf{v} \in \mathbb{R}^N \setminus \{\mathbf{0}\}$ due to $\mathbf{B}^T\mathbf{M}^{-1}\mathbf{B}$ being symmetric positive definite, stability is implied.

  From our analysis of the LSPG ROM applied to the Galerkin FEM model, it is straightforward to see that if the FOM has a symmetric positive definite mass matrix and a positive definite dynamics matrix, then the resulting LSPG ROM constructed in the inner product $\mathbf{W} = \mathbf{M}^{-1}$ will be stable in the sense of (35).
- **APG ROMs**. The APG ROM is derived from a formulation of the Mori–Zwanzig formalism, and a stability analysis has been undertaken for a model displaying a structural equivalence to APG in Ref. [65]. This analysis demonstrates that the so-called t-model (which is equivalent to APG for τ set to t) will be be dissipative when applied to a system that is energy conserving; this result directly implies a positive definite dynamics matrix. However, no result exists in the literature demonstrating stability of the APG ROM for systems that dissipate energy.

6.3 Error Bounds

We now summarize existing numerical analyses that attempt to bound the ROM error for the CDR system. We note that *a priori* error bounds for POD-based methods are typically

[11] No mass matrix was considered; it is known that treatment of the mass matrix can impact the performance of ROMs [6].

limited to reproductive cases (unless some assumption is made on the solution manifold), while *a posteriori* error bounds are typically valid in both the reproductive and predictive regime.

6.3.1 Continuous ROMs

- **Continuous Galerkin ROMs.** As a continuous Galerkin ROM arises from the Galerkin approximation of the CDR equation in a POD (or reduced-basis method (RBM)) subspace, its *a priori* error bound can be derived by leveraging the FEM error analysis for parabolic PDEs [161] together with the approximability properties of the POD [95] or RBM [67, 126] space. For example, error bounds for the POD-Galerkin ROM constructed using continuous projection were derived for parabolic linear systems and certain nonlinear systems by Kunisch and Volkwein in Ref. [95]. In a follow-up paper, the authors derived error bounds for equations pertaining to fluid dynamics [96], e.g., the two-dimensional incompressible Navier–Stokes equations. New error bounds were proved by Singler [152], who derived exact expressions for the POD data approximation errors considering four different POD projections and two different Hilbert space error norms. Error bounds for the RBM-Galerkin ROM constructed using continuous projection were derived for parabolic problems in [56, 57, 64], the convergence of POD-Greedy algorithm was analyzed in [63], and sharper error bounds using space-time formulations were obtained in [164, 177]. We emphasize that these Galerkin ROM error bounds for parabolic PDEs grow with the inverse of the coercivity constant, which scales with ϵ for the CDR system. Hence, there is no guarantee that the continuous Galerkin ROMs will provide an approximation comparable to the best-fit approximation in the limit of $\epsilon \to 0$.

  It is worth noting that error bounds and convergence analyses exist for ROMs built using continuous Galerkin projection for PDEs other than the CDR equation, e.g., hyperbolic equations. In [87], for example, Kalashnikova and Barone derived *a priori* error estimates for an energy-stability-preserving ROM formulation developed in [14] for linearized compressible flow. These error bounds were derived by adapting techniques traditionally used in the numerical analysis of spectral approximations to PDEs [51] and employed a carefully constructed stable penalty-like implementation of the relevant boundary conditions in the ROM.
- **Continuous SUPG ROMs.** Error analysis of the SUPG ROM was undertaken recently in Ref. [82], where it was demonstrated that the SUPG ROM could be equipped with robust error estimates that do not deteriorate as $\epsilon \to 0$. These estimates bound the error between the SUPG ROM solution and a corresponding SUPG FEM solution. To obtain Δt-independent error bounds, the authors employed POD snapshots that included the time-difference quotients [92, 95]; without these coefficients the resulting error bounds depend on Δt. In numerical experiments, however, it was observed that including the time-difference quotients did not lead to improved results, and thus the authors believe an important open question is the derivation of Δt-independent bounds for the case where the time-difference quotients are not included in the bases. Lastly, we note that Ref. [82] supports previous analysis of the SUPG ROM in [52].
- **Other stabilized ROMs.** To the best of our knowledge, no error analysis exists for the other stabilized ROMs considered here. We do note that error analyses have been done for the corresponding FEM formulations. We also note that error analysis exists for stabilized ROMs that are not residual-based, such as those outlined in Appendix 1 (see, e.g., Refs. [8, 21, 46, 78, 79, 129, 134, 141, 176]).

6.3.2 Discrete ROMs

- **Discrete Galerkin ROM**. Due to the equivalence between a discrete Galerkin ROM and its continuous counterpart, the error bounds derived for the continuous Galerkin ROM are applicable to the discrete Galerkin ROM constructed on top of their corresponding continuous FEM system. Various authors have derived error bounds for the discrete Galerkin ROM in a more generic context. In Ref. [128], error bounds are derived for the discrete Galerkin ROM within the context of a linear and nonlinear dynamical system $\dot{\boldsymbol{x}} = \boldsymbol{f}(\boldsymbol{x})$. Analogously, Ref. [29] derives error bounds for the discrete Galerkin ROM for OΔEs arriving from linear multistep and Runge–Kutta time discretizations of $\dot{\boldsymbol{x}} = \boldsymbol{f}(\boldsymbol{x})$. In the general nonlinear case, these error bounds depend on difficult-to-compute Lipschitz constants, grow exponentially in time, and lack sharpness. No error analysis of the discrete Galerkin ROM specialized to the CDR system exists to the best of our knowledge.
- **LSPG ROMs**. *A priori* and *a posteriori* upper error bounds for LSPG ROMs applied to generic time-discrete nonlinear dynamical systems are derived in Ref. [29]. These error bounds rely on the assumption of Lipschitz continuity of the nonlinear right-hand side velocity operator, which can be related to coercivity in the linear setting. The bounds demonstrate that the upper error bound of the LSPG ROM grows exponentially with the number of time steps, and that this upper error bound can be bounded by the maximum residual over a given time step. Further, [29] shows that LSPG can be equipped with an *a posteriori* upper error bound lower than the Galerkin

Table 1 Summary of continuous ROMs investigated

	Gal.	SUPG	GLS_{DS}	ADJ_{DS}	GLS_{ST}	ADJ_{ST}
ROM OΔE	Eq. (20)	Eq. (22)	Eq. (22)	Eq. (22)	Eq. (22)	Eq. (22)
Conditions	N/A	$\mathcal{Q} = \mathcal{Q}_{\text{DS-SUPG}}$	$\mathcal{Q} = \mathcal{Q}_{\text{DS-GLS}}$	$\mathcal{Q} = \mathcal{Q}_{\text{DS-ADJ}}$	$\mathcal{Q} = \mathcal{Q}_{\text{ST-GLS}}$	$\mathcal{Q} = \mathcal{Q}_{\text{ST-ADJ}}$

Table 2 Summary of LSPG ROMs investigated

	G–LSPG	SUPG–LSPG	GLS_{DS}–LSPG	ADJ_{DS}–LSPG	GLS_{ST}–LSPG	ADJ_{ST}–LSPG
ROM OΔE	Eq. (25)	Eq. (25)	Eq. (25)	Eq. (25)	Eq. (25)	Eq. (25)
FOM OΔE	Eq. (7)	Eq. (15)	Eq. (15)	Eq. (15)	Eq. (15)	Eq. (15)
Conditions	N/A	$\mathcal{Q} = \mathcal{Q}_{\text{DS-SUPG}}$	$\mathcal{Q} = \mathcal{Q}_{\text{DS-GLS}}$	$\mathcal{Q} = \mathcal{Q}_{\text{DS-ADJ}}$	$\mathcal{Q} = \mathcal{Q}_{\text{ST-GLS}}$	$\mathcal{Q} = \mathcal{Q}_{\text{ST-ADJ}}$
Inner product	$\mathbf{W} = \mathbf{M}^{-1}$	$\mathbf{W} = \mathbf{M}^{-1}$	$\mathbf{W} = \mathbf{M}^{-1}$	$\mathbf{W} = \mathbf{M}^{-1}$	$\mathbf{W} = \mathbf{M}^{-1}$	$\mathbf{W} = \mathbf{M}^{-1}$

ROM. The bounds presented in Ref. [29] are derived for the case where there is no mass matrix, and sharpness of the bounds is not addressed (thus, LSPG having a lower "upper bound" than Galerkin is not a robust statement of accuracy). Again, no error analysis of LSPG ROMs specialized to the CDR system exists to the best of our knowledge.

- **APG ROMs**. Ref. [121] derives *a priori* error bounds for the APG ROM for nonlinear dynamical systems and linear time-invariant dynamical systems. In the linear case, it is shown that, for sufficiently small τ, the upper bound on the error in the APG ROM is lower than in the Galerkin ROM. Similar to LSPG, however, the bounds are presented for the case where there is no mass matrix and sharpness is additionally not addressed (again, APG having a lower "upper bound" than Galerkin is not a robust statement of accuracy). Once again, no error analysis of APG ROMs specialized to the CDR system exists to the best of our knowledge.

6.4 Selection and Scaling of the Stabilization Parameter, τ

Lastly, we comment on analyses for selecting the ROM stabilization parameter. In standard FEM, numerical analysis arguments are generally used to determine the scaling of the stabilization parameter, τ, in residual-based stabilizations (see, e.g., the survey in [135]). The general approach used to determine the τ scaling is to (i) prove error bounds for the stabilized method, and (ii) choose a τ scaling with respect to the discretization parameters (e.g., the mesh size h and the time step Δt) that ensures an optimal error bound.

For residual-based ROM stabilizations, one heuristic approach for choosing the stabilization parameter, τ, is to use the same value as that used in the standard FEM (see, e.g., equation (13) in [118], equation (20) in [94], and equation (10) in [111]). We note that this approach is purely heuristic and does not use the numerical analysis arguments generally employed for standard FEM residual-based stabilized methods [135].

Table 3 Summary of APG ROMs investigated

	G–APG	SUPG–APG	GLS_{ST}–APG	ADJ_{ST}–APG
ROM OΔE	Eq. (27)	Eq. (28)	Eq. (28)	Eq. (28)
FOM OΔE	Eq. (7)	Eq. (15)	Eq. (15)	Eq. (15)
Conditions	N/A	$\mathcal{Q} = \mathcal{Q}_{\text{DS-SUPG}}$	$\mathcal{Q} = \mathcal{Q}_{\text{ST-GLS}}$	$\mathcal{Q} = \mathcal{Q}_{\text{ST-ADJ}}$
Inner product	$\mathbf{W} = \mathbf{I}$	$\mathbf{W} = \mathbf{I}$	$\mathbf{W} = \mathbf{I}$	$\mathbf{W} = \mathbf{I}$

A fundamentally different approach, which utilizes numerical analysis arguments to determine the τ scaling, was proposed in [52] for the SUPG-ROM. As explained in Section 3.5.1 in [52] (see also Sect. 4.3 of the present paper), since the ROM space is a subspace of the FEM space, two types of inverse estimates can be used to prove optimal error estimates for the SUPG-ROM: (i) a FEM inverse estimate, which yields the standard FEM scaling in which τ depends on the FEM mesh size, and (ii) a ROM inverse estimate [95], which yields a new ROM scaling in which τ depends on the ROM parameters (e.g., the ROM dimension, the POD basis functions, and the corresponding eigenvalues). The preliminary numerical investigation in [52] suggests that the FEM τ scaling yields more accurate results for large R values, but the ROM τ scaling is competitive for low R values. Further theoretical and numerical investigation is needed in order to determine optimal τ scalings for residual-based stabilized ROMs.

7 Numerical Experiments

7.1 Overview

We now present several studies to numerically assess the various ROM formulations for the CDR equation (1). We first provide specifics on the setup of the numerical experiments.

7.1.1 Investigated ROMs and Implementation Details

Table 1 details the continuous ROMs we investigate, while Tables 2 and 3 detail the LSPG and APG ROMs investigated. For continuous ROMs, we investigate the Galerkin, SUPG, ADJ, and GLS ROMs, as detailed in Sect. 4.2. For ADJ and GLS, we investigate formulations developed both through the "discretize-then-stabilize" approach (DS) and the "space–time" approach (ST), as discussed in Sect. 3.2. For discrete ROMs, we examine (1) LSPG ROMs based on the Galerkin FEM, SUPG FEM, ADJ_{DS} FEM, ADJ_{ST} FEM, GLS_{DS} FEM, and GLS_{ST} FEM, and (2) APG ROMs based on the Galerkin FEM, SUPG FEM, GLS_{ST} FEM, and ADJ_{ST} FEM. In what follows, we will abbreviate these discrete ROM formulations as "FEM type–discrete ROM type", e.g., "SUPG–LSPG" denotes an LSPG ROM of the SUPG FEM. All in all, we consider 16 ROM formulations. All ROMs employ the implicit Euler method for temporal discretization. The numerical experiments are carried out in the `FEniCS` package [5, 104–106]. *We emphasize that stabilization is carried out both at the FEM level and the ROM level*; this will be detailed in subsequent sections. Lastly, we additionally note that all experiments will focus only on reproductive ROMs.

7.1.2 Metrics

We use as metrics the (discrete) time-integrated relative $L^2(\Omega)$ error and the (discrete) time-integrated relative $\mathcal{H}^1(\Omega)$ error between the ROM solution and best-fit solution (i.e., the error between the ROM solution and the FOM solution projected onto the trial space). The time-integrated $L^2(\Omega)$ relative error is defined as

$$\overline{e}_{L^2}(\mathcal{V}) = \frac{\sum_{n=1}^{N_t} \|\mathsf{u}_{\text{r}}^n - \mathbb{P}_{L^2}(\mathcal{V})\mathsf{u}_*^n\|_{L^2(\Omega)}^2}{\sum_{n=1}^{N_t} \|\mathbb{P}_{L^2}(\mathcal{V})\mathsf{u}_*^n\|_{L^2(\Omega)}^2}, \tag{36}$$

where $\mathbb{P}_{L^2}(\mathcal{V})$ is the orthogonal $L^2(\Omega)$ projector onto $\mathcal{V}$. For ROMs, we measure the $\overline{e}_{L^2}\left(\mathcal{V}_{\text{r}}\right)$ error, which measures the error between the ROM solution and the FOM solution projected onto the ROM trial space. For FEM solutions, we similarly measure the $\overline{e}_{L^2}\left(\mathcal{V}_{\text{h}}\right)$ error. Analogously, the relative $\mathcal{H}^1(\Omega)$ error is defined as

$$\overline{e}_{\mathcal{H}^1}(\mathcal{V}) = \frac{\sum_{n=1}^{N_t} |\mathsf{u}_{\text{r}}^n - \mathbb{P}_{\mathcal{H}^1}(\mathcal{V})\mathsf{u}_*^n|_{\mathcal{H}^1(\Omega)}^2}{\sum_{n=1}^{N_t} |\mathbb{P}_{\mathcal{H}^1}(\mathcal{V})\mathsf{u}_*^n|_{\mathcal{H}^1(\Omega)}^2}, \tag{37}$$

where $|\cdot|_{\mathcal{H}^1(\Omega)}$ is the $\mathcal{H}^1(\Omega)$ semi-norm and $\mathbb{P}_{\mathcal{H}^1}(\mathcal{V})$ is the orthogonal projector onto $\mathcal{V}$ in the $\mathcal{H}^1(\Omega)$ semi-norm. We note that, in our studies, we execute the ROMs for varying time step sizes,[12] and as a result the ROM is executed on a different time grid than the high resolution FOM solution. We design our studies such that the ratio of the ROM time step to the high resolution time step is always a positive integer. The summations in Eqs. (36) and (37) are then performed on the coarser ROM time grid.

[12] This is done because the time step size impacts the stabilization.

7.1.3 Construction of ROM Trial Space

To construct the ROM basis functions, we use the following two criteria:

1. We consider a *realistic* setting for convection-dominated problems. To this end, we use an *under-resolved* FOM trial space, just as in the numerical simulation of realistic, convection-dominated (e.g., turbulent) flows.
2. We ensure *fairness* of the numerical comparison. Specifically, we require all the stabilized ROMs use the same ROM basis, which is generated without using stabilization.

To satisfy the first criterion (i.e., a realistic, under-resolved regime), we examine cases where the underlying FEM requires stabilization (this is the relevant case for real-world applications), and, as such, examine the scenario where the FEM trial space is under-resolved such that our FEM requires stabilization to be accurate. The natural approach to generate the ROM trial space in this setting is to (i) solve a FOM, which comprises a stabilized FEM model, and (ii) leverage the solution data to construct the ROM trial space. The ROM is then executed with the same stabilized form used to generate the snapshots; this is the so-called "offline–online stabilization strategy" outlined in Ref. [4] (see also [158]), which comprises a form of model consistency. This procedure, unfortunately, makes it difficult to ensure a fair comparison of the performance of different ROM stabilization techniques (i.e., to satisfy the second criterion listed above). For example, if we generated the FOM solution with SUPG, then comparing SUPG ROM solutions to LSPG ROM solutions becomes unfair. As a result, we are not using this approach to construct the ROM basis for the stabilized ROMs used in our numerical investigation.

To circumvent this issue, we generate the ROM trial spaces by projecting "truth data" onto a FOM trial space. As the problems we analyze in this section do not have analytical solutions, we generate the truth data via a high fidelity Galerkin FEM model that uses a high resolution trial space $[\mathcal{V}_{\text{h}}]_{\text{h-res}}$. We generate ROM bases by projecting this truth data onto the (lower-dimensional) FOM trial space $[\mathcal{V}_{\text{h}}]_{\text{fom}}$ in the $L^2(\Omega)$ sense and, e.g., performing an SVD. We emphasize that the high-fidelity Galerkin FEM model and the high resolution FEM trial space are used only for generating reference solutions and snapshots. At a high level, one may

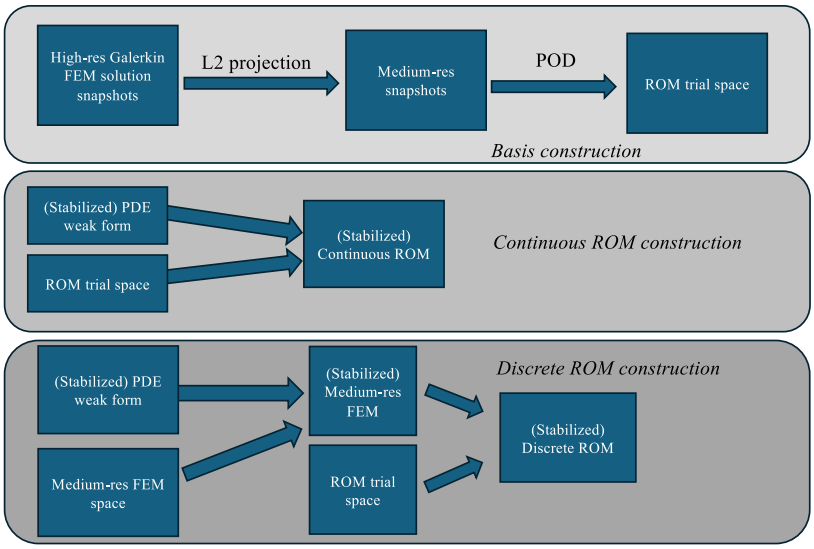

Fig. 3 Schematic depicting workflow for basis and ROM construction

think of this approach of constructing the ROM basis as the setting where the truth data comes from experimental measurements. We also note that a consequence of this approach is that none of our ROMs will be consistent with the high fidelity Galerkin FEM model that generated the truth data, meaning that adding ROM basis vectors will not necessarily result in a more accurate solution.

We emphasize that our strategy of generating the ROM basis, which is outlined in Algorithm 1 and depicted in Fig. 3, satisfies both criteria outlined at the beginning of this section. Specifically, the first criterion is satisfied since the snapshots are obtained from a realistic, under-resolved representation of the truth, i.e., a high-resolution solution that is projected onto an under-resolved FOM trial space. The second criterion is satisfied since all the stabilized ROMs use the same ROM basis. Furthermore, no stabilization method is used to generate snapshots used for basis construction, and, thus, none of the stabilized ROMs can claim an unfair advantage over the others. Thus, our strategy of generating the ROM basis ensures both a *realistic* and *fair* comparison of the stabilized ROMs.

7.1.4 Selection of Stabilization Parameters and Time Step

In addition to depending on the choice of inner product, all stabilized methods considered depend on the stabilization parameter τ, the time step Δt, or both. As discussed earlier, the *a priori* selection of τ is an area that is receiving attention in both the FEM and ROM communities [52, 70], and is still an outstanding issue for ROMs in particular. Further, while Δt is a discretization parameter, it impacts certain types of stabilization schemes because it shows up in the stabilization operator. Here we perform a grid sweep to explore this sensitivity. The grid sweep is obtained by executing ROM solves for $(\tau, \Delta t) \in \boldsymbol{\tau} \times \boldsymbol{\Delta t}$, where

$$\begin{aligned}\tau = \Delta t = \{&10^{-4},\ 2.5\times10^{-4},\ 5\times10^{-4},\ 10^{-3},\ 2\times10^{-3},\ 3\times10^{-3},\\ &4\times10^{-3},\ 5\times10^{-3},\ 6\times10^{-3},\ 7\times10^{-3},\ 8\times10^{-3},\\ &9\times10^{-3},\ 10^{-2},\ 1.5\times10^{-2},\ 2\times10^{-2},\ 2.5\times10^{-2},\\ &3\times10^{-2},\ 4\times10^{-2},\ 5\times10^{-2}, 6\times10^{-2}, 8\times10^{-2}, 10^{-1},\\ &2\times10^{-1}, \times10^{-1}, 4\times10^{-1}, 5\times10^{-1}\end{aligned}$$

Algorithm 1 Algorithm for generating high fidelity solutions and the ROM trial space

Input: Energy cutoff criterion, ϵ_{c}
Output: ROM bases, $\boldsymbol{\Psi}$
Steps:

1. Solve the Galerkin OΔE (7) with $\mathcal{V}_{\mathrm{h}} \leftarrow [\mathcal{V}_{\mathrm{h}}]_{\mathrm{h-res}}$ for $n = 1, \ldots, N_t$ to generate solutions $[\mathsf{u}_{\mathrm{h}}^n]_{\mathrm{h-res}}$, $n = 1, \ldots, N_t$.
2. Perform the restriction $[\mathsf{u}_{\mathrm{h}}]_{\mathrm{fom}}^n = \mathbb{P}_{L^2}([\mathcal{V}_{\mathrm{h}}]_{\mathrm{fom}})[\mathsf{u}_{\mathrm{h}}]_{\mathrm{h-res}}^n$, $n = 1, \ldots, N_t$.
3. Collect the FEM coefficients $[\mathbf{a}_{\mathrm{h}}]_{\mathrm{fom}}^n$ associated with $[\mathsf{u}_{\mathrm{h}}^n]_{\mathrm{FOM}}$, $n = 0, \ldots, N_t$ into the snapshot matrix
$$\mathbf{S}_{\mathbf{a}_{\mathrm{h}}} = \begin{bmatrix}[\mathbf{a}_{\mathrm{h}}]_{\mathrm{fom}}^1 & \cdots & [\mathbf{a}_{\mathrm{h}}]_{\mathrm{fom}}^{N_t}\end{bmatrix}.$$
4. Execute Algorithm 2 with inputs $\mathbf{S}_{\mathbf{a}_{\mathrm{h}}}$, ϵ_{c}, $\mathbf{P} = \mathbf{M}$ to obtain the ROM basis $\boldsymbol{\Psi}$ and trial space $\mathcal{V}_{\mathrm{r}} = \mathrm{Range}(\boldsymbol{\Psi})$.

. We note that the SUPG–APG, GLS_{ST}–APG, and ADJ_{ST} –APG ROMs depend upon both the APG stabilization parameter and the FEM stabilization parameter. As will be seen, these methods are well-behaved in the low time-step limit and as such we execute these methods for $\tau_{\text{APG}}, \tau \in \boldsymbol{\tau} \times \boldsymbol{\tau}$ with a fixed time step $\Delta t = 10^{-3}$ equal to the FOM time step. As will be detailed in the following section, we note that all ROMs and FOMs will be performed on the same spatial grid.

7.2 Example 1: Boundary Layer

The first numerical experiment we consider is a transient version of the setup used by Codina in [39]. We solve Eq. (1) with a final time $T = 5$ and a physical domain $x \in \Omega = (0,1) \times (0,1)$. We take the parameters to be a slightly modified version of those used in by Codina in [39], where we set $\epsilon = 10^{-3}$, $f = 1$, $\sigma = 1$, and $\mathbf{b} = \frac{1}{2}\left[\cos(\pi/3)\ \sin(\pi/3)\right]^T$. The high-resolution trial space $[\mathcal{V}_{\text{h}}]_{\text{h-res}}$ is obtained via a uniform triangulation of Ω into $N_{\text{el}} = 2 \times 128^2$ elements equipped with a $\mathcal{C}^0(\Omega)$ continuous discretization with polynomials of order $p = 2$. The grid Peclet number is $\text{Pe}_{\text{h}} = 1.953125$, where we used $h = (128p)^{-1}$. Analogously, the FOM trial space $[\mathcal{V}_{\text{h}}]_{\text{fom}}$ is obtained via a uniform triangulation of Ω based on 32 nodes in each direction into $N_{\text{el}} = 2048$ elements equipped with a $\mathcal{C}^0(\Omega)$ continuous discretization with polynomials of order $p = 2$. The grid Peclet number is $\text{Pe}_{\text{h}} = 7.8125$, where we used $h = (32p)^{-1}$. In both cases, the triangulations are obtained via a partition of Ω into uniform square cells. The triangles are then cut from bottom-left to top-right of each cell. The Galerkin method equipped with the high-resolution trial space is mesh-converged and accurate. The Galerkin method equipped with the FOM trial space yields inaccurate solutions; this error will be quantified later in this section and we consider this case as this is representative of practical problems. Lastly, the ROM trial space is obtained by executing Algorithm 1. Figure 4 presents the residual statistical energy as a function of basis dimension, where it is seen that the first five basis vectors capture over 99.999% of the statistical energy (in $L^2(\Omega)$).

7.2.1 Coarse-Grid FEM Results

We first present results of the various FEMs considered and re-emphasize that (1) these FEMs are executed on a coarse trial space such that the they require stabilization to be accurate and (2) the data from these FEMs are *not* used to construct the ROM trial subspace; instead, we employ high-fidelity data as described in Sect. 7.1.3. We present the FEM solutions to quantify the underlying FEM error of a given method on this coarse mesh. We re-emphasize that we examine the case where the FEM requires stabilization as this is representative of practical problems. Figure 5 presents the various FEM solutions at the final time, $t = 5$, while Table 4 tabulates the solution errors and stabilization parameters employed in the simulations; these parameters were selected by executing the FEMs on the $\boldsymbol{\tau} \times \boldsymbol{\Delta t}$ grid described above and extracting solutions with the lowest $L^2(\Omega)$ error. The errors reported in Table 4 measure the (time integrated) difference between the FEM solutions and the "truth" solution projected onto the FEM trial space, as described in Sect. 7.1.2. We observe the following:

- The Galerkin, GLS_{DS}, and ADJ_{DS} FEMs are the worst performing methods, and all result in solutions with large oscillations at the boundary.
- The SUPG, GLS_{ST}, and ADJ_{ST} FEM provide the best solutions. These methods result in solution errors that are approximately an order of magnitude better than the Galerkin FEM and provide qualitatively accurate solutions.
- The "space–time" GLS_{ST} and ADJ_{ST} FEMs perform much better than the "discretize-then-stabilize" GLS_{DS} and ADJ_{DS} FEMs.

7.2.2 Reduced-Order Model Results as a Function of Basis Dimension

We next examine the performance of the various ROMs as the dimension of the ROM basis is varied for $1 \leq R \leq 20$. For each basis dimension, we present results for optimal $(\tau, \Delta t)$ as measured by the $L^2(\Omega)$ error. Figure 6 shows the convergence of the $L^2(\Omega)$-error and $\mathcal{H}^1(\Omega)$-error as a function of RB size, while Fig. 7 shows the corresponding optimal stabilization parameters and time steps. We emphasize that the measured error is defined as the discretely time-integrated

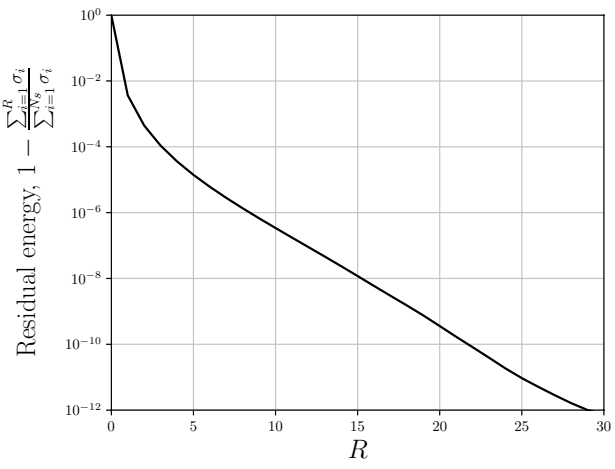

Fig. 4 Example 1, boundary layer. Residual statistical energy as a function of basis dimension

error between the ROM solution and the FOM solution projected onto the ROM trial space, as described in Sect. 7.1.2. We make the following observations about the *accuracy* of the various ROMs.

- No method results in a monotonic decrease in error in both the $L^2(\Omega)$ and $\mathcal{H}^1(\Omega)$ norms. This is, in part, a result of the fact that the ROMs are not consistent with the high resolution reference solution (see the discussion in Sect. 7.1.3).
- The Galerkin ROM performs poorly for all basis dimensions.
- SUPG–APG, ADJ_{ST}–APG, GLS_{ST}, and SUPG–LSPG are the best performing ROMs.
- GLS_{ST} and ADJ_{ST} are consistently more accurate than SUPG.
- The "discretize-then-stabilize" ROMs outperform the Galerkin ROM, but are consistently worse than their space–time counterparts.
- LSPG ROMs outperform their continuous counterparts in all cases.
- APG ROMs outperform their continuous counterparts in all cases except for GLS_{ST}–APG.
- It is interesting to note that the G–APG and G–LSPG ROMs perform significantly better than the standard Galerkin ROM for large number of bases, even though these two methods formally converge to the Galerkin ROM in the limit of a full basis.
- While not always the case, a decrease in error in the $L^2(\Omega)$ norm, in general, corresponds to a decrease in error in the $\mathcal{H}^1(\Omega)$ semi-norm.
- Comparing Fig. 6 to Table 4, it is interesting to observe that, while the same trends are observed, some ROMs are more accurate than their corresponding FEM models. This is again likely a result of the inconsistency between the ROMs and the high-resolution reference solution.

Examining Fig. 7, we make the following observations about the behavior of the stabilization parameters of the various ROMs.

- The optimal stabilization parameters for the SUPG, ADJ_{ST}, GLS_{ST}, and APG ROMs are more or less constant for all reduced basis dimensions (with the exception of a few APG solutions at very small basis dimensions).
- The GLS_{DS}, ADJ_{DS}, and LSPG-based ROMs are optimal for time step sizes larger than the FOM. In particular, the optimal time step for almost all LSPG ROMs occurs at an intermediate time step. This is well documented in the literature [29].
- It is difficult to decipher any pattern in the optimal stabilization parameters for the LSPG-based ROMs. We expect that this is, in part, due to the complex interplay between the dependence of the time-step and stabilization parameters on the LSPG ROM performance.

Next, Fig. 8 presents solution profiles for the various ROMs at a reduced basis dimension of $R = 5$, which corresponds to an energy criterion of $\epsilon_{\text{c}} = 0.99999$, and at optimal values of τ and Δt (and τ_{APG}) for APG ROMs) for the final time instance, $t = 5$. We observe that the projected truth solution displays a small oscillation at the boundary. This oscillation is a result of the FOM trial space $[\mathcal{V}_{\text{h}}]_{\text{fom}}$ being unable to fully resolve the boundary layer. Next, we see that the Galerkin ROM results in inaccurate solutions with large-scale oscillations. All stabilized ROMs are qualitatively accurate with minimal variation between their solutions.

7.2.3 Sensitivity to Time Step and Stabilization Parameters

The performance of the stabilized methods can depend on both the stabilization parameter τ and the time step Δt (and, for APG, the APG stabilization parameter τ_{APG}). To quantify this sensitivity, Fig. 9 presents results for the continuous and LSPG ROM solutions obtained on the parameter grid $(\tau, \Delta t) \in \boldsymbol{\tau} \times \boldsymbol{\Delta t}$. Figure 10 presents results for the G–APG ROM solution obtained on the parameter grid $(\tau_{\text{APG}}, \Delta t) \in \boldsymbol{\tau} \times \boldsymbol{\Delta t}$ and the remaining APG ROM solutions (which depend on three parameters, Δt, τ, and τ_{APG}) obtained on the parameter grid $(\tau, \tau_{\text{APG}}) \in \boldsymbol{\tau} \times \boldsymbol{\tau}$ with a fixed time step $\Delta t = 10^{-3}$. All ROM results are shown for a reduced basis dimension $R = 5$. As a reference, Fig. 11 shows the same results, but for full-order finite element simulations executed on the FOM trial space. We observe the following.

- In the limit that $\tau \to 0$ (or $\Delta t \to 0$ for LSPG), all ROMs converge to the standard G-ROM with the exception of ADJ_{DS}. This ROM displays poor behavior in the low time-step limit when $\tau \approx \Delta t$.
- The SUPG (Fig. 9b), GLS_{ST} (Fig. 9e), ADJ_{ST} (Fig. 9f), and G–APG (Fig. 10a) ROMs again all display a similar dependence on the time step and stabilization parameter. Optimal results are obtained for an intermediate value of τ, and the solutions all converge in the limit of $\Delta t \to 0$.
- All LSPG ROMs (Fig. 9g-9f) yield optimal results at an intermediate time step, and are thus not robust in the low time-step limit [29].
- Errors in the GLS_{DS}(Fig. 9c) and ADJ_{DS} (Fig. 9d) ROMs start to increase once the time step becomes small enough, and thus these ROMs are not robust in the low time-step limit.
- The Galerkin (Fig. 9a), SUPG (Fig. 9b), GLS_{ST}(Fig. 9e), and ADJ_{ST} (Fig. 9f) ROMs display a similar dependence to the stabilization parameter and time step as their cor-

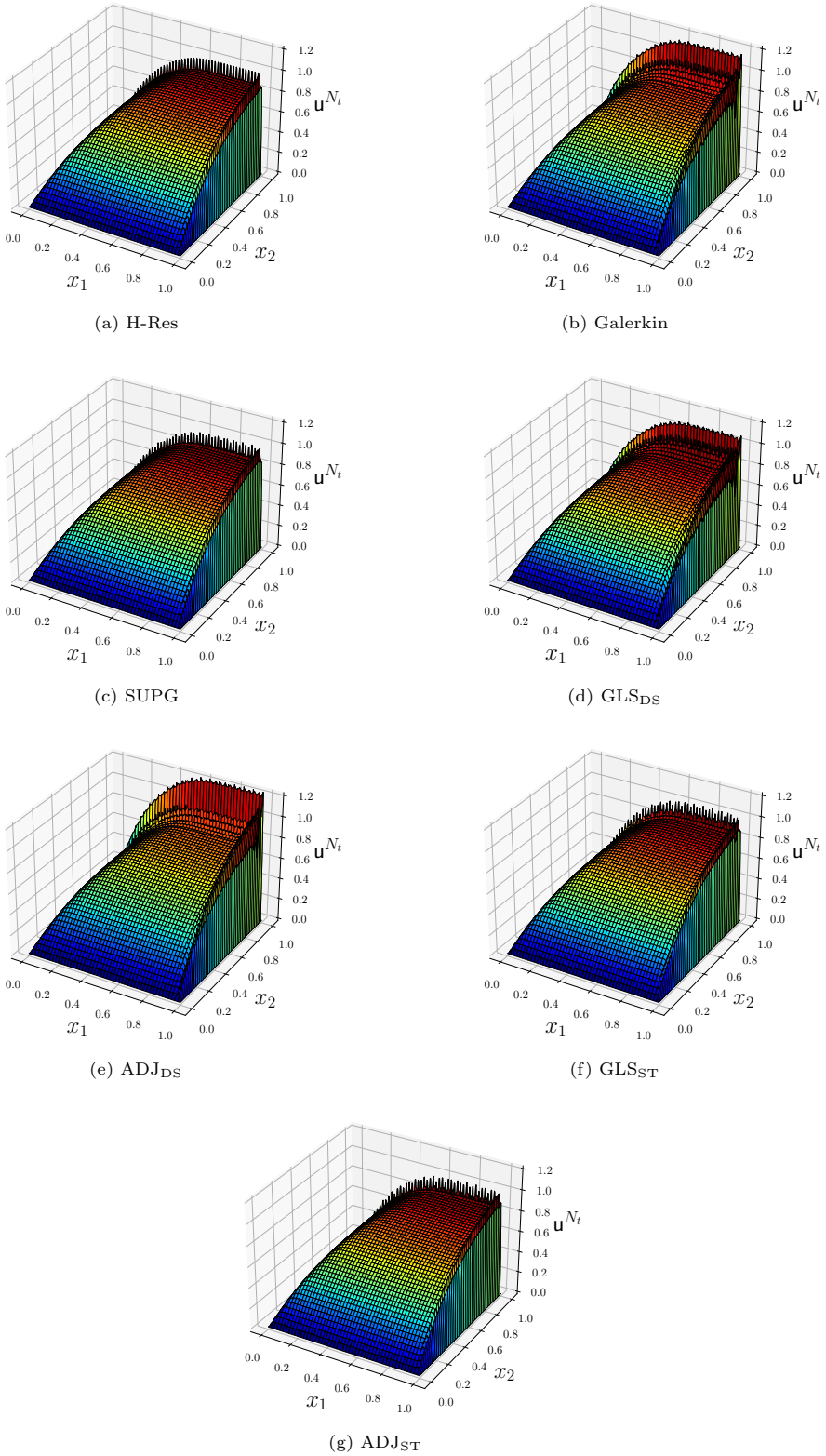

(a) H-Res (b) Galerkin

(c) SUPG (d) $\mathrm{GLS}_{\mathrm{DS}}$

(e) $\mathrm{ADJ}_{\mathrm{DS}}$ (f) $\mathrm{GLS}_{\mathrm{ST}}$

(g) $\mathrm{ADJ}_{\mathrm{ST}}$

Fig. 5 Example 1, boundary layer. FEM solutions to the CDR equation at $t = 5$. Note that Fig. 5a shows the high-resolution FEM solution projected onto the medium resolution FOM trial space

responding FOMs (Fig. 11a–9f). The behaviors of the $\mathrm{GLS}_{\mathrm{DS}}$ and $\mathrm{ADJ}_{\mathrm{DS}}$ ROMs display some qualitative similarities with their corresponding FEM solutions, but in general are different.

- For APG ROMs built on top of a stabilized FEM model (Figs. 10b-10d), optimal results are obtained for either an intermediate value of τ_{APG} and low value of τ, or vice versa. It is interesting to note that the solutions are almost

Table 4 Example 1, boundary layer. Time integrated (relative) $L^2(\Omega)$ and $\mathcal{H}^1(\Omega)$ errors of various FEMs presented in Fig. 5, along with the stabilization parameters at which the FEMs were executed

	Galerkin	SUPG	GLSDS	ADJDS	GLSST	ADJST
$\overline{e}_{L^2}([\mathcal{V}_h]_{\text{fom}})$	1.83×10^{-3}	2.11×10^{-4}	1.69×10^{-3}	2.09×10^{-3}	4.34×10^{-4}	2.38×10^{-4}
$\overline{e}_{\mathcal{H}^1}([\mathcal{V}_h]_{\text{fom}})$	1.56×10^{-3}	1.62×10^{-4}	1.48×10^{-3}	1.61×10^{-3}	3.52×10^{-4}	2.04×10^{-4}
τ	N/A	1.00×10^{-2}	1.00×10^{-4}	1.00×10^{-4}	1.00×10^{-2}	1.00×10^{-2}
Δt	1.00×10^{-3}	1.00×10^{-3}	1.00×10^{-3}	1.00×10^{-3}	1.00×10^{-3}	1.00×10^{-3}

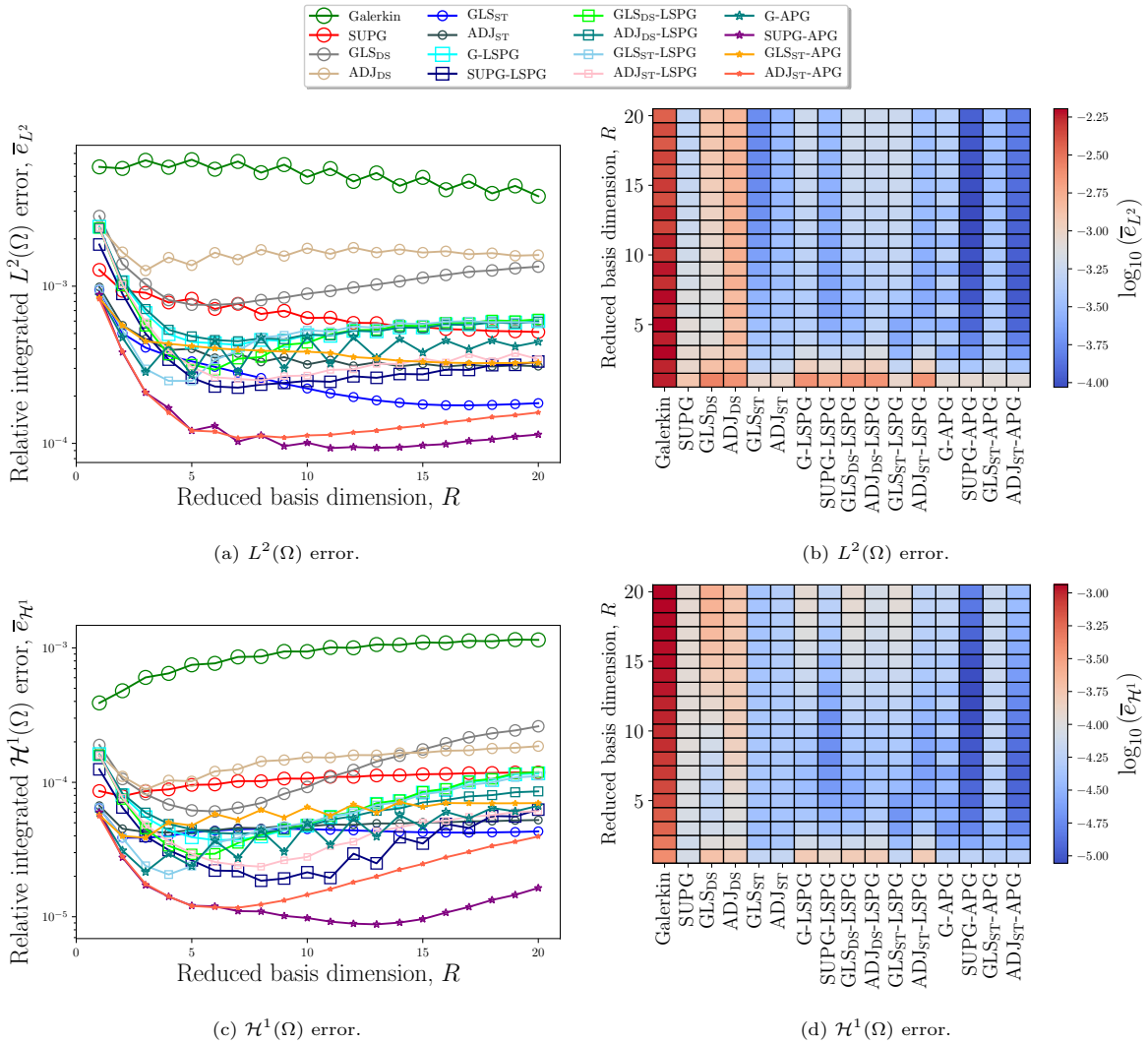

(a) $L^2(\Omega)$ error.

(b) $L^2(\Omega)$ error.

(c) $\mathcal{H}^1(\Omega)$ error.

(d) $\mathcal{H}^1(\Omega)$ error.

Fig. 6 Example 1, boundary layer. $L^2(\Omega)$ (top) and $\mathcal{H}^1(\Omega)$ (bottom) error as a function of ROM basis dimension for the various ROMs evaluated. We note that the left and right figures show the same quantities, but with different visualization techniques. Results are shown for optimal values of t, τ, as discussed in Sect. 7.1.4

symmetric with respect to these two parameters. In addition, we see regions of instability for high values of τ_{APG}.

7.3 Example 2: Advecting Front

The second numerical experiment we consider examines the CDR equation in a setting that yields an advecting front. ROMs of this problem require more basis vectors to accurately characterize the system and it is easier to examine the regime where the ROM itself is under-resolved.

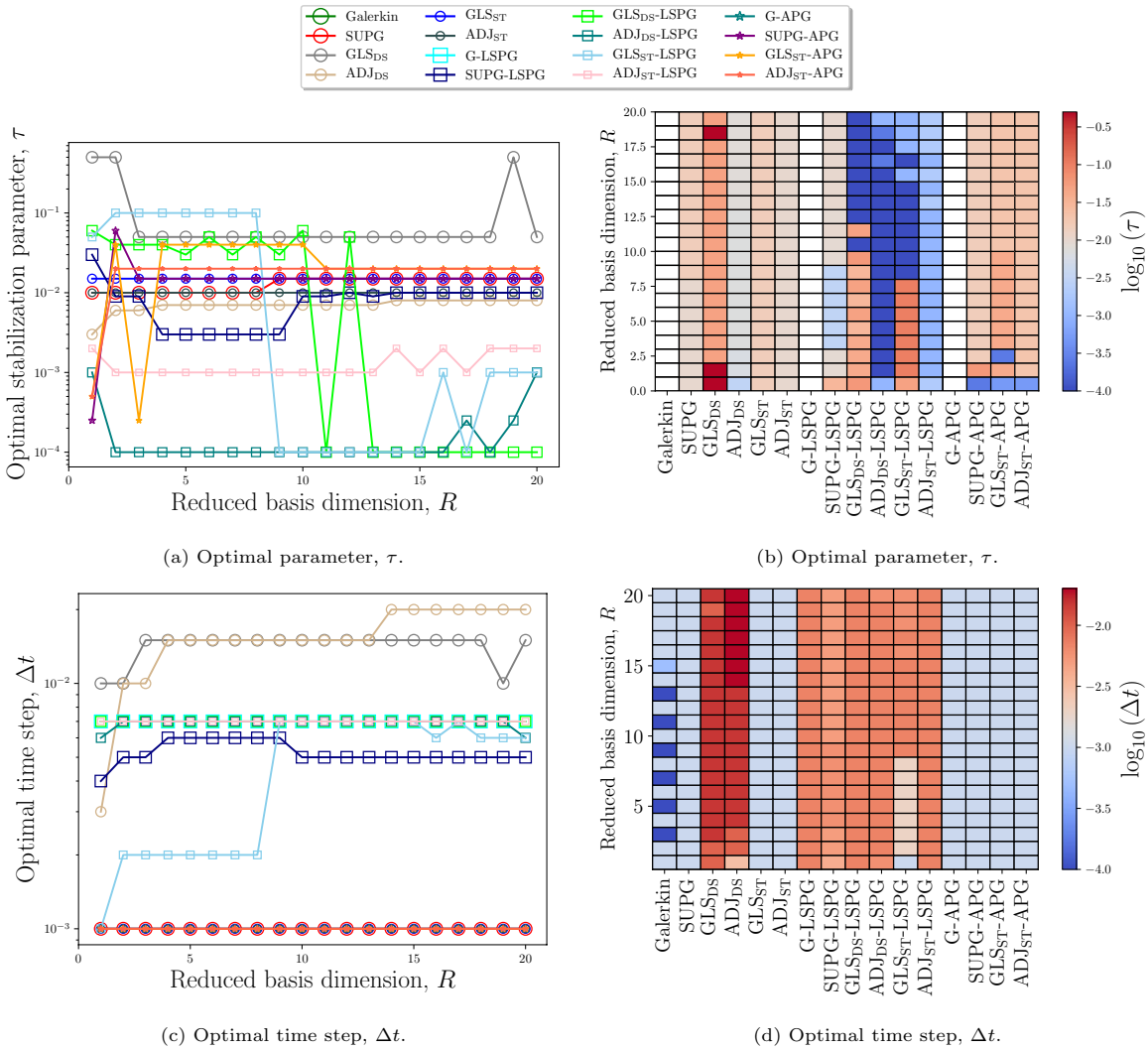

(a) Optimal parameter, τ.

(b) Optimal parameter, τ.

(c) Optimal time step, Δt.

(d) Optimal time step, Δt.

Fig. 7 Example 1, boundary layer. Optimal stabilization parameter (top) and time step (bottom) as a function of ROM basis dimension for the various ROMs evaluated. We note that the left and right figures show the same quantities, but with different visualization techniques. Results are shown for optimal values of t, τ, as discussed in Sect. 7.1.4

7.3.1 Description of Problem Setup, Full-Order Model, and Generation of Trial Spaces

We solve Eq. (1) with a final time $T = 2$ and a spatial domain $\Omega = (0,1) \times (0,1)$. We take $\epsilon = 10^{-4}$, $\sigma = 1$, and $\mathbf{b} = \frac{1}{2}\left[\cos(\pi/3)\ \sin(\pi/3)\right]^T$. The Peclet number is $\mathrm{Pe} := ||\mathbf{b}||_2/\epsilon = 5000$. The forcing is set as

$$f = \begin{cases} 1 & 0 \le x \le 0.5 \ \text{ and } \ 0 \le y \le 0.25 \\ 0 & x > 0.5 \ \text{ and } \ y > 0.25. \end{cases}$$

The high-resolution trial space $[\mathcal{V}_h]_{h-res}$ is obtained via a uniform triangulation of Ω into $N_{el} = 2 \times 256^2$ elements equipped with a $\mathcal{C}^0(\Omega)$ continuous discretization with polynomials of order $p = 2$. The grid Peclet number is $\mathrm{Pe}_g = 9.77$, where we used $h = (256p)^{-1}$. Analogously, the FOM trial space $[\mathcal{V}_h]_{fom}$ is obtained via a uniform triangulation of Ω into $N_{el} = 2 \times 32^2$ elements equipped with a $\mathcal{C}^0(\Omega)$ continuous discretization with polynomials of order $p = 2$. The grid Peclet number is $\mathrm{Pe}_g = 78.125$, where we used $h = (32p)^{-1}$. The triangulations are obtained in the same manner as in the previous experiment. The ROM trial space is obtained by executing Algorithm 1; Fig. 12 presents the residual statistical energy as a function of basis dimension. More basis vectors are required to characterize the system as compared to the previous example.

7.3.2 Full-Order Model Results

We again first present results of the various FOMs considered (again for optimal stabilization parameters and time

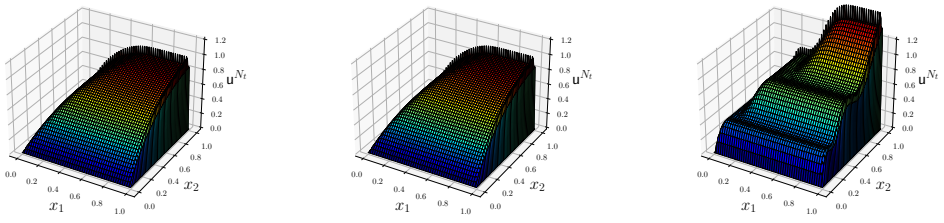

(a) H-Res ($L^2(\Omega)$ best fit) (b) H-Res ($\mathcal{H}^1(\Omega)$ best fit) (c) Galerkin

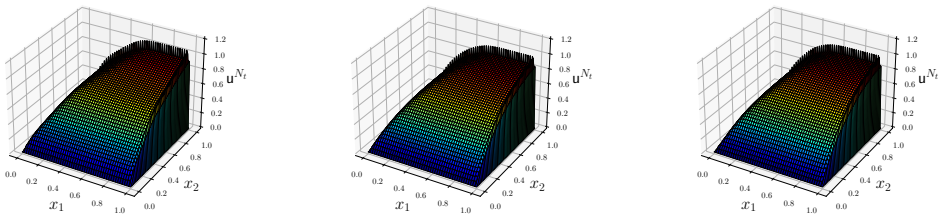

(d) SUPG (e) $\mathrm{GLS}_{\mathrm{DS}}$ (f) $\mathrm{ADJ}_{\mathrm{DS}}$

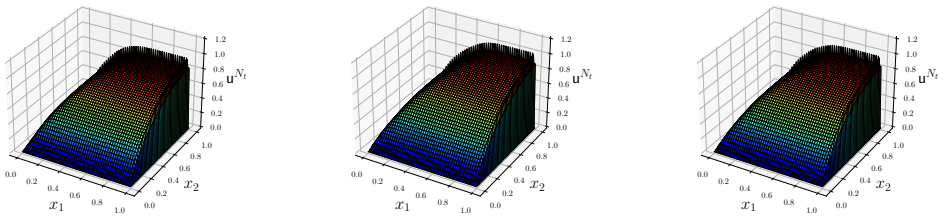

(g) $\mathrm{GLS}_{\mathrm{ST}}$ (h) $\mathrm{ADJ}_{\mathrm{ST}}$ (i) G–LSPG

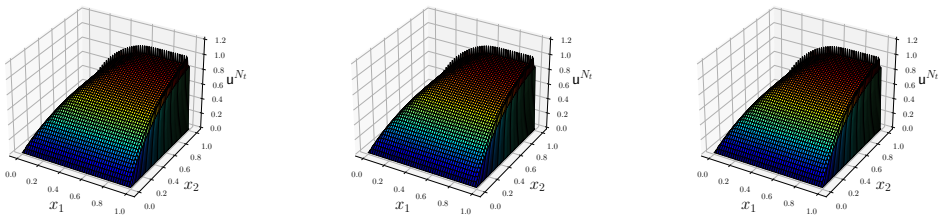

(j) SUPG–LSPG (k) $\mathrm{ADJ}_{\mathrm{DS}}$–LSPG (l) $\mathrm{ADJ}_{\mathrm{DS}}$–LSPG

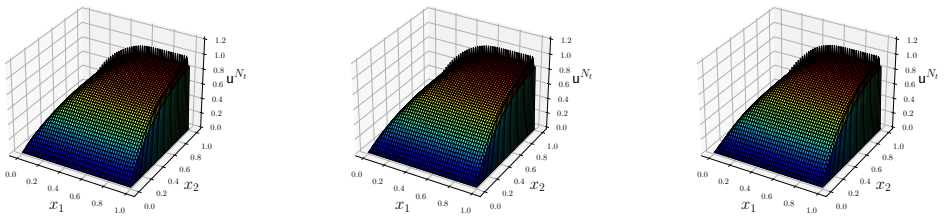

(m) $\mathrm{GLS}_{\mathrm{ST}}$–LSPG (n) $\mathrm{ADJ}_{\mathrm{ST}}$–LSPG (o) G–APG

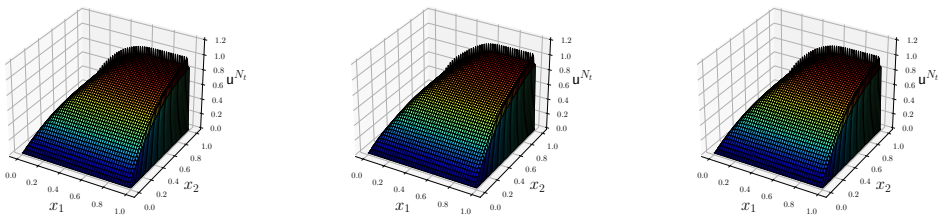

(p) SUPG–APG (q) $\mathrm{GLS}_{\mathrm{ST}}$–APG (r) $\mathrm{ADJ}_{\mathrm{ST}}$–APG

Fig. 8 Example 1, boundary layer. ROM solutions to the CDR equation at $t = 5$. Results are shown for solutions obtained with $R = 5$ and with the optimal time step and stabilization parameter as measured by the $L^2(\Omega)$-error

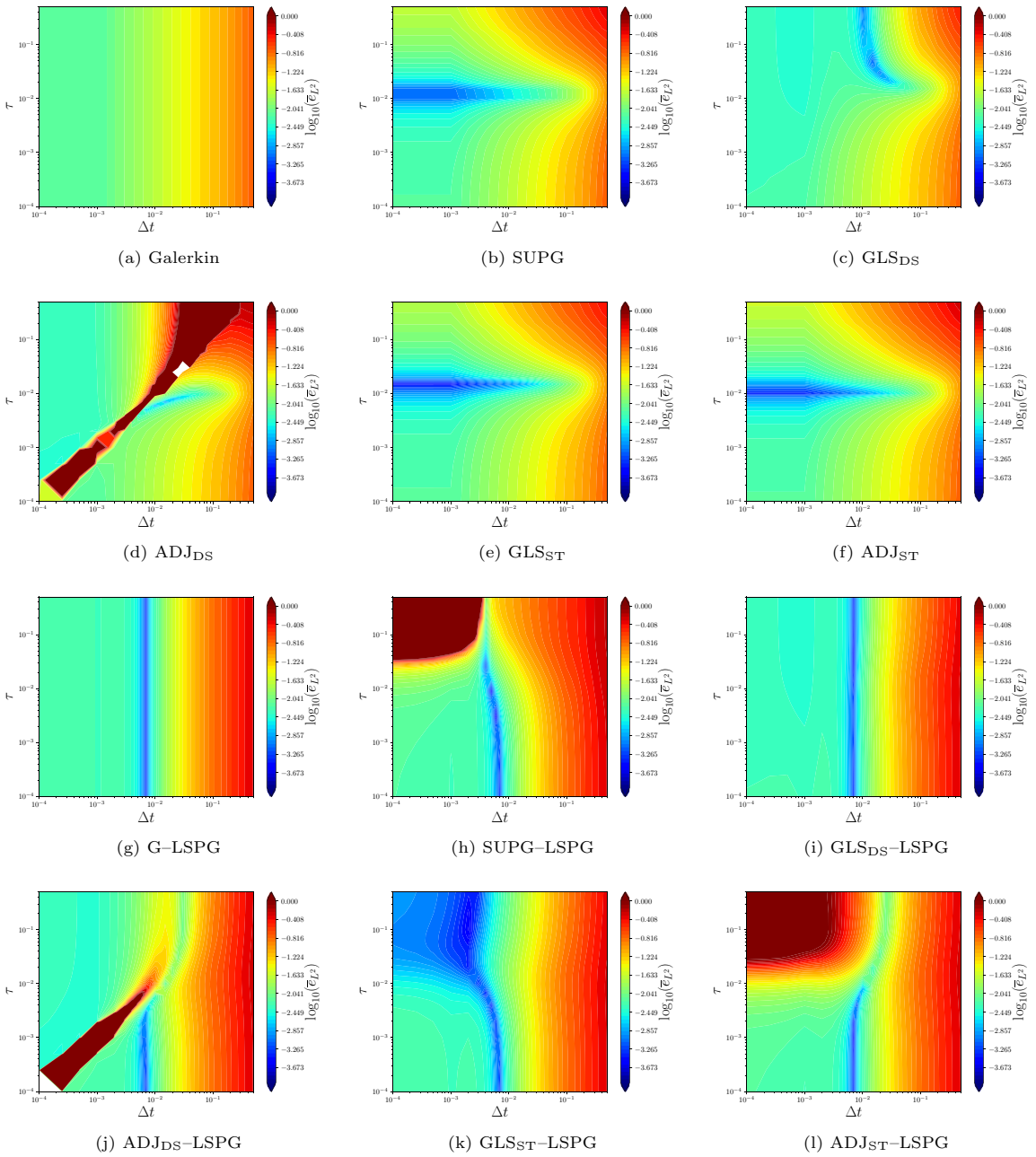

Fig. 9 Example 1, boundary layer. Time integrated $L^2(\Omega)$ best-fit error as a function of time step and stabilization parameter for the various ROMs evaluated. Note that Galerkin and LSPG display no dependence on the stabilization parameter. White regions indicate regions where the solution diverged to NaN

steps). Figure 13 presents the various FOM solutions at the final time, $t = 2$, while Table 5 tabulates the solution errors and stabilization parameters employed in the simulations. We observe the following.

- The Galerkin, ADJ$_{\mathrm{DS}}$, and GLS$_{\mathrm{DS}}$ FEM FOMs are the worst performing methods and all result in oscillatory solutions.
- SUPG, GLS$_{\mathrm{ST}}$, and ADJ$_{\mathrm{ST}}$ all provide solutions of a similar qualitative and quantitative quality, and are all able to suppress the oscillations seen in the Galerkin FEM solution.
- The "space–time" GLS$_{\mathrm{ST}}$ and ADJ$_{\mathrm{ST}}$ FEMs again perform much better than the "discretize-then-stabilize" GLS$_{\mathrm{DS}}$ and ADJ$_{\mathrm{DS}}$ FEM FOMs.

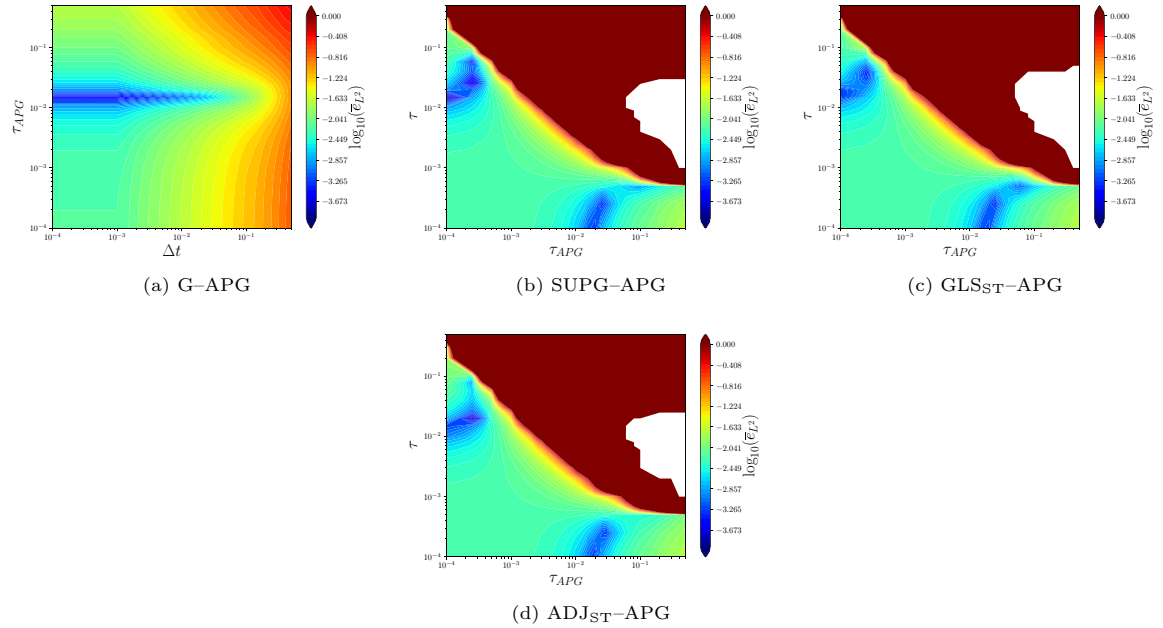

(a) G–APG (b) SUPG–APG (c) GLS_{ST}–APG

(d) ADJ_{ST}–APG

Fig. 10 Example 1, boundary layer. Time integrated $L^2(\Omega)$ error as a function of time step and stabilization parameter for the APG ROMs evaluated. White regions indicate regions where the solution diverged to NaN

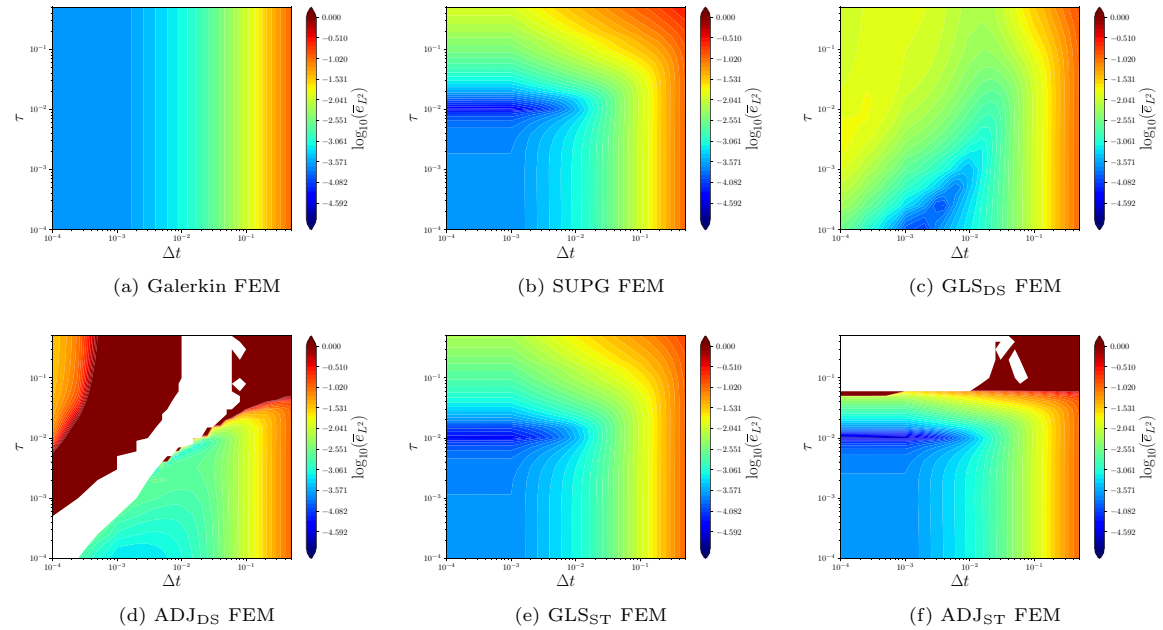

(a) Galerkin FEM (b) SUPG FEM (c) GLS_{DS} FEM

(d) ADJ_{DS} FEM (e) GLS_{ST} FEM (f) ADJ_{ST} FEM

Fig. 11 Example 1, boundary layer. Time integrated $L^2(\Omega)$ error as a function of time step and stabilization parameter for various FEM models. Results are shown for full-order FEM solutions executed on the FOM trial space. White regions indicate regions where the solution diverged to NaN

These results are similar to those obtained for example 1 (Sect. 7.2.1).

7.3.3 Results as a Function of RB Dimension

Figure 14 shows the time integrated relative$L^2(\Omega)$ error and $\mathcal{H}^1(\Omega)$ error for each of the ROMs considered as a

function of RB size. Results are presented for the value of τ and Δt that led to the lowest $L^2(\Omega)$ error; Fig. 15 shows these optimal stabilization parameters and time steps for each basis dimension.

Examining Fig. 14, we make the following observations about the *accuracy* of the various ROMs.

- The APG-based, SUPG, ADJ_{ST}, and GLS_{ST} ROMs are the best overall performing methods.
- The "discretize-then-stabilize" ROMs outperform the Galerkin ROM, but are consistently worse than their space–time stabilized counterparts for all ROM dimensions. In general, even when equipped with LSPG, the discretize-then-stabilize methods perform quite poorly.
- When applied to the standard Galerkin and GLS_{DS} FEM models, LSPG leads to slightly improved solutions. LSPG does not lead to improved solutions for SUPG, GLS_{ST}, or ADJ_{ST}.
- It is again interesting to note the improved performance of G–APG over the standard Galerkin method at high reduced basis dimensions, given that G–APG will converge to the Galerkin method in the limit of a full reduced basis. The improved performance is also seen for G–LSPG, but to a lesser extent.
- Once again, while not always the case, a decrease in error in the $L^2(\Omega)$ norm generally corresponds to a decrease in error in the $\mathcal{H}^1(\Omega)$ norm.
- Comparing Fig. 14 to Table 5, we again observe that some ROMs are more accurate than their corresponding FEM.

Examining Fig. 15, where we show the optimal stabilization parameters and time steps associated with Fig. 14, we make the following observations about the behavior of the stabilization parameters of the various ROMs.

- The optimal stabilization parameters for the SUPG, ADJ_{ST}, GLS_{ST}, and APG ROMs decrease as R grows (Fig. 15a). This result is consistent with analyses performed for SUPG ROMs in [52] and APG ROMs in [121], which suggest that the optimal stabilization parameter decreases with increasing ROM dimension; we refer the reader to the discussion in Sect. 4.3 regarding the scaling of the stabilization parameter with the mesh size and ROM size.
- The optimal stabilization parameter for GLS_{DS} is quite high for all ROM dimensions.
- The optimal time step for all LSPG ROMs occurs at an intermediate time step larger than the FEM FOM.
- Interestingly, the optimal time step for G–LSPG is the same as the optimal time step for GLS_{DS}.
- The reader may observe that the optimal time step for SUPG, GLS_{ST}, and ADJ_{DS} decreases for moderately high ROM dimensions; we note that this improvement is very minor as will be seen in Fig. 17.

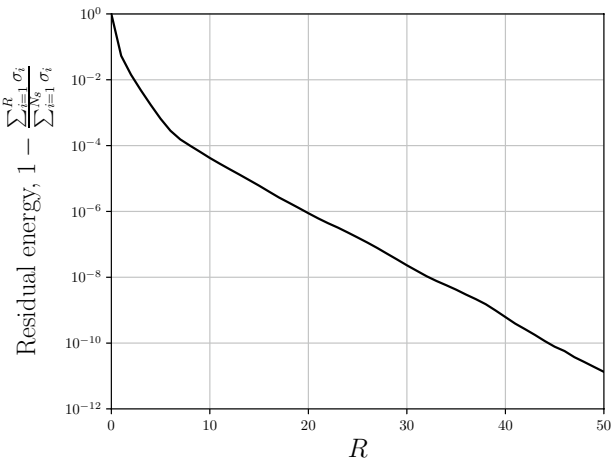

Fig. 12 Example 2, advecting front. Residual statistical energy as a function of basis dimension

Next, Fig. 16 presents physical space solution profiles for the various ROMs for a reduced basis dimension of $R = 5$ at the final time instance, $t = 2.0$. We observe that all methods yield qualitatively accurate solutions with the exception of Galerkin, G–LSPG, and GLS_{DS}; these three methods underpredict the magnitude of the solution in the lower-left quadrant of the domain ($x_1, x_2 \leq 0.4$). It is interesting to note that, although Fig. 14 showed that ADJ_{DS} and the non-Galerkin LSPG ROMs clearly perform less well than the other formulations, Fig. 16 shows that their physical space solutions still show a significant improvement over the standard Galerkin ROM. We additionally note that even the best performing methods are unable to fully capture the peak in the solution in the lower-left quadrant of the domain. The ROM solutions may appear overly dissipative relative to the $L^2(\Omega)/\mathcal{H}^1(\Omega)$ best fit solutions, and hence one may deduce that a smaller value of τ may improve the solution. However, we recall that all stabilized ROM methods use the τ optimized to minimize the error, and hence the lack of sharpness is due to adding non-optimal kind (i.e., mode) of dissipation, and it cannot be corrected by adjusting the amount (i.e., scale) of dissipation.

7.3.4 Sensitivity to Time Step and Stabilization Parameters

We now quantify the sensitivity of the various methods to their stabilization parameters and the time step. Figure 17 presents results for the continuous and LSPG ROM solutions obtained at $R = 5$ on the parameter grid $(\tau, \Delta t) \in \boldsymbol{\tau} \times \boldsymbol{\Delta t}$,

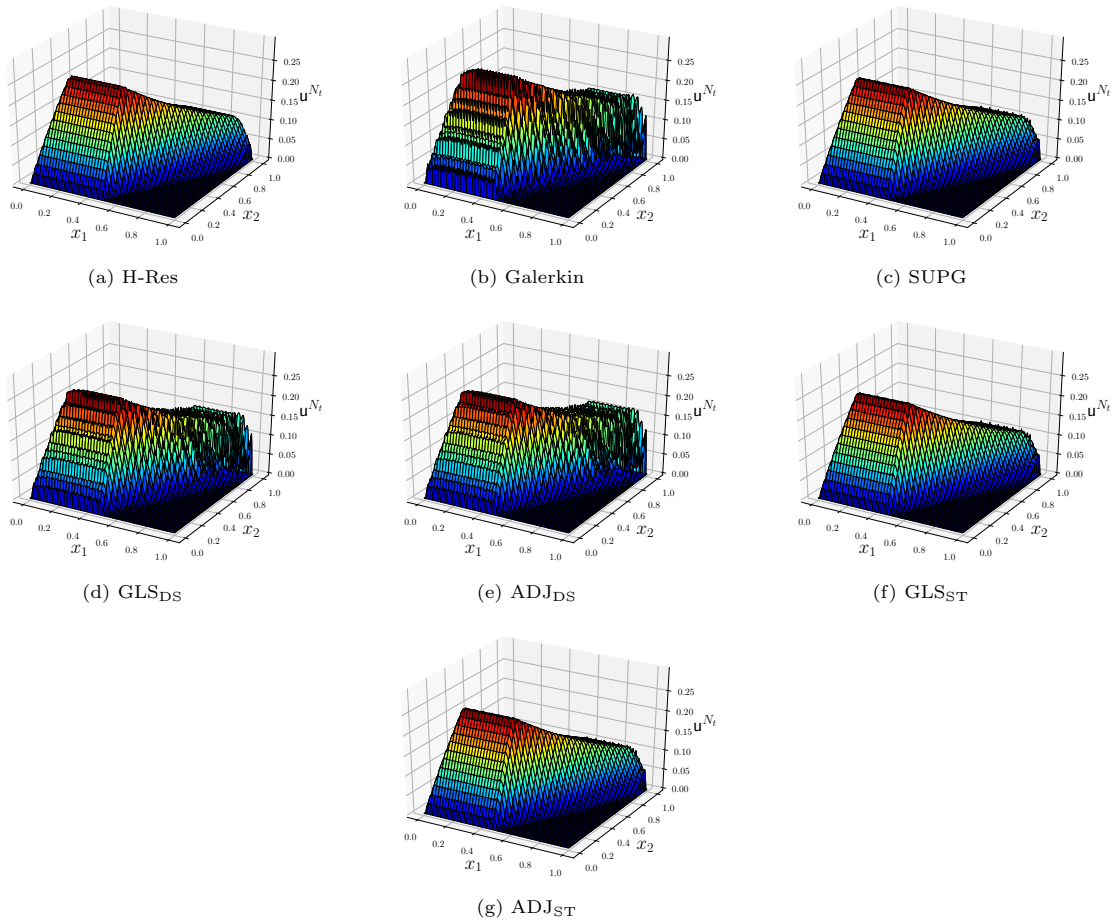

(a) H-Res (b) Galerkin (c) SUPG

(d) $\mathrm{GLS_{DS}}$ (e) $\mathrm{ADJ_{DS}}$ (f) $\mathrm{GLS_{ST}}$

(g) $\mathrm{ADJ_{ST}}$

Fig. 13 Example 2, advecting front. FOM solutions to the CDR equation at $t = 5$

Table 5 Example 2, advecting front. Integrated (relative) $L^2(\Omega)$ and $\mathcal{H}^1(\Omega)$ errors of various FOMs presented in Fig. 13, along with the stabilization parameters at which the FOMs were executed

	Galerkin	SUPG	GLSDS	ADJDS	GLSST	ADJST
$\bar{e}_{L^2}([\mathcal{V}_\mathrm{h}]_\mathrm{fom})$	2.76×10^{-2}	6.62×10^{-3}	2.24×10^{-2}	2.19×10^{-2}	6.66×10^{-3}	6.59×10^{-3}
$\bar{e}_{\mathcal{H}^1}([\mathcal{V}_\mathrm{h}]_\mathrm{fom})$	9.30×10^{-2}	5.37×10^{-3}	7.53×10^{-2}	7.32×10^{-2}	5.81×10^{-3}	5.02×10^{-3}
τ	*N/A*	1.00×10^{-2}	1.00×10^{-4}	1.00×10^{-4}	1.00×10^{-2}	1.00×10^{-2}
Δt	1.00×10^{-3}	1.00×10^{-3}	1.00×10^{-3}	1.00×10^{-3}	1.00×10^{-3}	1.00×10^{-3}

while Fig. 18 presents results for the G–APG ROM solutions obtained at $R = 5$ on the parameter grid $(\tau_\mathrm{APG}, \Delta t) \in \boldsymbol{\tau} \times \boldsymbol{\Delta t}$ and the remaining APG ROM solutions (which depend on three parameters, Δt, τ, and τ_APG) obtained at $R = 5$ on the parameter grid $(\tau, \tau_\mathrm{APG}) \in \boldsymbol{\tau} \times \boldsymbol{\tau}$ with a fixed time step $\Delta t = 10^{-3}$. As a reference, Fig. 19 shows the same sensitivities but for full-order FEM simulations executed on the FOM trial space. We make the following observations.

- The SUPG (Fig. 17b), $\mathrm{GLS_{ST}}$ (Fig. 17e), $\mathrm{ADJ_{ST}}$ (Fig. 17f), and G–APG (Fig. 18g) ROMs again all display a dependence on the time step and stabilization parameter that is similar to the first example. Optimal results are obtained for an intermediate value of τ, and the solutions all converge in the limit of $\Delta t \to 0$.
- G–LSPG (Fig. 17g), which contains no dependence on τ, yields optimal results at an intermediate time step.
- For sufficiently large τ, the dependence of $\mathrm{GLS_{DS}}$ (Fig. 17c) on the time step is similar to that of LSPG (Fig. 17g).
- Neither $\mathrm{GLS_{DS}}$ nor $\mathrm{ADJ_{DS}}$ ROMs have optimal results at the minimum time step, suggesting that these methods

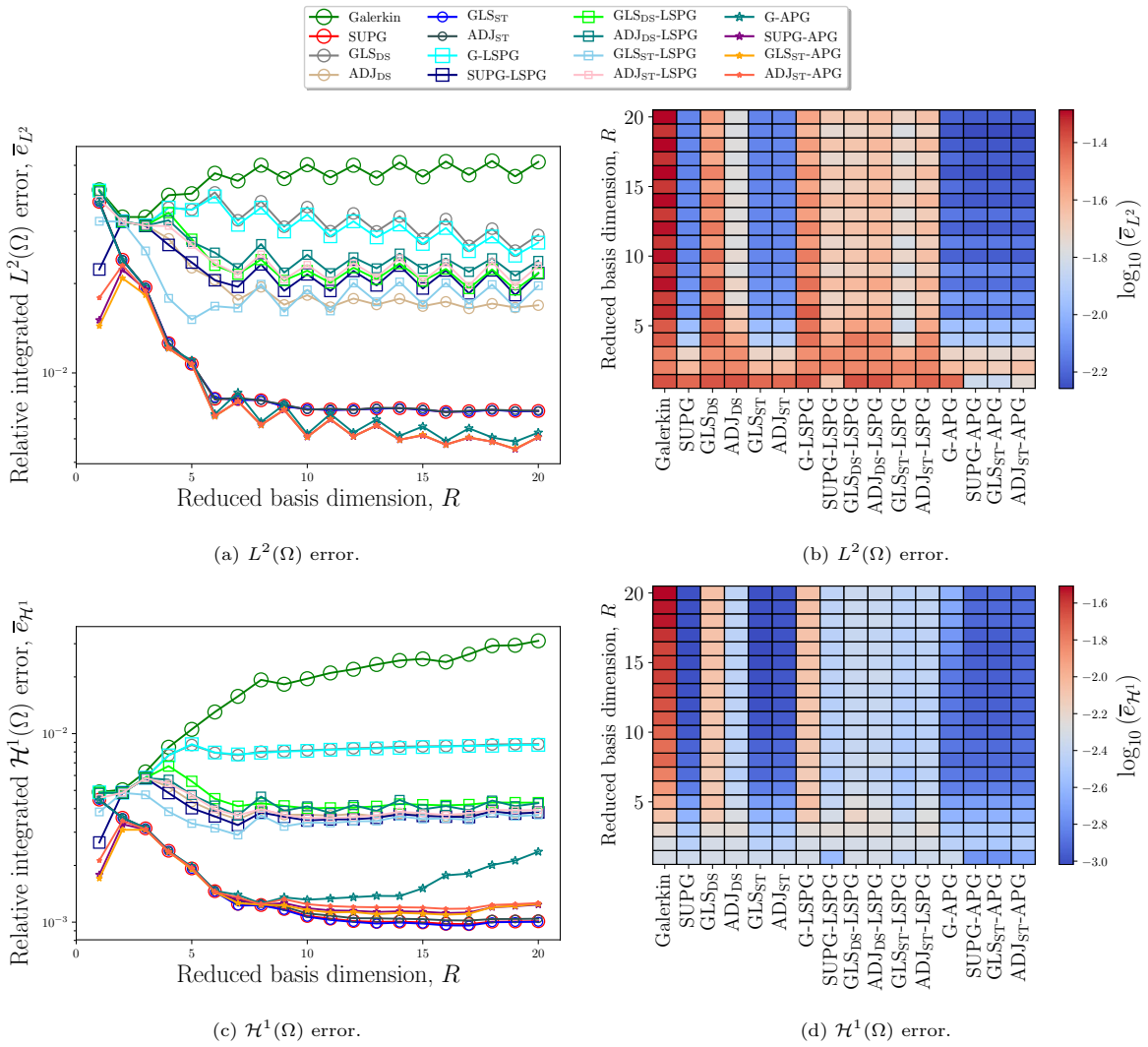

(a) $L^2(\Omega)$ error.

(b) $L^2(\Omega)$ error.

(c) $\mathcal{H}^1(\Omega)$ error.

(d) $\mathcal{H}^1(\Omega)$ error.

Fig. 14 Example 2, advecting front. $L^2(\Omega)$ (top) and $\mathcal{H}^1(\Omega)$ (bottom) error as a function of RB dimension for the various ROMs evaluated. We note that the left and right figures show the same quantities, but with different visualization techniques. Results are shown for optimal values of $\Delta t, \tau$ as discussed in Sect. 7.1.4

are not well-behaved in the low time-step limit. This result reinforces those presented in Fig. 15c.

- All continuous ROMs (Fig. 17a–f) display a similar dependence to the stabilization parameter and time step as their corresponding FOMs (Fig. 19a–f).
- Lastly, for APG ROMs built on top of a stabilized FEM (Fig. 18c–e), optimal results are obtained for either an intermediate value of τ_{APG} and low value of τ, or vice versa. It is interesting to note that the solutions are almost symmetric with respect to these two parameters.

7.4 Summary of Numerical Experiments and Empirical Findings

Sections 7.2 and 7.3 presented results for stabilized ROMs applied to the CDR system for two different configurations. Across both cases, we observed that the "space–time" stabilized continuous ROM formulations were superior to their "discretize-then-stabilize" counterparts: the space–time stabilization formulations had lower errors, were well-behaved in the low time-step limit (the discretize-then-stabilized methods were not), and had a smoother, more intuitive dependence on the time step and stabilization parameter.

ROMs constructed from LSPG projection had mixed results in terms of accuracy. In the first numerical experiment, ROM solutions computed via LSPG projection

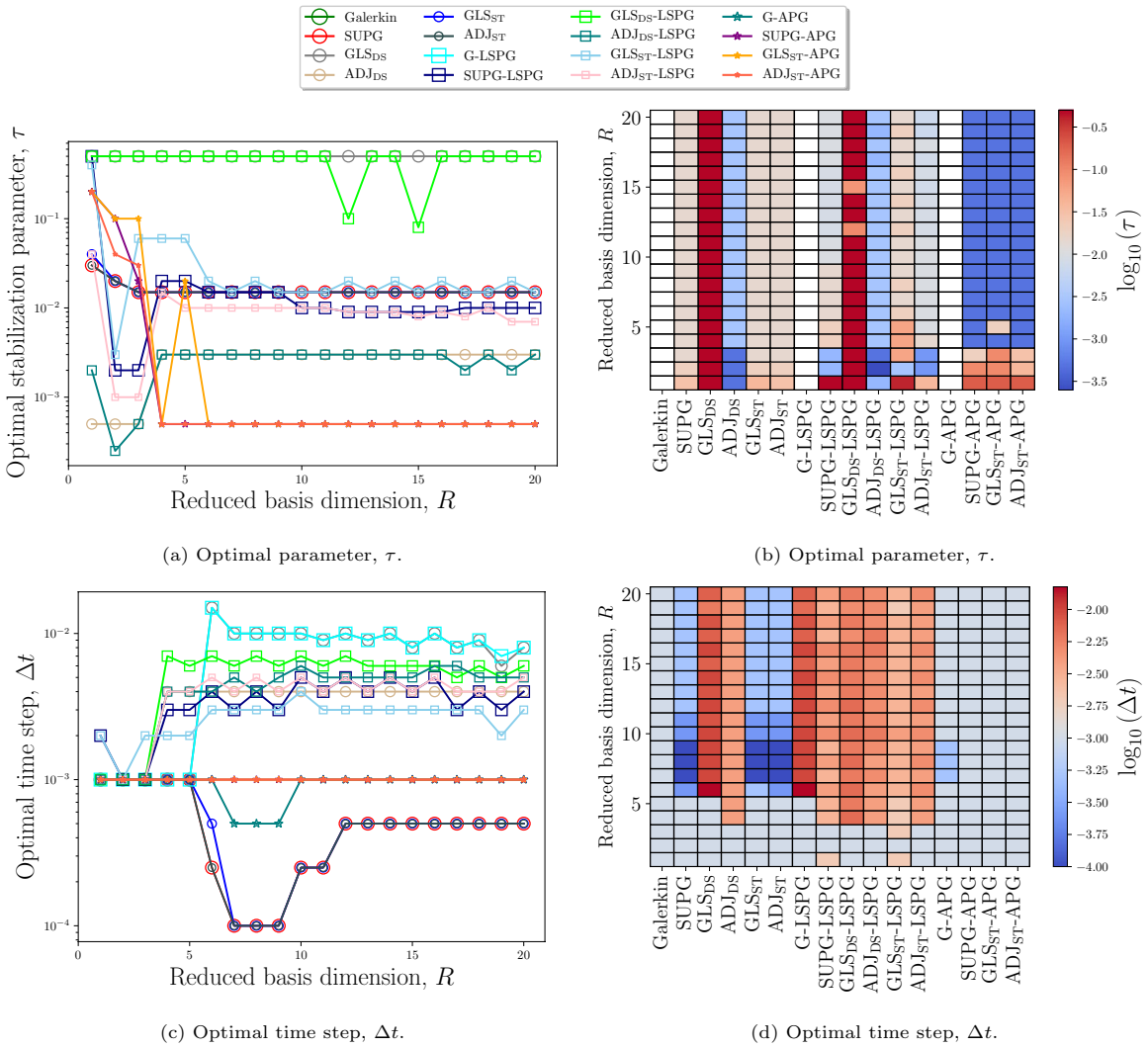

(a) Optimal parameter, τ.

(b) Optimal parameter, τ.

(c) Optimal time step, Δt.

(d) Optimal time step, Δt.

Fig. 15 Example 2, advecting front. Optimal stabilization parameter (top) and time step (bottom) as a function of RB dimension. We note that the left and right figures show the same quantities, but with different visualization techniques. Results are shown for optimal values of $\Delta t, \tau$ as discussed in Sect. 7.1.4

tended to be slightly better than their non-stabilized (e.g., discrete Galerkin) ROM counterparts. In the second example, however, the performance was mixed. While G–LSPG and GLS$_{DS}$–LSPG led to better solutions than Galerkin and GLS$_{DS}$, respectively, SUPG–LSPG, ADJ$_{DS}$–LSPG, GLS$_{ST}$–LSPG, and ADJ$_{ST}$–LSPG all performed worse than SUPG, ADJ$_{DS}$, GLS$_{ST}$, and ADJ$_{ST}$, respectively. Further, all LSPG ROMs were optimal for intermediate time steps and, when built on top of a stabilized FEM solution, displayed a complex sensitivity to both the stabilization parameter and time step. The *a priori* selection of an optimal time step appears difficult, and is likely problem dependent.

Constructing ROMs with APG stabilization tended to have a positive result in terms of accuracy. In the first example, APG ROMs outperformed their non-stabilized (i.e., discrete Galerkin) counterpart for all cases with the exception of GLS$_{ST}$. In the second example, APG-based ROMs were better than their non-stabilized counterparts for all FEM formulations. APG was well-behaved in the low time step limit. However, building an APG ROM on top of a stabilized FEM solution led to complex behavior for the stabilization parameter: high values of τ for the stabilized FEM models required low values of τ_{APG} for the ROM, and vice versa. The *a priori* selection of these parameters again appears difficult.

Figure 20 summarizes the performance of the various ROMs by tabulating the number of times a given ROM formulation led to the lowest errors in the $L^2(\Omega)$ and $\mathcal{H}^1(\Omega)$ -norm. Results are compiled for ROMs of basis dimensions $R = 1, \ldots, 20$ across both numerical experiments. We observe that SUPG–APG was the best performing ROM for both error metrics. The next best performing ROMs were ADJ$_{ST}$–APG and GLS$_{ST}$–APG, followed closely by GLS$_{ST}$,

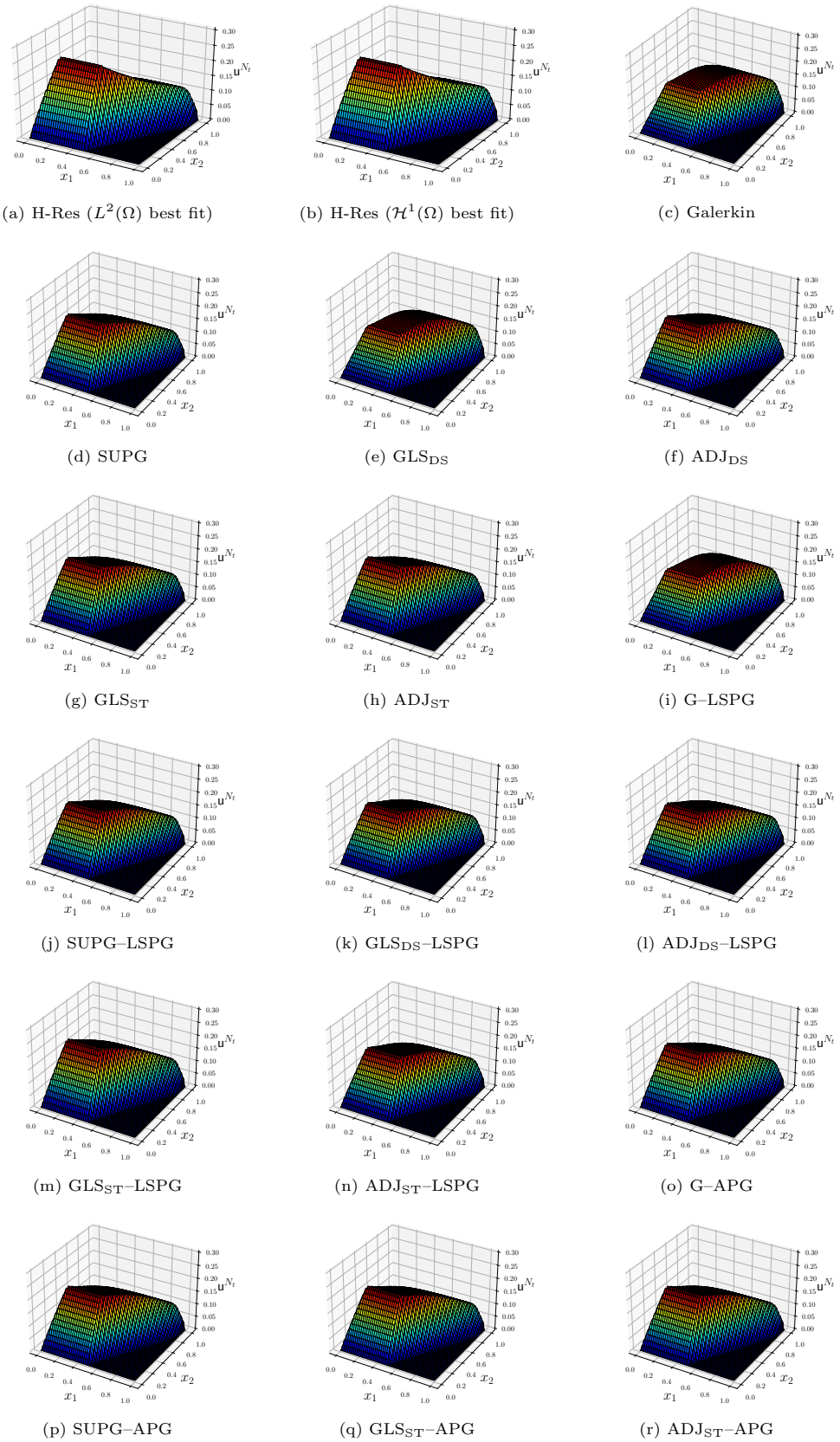

(a) H-Res ($L^2(\Omega)$ best fit) (b) H-Res ($\mathcal{H}^1(\Omega)$ best fit) (c) Galerkin

(d) SUPG (e) GLS_{DS} (f) ADJ_{DS}

(g) GLS_{ST} (h) ADJ_{ST} (i) G–LSPG

(j) SUPG–LSPG (k) GLS_{DS}–LSPG (l) ADJ_{DS}–LSPG

(m) GLS_{ST}–LSPG (n) ADJ_{ST}–LSPG (o) G–APG

(p) SUPG–APG (q) GLS_{ST}–APG (r) ADJ_{ST}–APG

Fig. 16 Example 2, advecting front. ROM solutions to the CDR equation at $t = 2.0$. Results are shown for $R = 5$

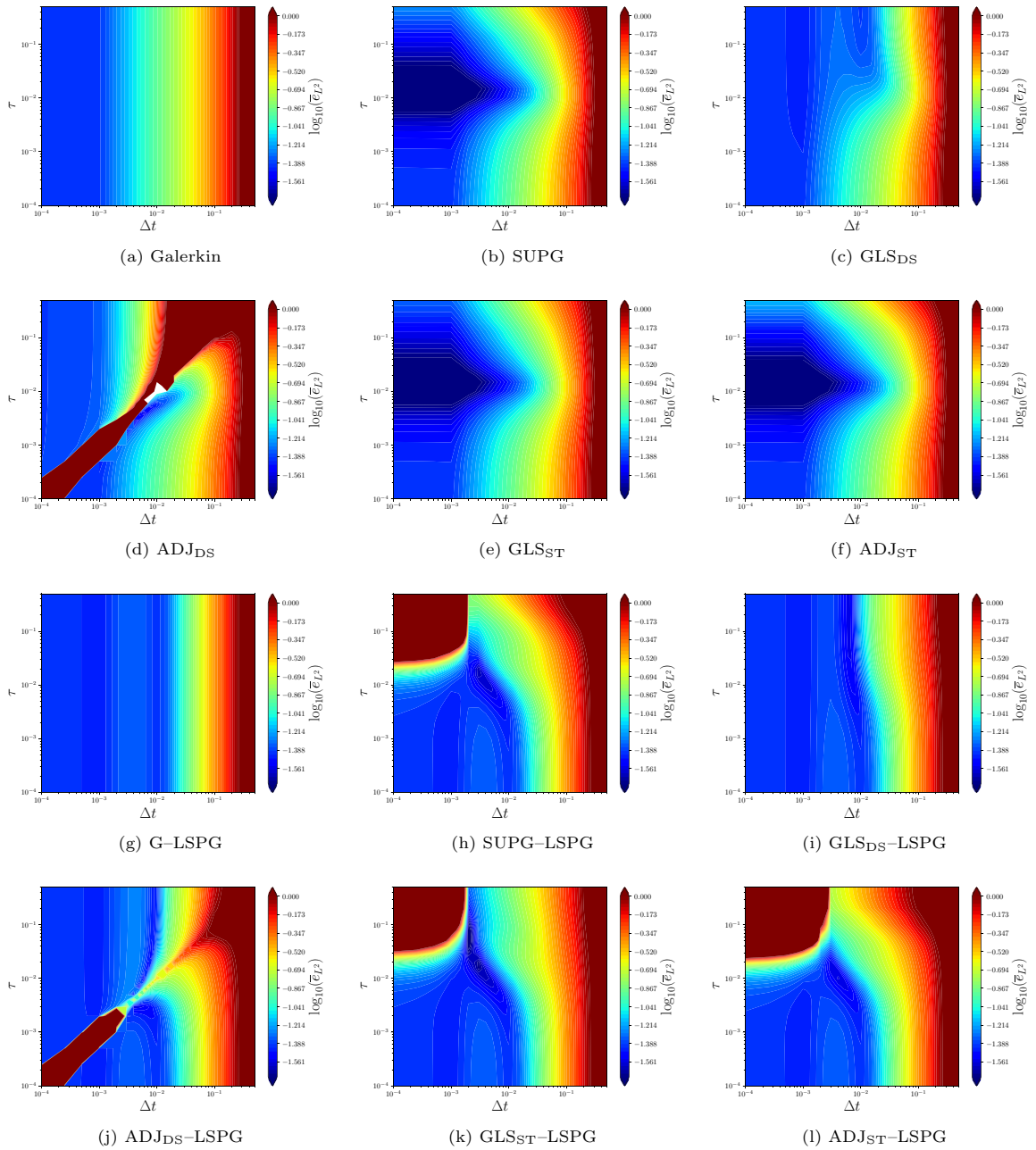

Fig. 17 Example 2, advecting front. Time integrated $L^2(\Omega)$ error as a function of time step and stabilization parameter for the various ROMs evaluated. Note that Galerkin and LSPG display no dependence on the stabilization parameter. White regions indicate solutions that diverged to NaN

SUPG, and ADJ$_{\mathrm{ST}}$. It is interesting to note that the two different error measures lead to slightly different measure of optimality (SUPG is never a top-performing method in $L^2(\Omega)$ but is consistently a top-performing method in $\mathcal{H}^1(\Omega)$).

Lastly, Fig. 21 attempts to rank the various ROM formulations by scoring their performance. For a given basis dimension, we scored a ROM on a scale of $1 - N_{\mathrm{ROMS}}$, where $N_{\mathrm{ROMS}} = 16$ is the number of ROM formulations considered. The best ROM gets a score of N_{ROMS}, the second best ROM gets a score of $N_{\mathrm{ROMS}} - 1$, and so on until the worst-performing ROM gets a score of 1. The total score for each ROM formulation is computed by summing the individual scores across all basis dimensions and both numerical experiments. By this scoring system, we find that SUPG–APG is the best performing ROM in both error measures, followed closely

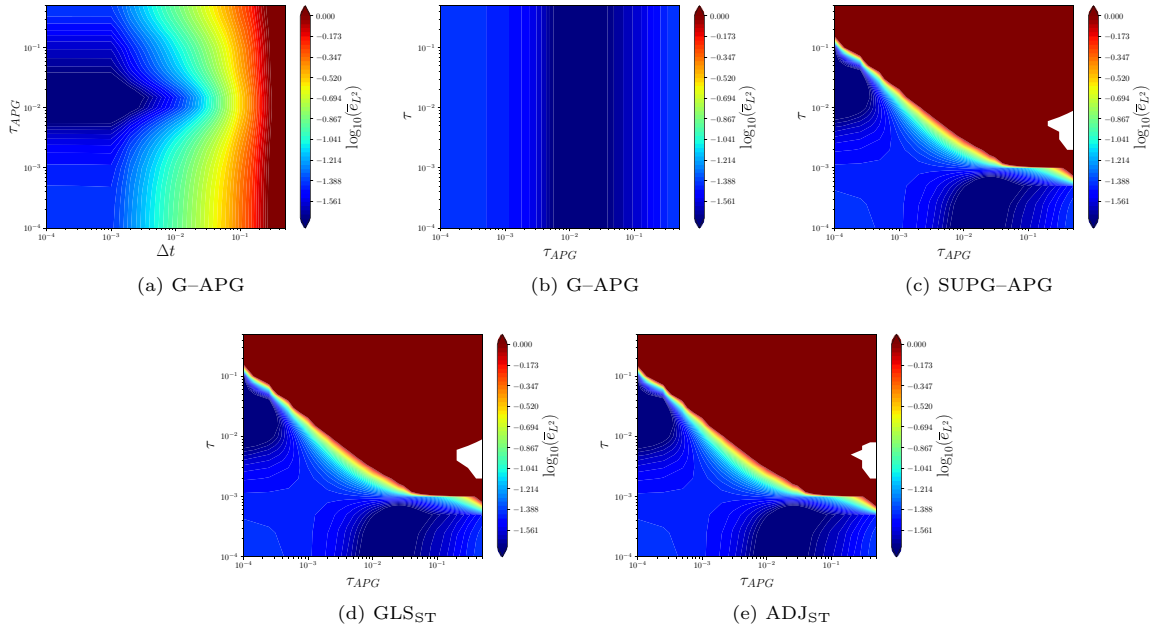

(a) G–APG (b) G–APG (c) SUPG–APG

(d) $\mathrm{GLS_{ST}}$ (e) $\mathrm{ADJ_{ST}}$

Fig. 18 Example 2, advecting front. Time integrated $L^2(\Omega)$ error as a function of time step and stabilization parameter for the various ROMs evaluated. Note that Galerkin and LSPG display no dependence on the stabilization parameter. White regions indicate errors higher than the color limit

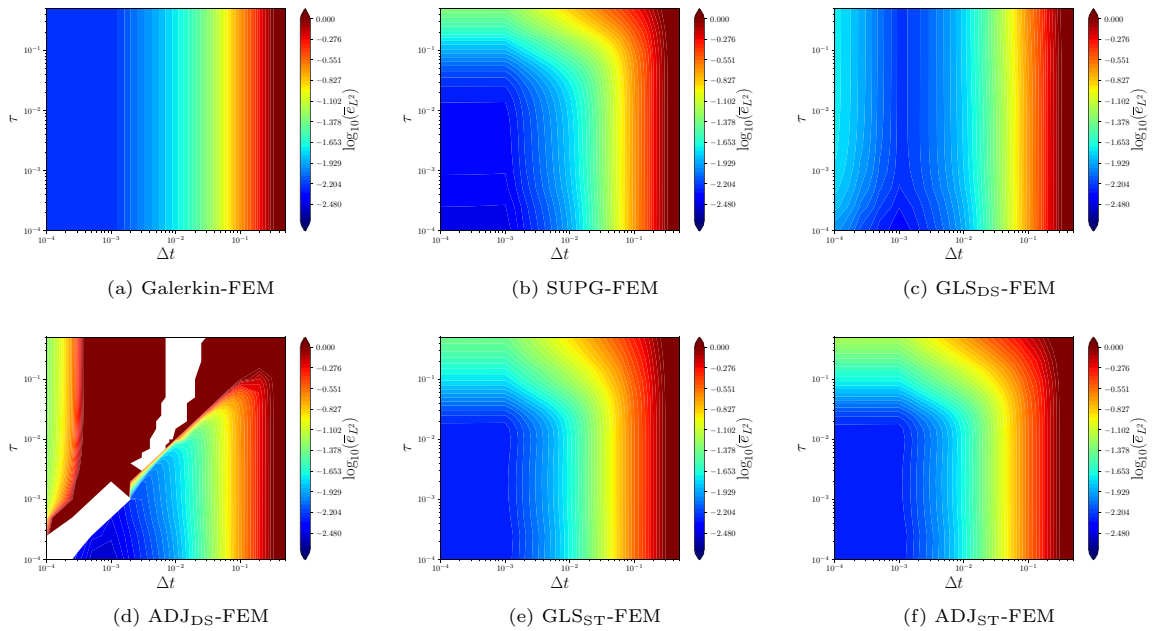

(a) Galerkin-FEM (b) SUPG-FEM (c) $\mathrm{GLS_{DS}}$-FEM

(d) $\mathrm{ADJ_{DS}}$-FEM (e) $\mathrm{GLS_{ST}}$-FEM (f) $\mathrm{ADJ_{ST}}$-FEM

Fig. 19 Example 2, advecting front. Time integrated $L^2(\Omega)$ error as a function of time step and stabilization parameter. Results are shown for full-order FEM solutions executed on the FOM trial space. White regions indicate errors higher than the color limit

by $\mathrm{ADJ_{ST}}$–APG, $\mathrm{GLS_{ST}}$, and $\mathrm{GLS_{ST}}$–APG. The $\mathrm{GLS_{ST}}$ ROM is the best continuous ROM considered in this work, while the Galerkin ROM performs the worst.

We end the discussion with notes on robustness and computational cost. First, while APG-based methods constructed on top of SUPG, $\mathrm{GLS_{ST}}$, and $\mathrm{ADJ_{ST}}$ led to solutions with the highest errors, these methods had a complex dependence

on stabilization parameters and were, at times, unstable. To fully realize the potential of these methods, analyses are needed for optimal selection of stabilization parameters. Second, while we did not report wall-clock times for running the various models considered in this work, we remark that, for linear problems, all ROM methods considered herein have similar online computational costs. The costs will differ for nonlinear problems, and will depend on the choice of hyper-reduction method used to handle the online evaluation of the nonlinearities in the governing problem. Extension of the analysis presented herein to nonlinear problems will be the subject of future work.

8 Conclusions

The development of robust ROMs for time-critical and many-query scenarios remains an active research area. This work outlined the construction of stabilized ROMs for the transient CDR equation via two differing approaches that have emerged within the community: discrete and continuous projections. We outlined the standard Galerkin, SUPG, GLS_{DS}, ADJ_{DS}, GLS_{ST}, and ADJ_{ST} continuous ROMs developed via traditional stabilized finite elements. We additionally outlined the construction of the discrete Galerkin, LSPG, and APG ROMs. These discrete ROMs can be constructed from a standard Galerkin FEM model, or they can also be constructed from a stabilized FEM model. We highlighted the well-established equivalences between constructing ROM basis vectors at the discrete and continuous levels. We additionally highlighted the established equivalence conditions between discrete ROM formulations and continuous ROM formulations. Lastly, a brief summary of existing numerical analyses was provided, where we discussed consistency, stability, and error bounds of the various methods.

Numerical experiments were conducted for two configurations of the CDR system. These experiments demonstrated that all stabilized ROMs result in superior performance over a standard Galerkin ROM built via continuous projection. APG and GLS_{ST}-based ROMs proved to be the best performing methods, while GLS_{DS}, ADJ_{DS}, and G–LSPG proved to be the worst performing stabilized methods. In particular, we found that equipping a stabilized FEM model with APG or LSPG projection can result in more accurate solutions. This improvement in accuracy comes at the cost of a more complex dependence on the stabilization parameters and time step. In the case of LSPG, results are optimal at an intermediate time step which is hard to select *a priori*. Further, the accuracy of LSPG-based methods degrades in the small time step limit as it is known to revert to Galerkin projection [29]. In the case of APG, we observed a non-trivial relationship between τ in the stabilized FEM model and τ_{APG} in the APG projection. Low values of τ in the stabilized FEM model required high values of τ_{APG}, and vice versa. There exist minimal methods for the *a priori* selection of these optimal stabilization parameters. However, APG-based ROMs were robust for small time steps. Lastly, we observed that ROMs built via continuous projection from the "space–time" approach were clearly superior to ROMs built via the "discretize-then-stabilize" approach: the space-time stabilization formulations had lower errors, were well-behaved in the low time-step limit (the discretize-then-stabilize methods were not), and had a smoother, more intuitive dependence on the time step and stabilization parameter.

In addition, our study highlighted several points (most of which are well-established in the literature) which we reiterate here.

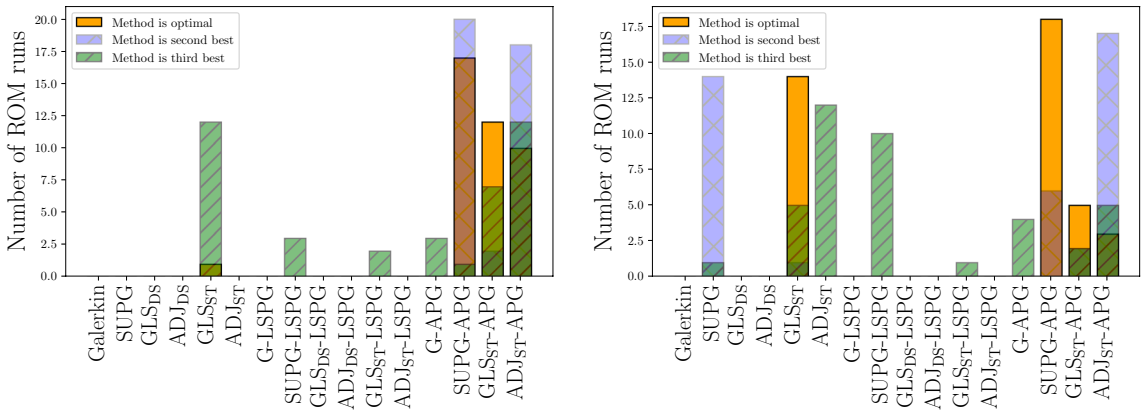

(a) $L^2(\Omega)$-norm (b) $\mathcal{H}^1(\Omega)$-norm

Fig. 20 Summary of numerical experiments. Number of times a given ROM formulation led to lowest errors in the $L^2(\Omega)$-norm (left) and $\mathcal{H}^1(\Omega)$ -norm (right). Results are compiled across both numerical examples for all basis dimensions

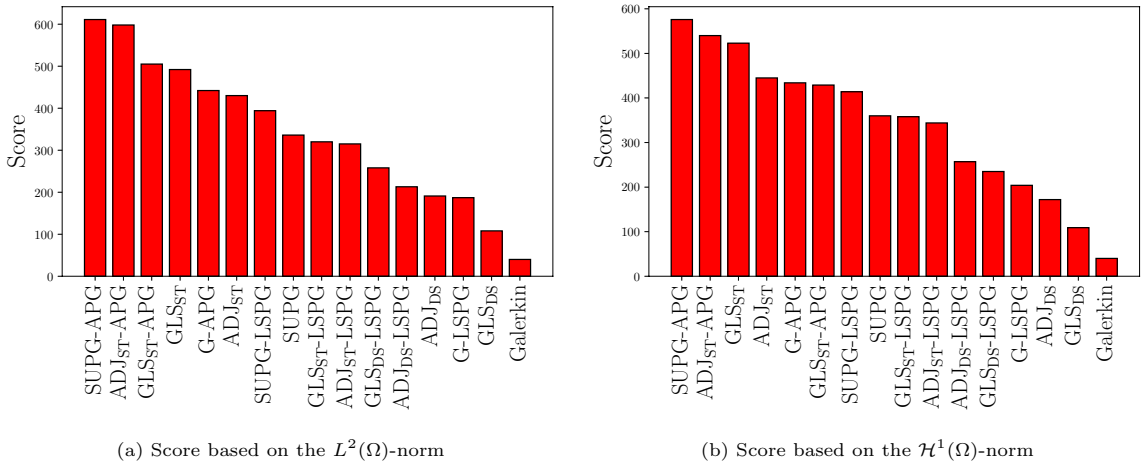

(a) Score based on the $L^2(\Omega)$-norm

(b) Score based on the $\mathcal{H}^1(\Omega)$-norm

Fig. 21 Summary of numerical experiments. Score as measured by the $L^2(\Omega)$-norm (left) and $\mathcal{H}^1(\Omega)$-norm (right). For a given basis dimension, we scored a ROM on a scale of 1 to N_{ROMS}, where $N_{\text{ROMS}} = 16$ is the number of ROM formulations considered. The best ROM gets a score of N_{ROMS}, the second best ROM gets a score of $N_{\text{ROMS}} - 1$, and so on until the worst ROM gets a score of 1. The total score for each ROM formulation is computed by summing the individual scores across all basis dimensions and both numerical experiments

- In the case of discrete projection, the POD basis must be obtained in an inner product that is $\mathbf{M}$-orthogonal to recover the POD basis obtained via continuous projection. This is well established in the literature.
- Both the Galerkin and stabilized ROMs obtained via continuous projection can be obtained via the Galerkin ROM obtained via discrete projection. This is additionally well-established.
- G–LSPG approximates a continuous minimization principle if the discrete norm is minimized in the $\mathbf{M}^{-1}$ inner product.
- All stabilized methods depend on a stabilization parameter, τ, the time step, Δt, or both. The dependency on these parameters is complex, and more work needs to be done for proper *a priori* selection of the stabilization parameters.

Future work should focus on several aspects. First, theory for discretely stabilized ROMs such as LSPG and APG is lacking for linear problems: minimal analyses exist studying the stability of these methods as well as their accuracy, and future work should address this. Second, future work should focus on the *a priori* selection of the stabilization parameters and optimal time steps (or, alternatively, data-driven calibration of these parameters). Minimal analyses exists for the appropriate *a priori* selection of these parameters within the context of ROMs: SUPG is studied in Refs. [52, 82], LSPG is studied in [29], and APG is studied in [121]. Third, future work should focus on extension to nonlinear and vector-valued systems. Here, hyper-reduction is important and the extension of stabilization techniques to this setting offers numerous interesting and important questions. Lastly, future work should focus on extension to predictive problems, wherein truncation errors are relevant and can dominate predicitive accuracy.

Appendix 1: Brief Review of Non-residual-Based Stabilization Techniques

Although the main focus of this paper is on residual-based stabilized ROMs for the CDR equation, in this Appendix we briefly outline some of the stabilized ROMs not covered herein for completeness. This work includes, but is not limited to, ROM stabilizations that are not residual-based, and ROM stabilizations for equations different from the convection–diffusion–reaction equation (e.g., the incompressible Navier–Stokes equations and, especially, the compressible Euler equations). We outline several such techniques here:

- *Closure models* that add additional "closure" terms to the ROM in order to account for the impact of truncated modes. For classical numerical discretizations (e.g., finite element, finite volume, or spectral methods) of turbulent incompressible or compressible flows, there is an extensive literature on closure models, especially in large eddy simulation (LES) [143]. Closure models for ROMs (see [3, 146] for surveys) have also been developed, using ideas from different fields, e.g., image processing [175], data-driven modeling [68, 173], machine learning [144], information theory [110] the Mori-Zwanzig formalism

from statistical mechanics [102], or dynamical systems [36]. We emphasize, however, that (just as in LES) arguably the most popular type of ROM closure models are the eddy viscosity models [69, 129, 170], which add a dissipative term to the standard ROM. These eddy viscosity ROM closures are generally built by invoking physical arguments, i.e., the concept of energy cascade, which states that in three-dimensional (3D) turbulent flows energy is transferred from large scales to small scales where the energy is dissipated [43, 143]. We note that eddy viscosity ROM closure models are similar *in spirit* to residual-based ROM stabilization methods since they both increase the numerical stability of the ROM. There are, however, notable differences. From one perspective, eddy viscosity ROM closures can be viewed as a phenomenological modeling approach that model the *physics* associated with truncation, i.e., the cascade of energy from large resolved scales to unresolved fine scales through diffusion. Residual-based ROM stabilization methods, on the other hand, can be interpreted as targeting errors arising from numerical discretization of the partial differential equation; the notable exception to this interpretation would be VMS residual-based stabilizations, which are typically interpreted as modeling the fine scales. Both methods have advantages and disadvantages, depending on the application.

- Stabilizing *inner products*, which are used to construct more stable ROMs. One of the earliest examples of stabilizing inner products is the $\mathcal{H}^1(\Omega)$ inner product that is used in [81] instead of the standard L^2 inner product. Other examples of stabilizing inner products are present in the literature for ROMs applied to multistate systems where a classic vector L^2 inner product does not result in a physically meaningful energy principle. For example, energy-based projections are proposed for compressible flows in Refs. [14, 81, 85, 138, 148], which use different inner products and flow variables to construct stabilized ROMs. Recently, Ref. [91] has proposed similar ideas within the context of magnetohydrodynamics. We note that the LSPG ROM-based preconditioning approach developed in [103] can be interpreted as a modification to the underlying inner product that has the effect of scaling different solution components to ensure that they are all of roughly the same magnitude.
- *Inf-sup* stabilizations, that aim at enforcing the *inf-sup* (or the Ladyzhenskaya-Babuska-Brezzi (LBB)) condition in incompressible Stokes and Navier–Stokes equations. We emphasize that the *inf-sup* condition is used to ensure the well-posedness of saddle-point problems, such as the incompressible Stokes and Navier–Stokes equations. Thus, the *inf-sup* stabilizations are different from the stabilization of convection-dominated systems, such as those we consider in this paper. In standard (e.g., FEM) numerical discretizations of the Stokes and the Navier–Stokes equations, it is well-known that not enforcing the *inf-sup* condition can yield spurious numerical oscillations in the pressure field. There are two main approaches to tackle this issue: (i) choose finite elements that do satisfy the *inf-sup* condition, or (ii) choose finite elements that do not satisfy the *inf-sup* condition and add pressure stabilization. In the ROM community, the first *inf-sup* stabilizations have been proposed in [140], which developed ROMs that satisfy the *inf-sup* condition (which is a significantly more difficult task than for finite elements, since the velocity and pressure ROM bases are problem dependent). Recognizing that enforcing the *inf-sup* condition at a ROM level can be prohibitively expensive [13], more efficient stabilized ROMs that do not satisfy the *inf-sup* condition were devised by using, e.g., the penalty method [18, 27], artificial compressibility [45], or local projection stabilization [141].
- *Structure preserving* methods that guarantee that the ROM satisfies the same physical constraints as those satisfied by the underlying equations. As for classical numerical discretizations, preserving these physical constraints generally yields more stable ROMs. For example, for the incompressible Navier–Stokes equations, ROMs in which the nonlinear terms preserve the kinetic energy are more stable than standard ROMs [93, 107] (see also [112] for ROM closure modeling and [91] for work in magnetohydrodynamics). Furthermore, ROMs that preserve Lagrangian structure were developed in [33, 97, 174], and ROMs that preserve Hamiltonian structure were constructed in [2, 55, 60, 61, 123, 150, 151, 153]. The recent work by Gruber et al. is the first to construct ROMs in which the more general metriplectic structure is preserved [59].
- Stabilizing *basis modification* methods designed to remedy the so-called "mode truncation instability", that is, to account for truncated modes *a priori* [7, 11, 12]. In [7], Amsallem and Farhat develop a non-intrusive method for stabilizing linear time-invariant (LTI) ROMs through the minimal modification of the left ROM basis. The new reduced-order basis is obtained by formulating and solving a small-scale convex constrained optimization problem in which the constraint imposes asymptotic stability of the modified ROM. In [11, 12], Balajewicz et al. demonstrate that a ROM for (nonlinear) fluid flow can be stabilized through a *stabilizing rotation* of the projection subspace. Specifically, the projection subspace is "rotated" into a more dissipative regime by modifying the eigenvalue distribution of the linear operator. Mathematically, the approach is formulated as a trace minimization on the Stiefel manifold. Like the approach in [7], the methods in [11, 12] are non-intrusive.

- *Spatial filtering*-based stabilization [62, 77, 90, 162, 171], in which explicit filtering performed either in the physical space or in the ROM space (see [131] for an extension to neural networks) is used to regularize/smooth different terms in the underlying equations, e.g., the convective term in the incompressible Navier–Stokes equations. Due to their simplicity, minimal invasive character, modularity, and effectiveness, spatially-filtered regularized models have been extensively studied in standard CFD (e.g., with finite element discretizations, surveyed in [98]). In contrast, only a few regularized ROMs have been proposed in deterministic [90, 142, 171] and stochastic [62, 77] settings.
- *Eigenvalue reassignment methods*, which calculate a stabilizing correction to an unstable ROM after the ROM has been constructed. The correction is computed offline by solving a constrained optimization problem. The approach was originally developed in Kalashnikova et al. [89] in the context of LTI systems, for which it is natural to impose a constraint on the Lyapunov stability of the ROM system by requiring that the eigenvalues of the ROM matrix defining the problem have negative real parts. The approach was subsequently extended to the nonlinear compressible flow equations by Rezaian and Wei in [132]. Here, appropriate constraints on the system energy, namely that it is non-increasing, were developed and applied. Eigenvalue reassignment methods are non-intrusive by construction, as they operate on a ROM *a posteriori* (i.e., after the ROM has been constructed), and can be effective regardless of the nature of the instability. The methods can also be used to assimilate data into a given ROM, again after the model has been constructed.

Appendix 2: Correspondence of LSPG to a Continuous Minimization Principle

This section outlines the equivalence between LSPG and a continuous minimization principle. We define the time-discrete, spatially continuous residual of the PDE (1) as

$$\mathsf{R}_{\mathrm{cdr}} : (\mathsf{w};\mathsf{z}) \mapsto \frac{\mathsf{w}-\mathsf{z}}{\Delta t} - \nu\nabla^2\mathsf{w} + \mathbf{b}\cdot\nabla\mathsf{w} + \sigma\mathsf{w} - f.$$

Under the assumption that the state is sufficiently regular[13], the residual of the Galerkin FOM OΔE can be written as

$$\mathbf{r}_{\mathrm{G}}t_i : (\mathbf{w};\mathbf{z}) \mapsto m\big(\mathsf{v}_i, \mathsf{R}_{\mathrm{cdr}}(\mathsf{v}\mathbf{w};\mathsf{v}\mathbf{z})\big), \qquad \forall \mathsf{v} \in \mathcal{V}_{\mathrm{h}}.$$

The FEM coefficients of the $L^2(\Omega)$ orthogonal projection of this residual onto the trial space $\mathcal{V}_{\mathrm{h}}$ are given by

$$\mathbf{r}_{\mathrm{G}}^{\|} : (\mathbf{w};\mathbf{z}) \mapsto \mathbf{M}^{-1}\mathbf{r}_{\mathrm{G}}(\mathbf{w};\mathbf{z}).$$

Analogously, at the spatially continuous level

$$\mathsf{R}_{\mathrm{G}}^{\|} : (\mathsf{w};\mathsf{z}) \mapsto \mathsf{v}\mathbf{M}^{-1}m\big(\mathsf{v}, \mathsf{R}_{\mathrm{cdr}}(\mathsf{w};\mathsf{z})\big).$$

The square residual integrated over the domain is then given by

$$\int_\Omega \left(\mathsf{R}_{\mathrm{G}}^{\|}(\mathsf{u}^n;\mathsf{u}^{n-1})\right)^2 dx = \left[\mathbf{M}^{-1}\mathbf{r}_{\mathrm{G}}(\mathbf{a}_{\mathrm{h}}^n;\mathbf{a}_{\mathrm{h}}^{n-1})\right]^T \mathbf{M}\mathbf{M}^{-1}\mathbf{r}_{\mathrm{G}}(\mathbf{a}_{\mathrm{h}}^n;\mathbf{a}_{\mathrm{h}}^{n-1}). \tag{38}$$

Setting $\mathbf{r} \leftarrow \mathbf{r}_{\mathrm{G}}$ and $\mathbf{P} \leftarrow \mathbf{M}^{-1}$ in optimization problem (25), LSPG corresponds to the continuous minimization principle for $\mathsf{u}_{\mathrm{r}}^n$, $n = 1, \ldots, N_t$

$$\mathsf{u}_{\mathrm{r}}^n = \underset{\mathsf{u}\in\mathcal{V}_{\mathrm{r}}}{\arg\min} \int_\Omega \left(\mathsf{R}_{\mathrm{G}}^{\|}(\mathsf{u};\mathsf{u}_{\mathrm{r}}^{n-1})\right)^2 dx. \tag{39}$$

LSPG computes the solution $\mathsf{u}_{\mathrm{r}}^n$ within the ROM trial space $\mathcal{V}_{\mathrm{r}}$ that minimizes the $L^2(\Omega)$-norm of the time-discrete, spatially continuous residual projected onto the finite element trial space $\mathcal{V}_{\mathrm{h}}$. Analogously, LSPG can be defined on the stabilized FOM OΔE (15). Setting $\mathbf{r} \leftarrow \mathbf{r}_{\mathrm{S}}$, the optimality conditions become

$$m_d\left(\frac{\mathbf{M}\boldsymbol{\Psi}}{\Delta t} + \mathbf{B}\boldsymbol{\Psi} + \mathbf{Q}\boldsymbol{\Psi}, \mathbf{r}_{\mathrm{S}}(\boldsymbol{\Psi}\hat{\mathbf{y}};\boldsymbol{\Psi}\hat{\mathbf{x}}^{n-1})\right) = \mathbf{0}.$$

Appendix 3: Derivation of the Adjoint Petrov–Galerkin Method

The APG method was derived in Ref. [121] in the case where the coarse- and fine-scale bases are orthogonal in a standard ℓ^2 discrete inner product. In FEM discretizations it is more appropriate to construct the spaces to be orthogonal in an $\mathbf{M}$ inner product. As such, in this section we derive the APG method for the case where the fine and coarse scales are $\mathbf{M}$-orthogonal. We consider application to the dynamical system given by

$$\mathbf{M}\frac{d\mathbf{x}}{dt} + \mathbf{A}\mathbf{x} - \mathbf{f} = \mathbf{0},$$

where $\mathbf{M} \in \mathbb{S}^N$ is the mass matrix, $\mathbf{x} : [0,T] \to \mathbb{R}^N$ is the state, $\mathbf{A} \in \mathbb{R}^{N\times N}$ is the system matrix, and $\mathbf{f}$ is a forcing term. The derivation begins by decomposing $\mathbb{R}^N$ into a coarse-scale space V_r and a fine-scale space V_r' such that $V_r \oplus V_r' \equiv \mathbb{R}^N$. The coarse-scale space $V_r \subset \mathbb{R}^N$ corresponds to the standard ROM space and is of dimension $\dim(V_r) = R$, while the fine-scale space V_r' comprises the $\mathbf{M}$-orthogonal complement of the coarse-scale space and has dimension

[13] We remark that this assumption does *not* hold for standard $\mathcal{C}^0(\Omega)$ FEM discretizations, in which case the state is not twice continuously differentiable.

$\dim(V_r') = N - R$. We equip the coarse- and fine-scale spaces with $\mathbf{M}$-orthogonal bases $\boldsymbol{\Psi} \in \mathbb{R}^{N\times R}$ and $\boldsymbol{\Psi}' \in \mathbb{R}^{N\times(N-R)}$. Note that $\boldsymbol{\Psi}^T\mathbf{M}\boldsymbol{\Psi}' = \mathbf{0}$ by definition.

The APG derivation proceeds by expressing the dynamical system in terms of the generalized coordinates associated with the coarse and fine-scale bases. This process results in a coupled system for the coarse and fine scales

$$\boldsymbol{\Psi}^T\mathbf{M}\frac{d}{dt}\boldsymbol{\Psi}\hat{\mathbf{x}} + \boldsymbol{\Psi}^T\mathbf{A}\left[\boldsymbol{\Psi}\hat{\mathbf{x}} + \boldsymbol{\Psi}'\hat{\mathbf{x}}'\right] - \boldsymbol{\Psi}^T\mathbf{f} = \mathbf{0}$$
$$\left[\boldsymbol{\Psi}'\right]^T\mathbf{M}\frac{d}{dt}\boldsymbol{\Psi}'\hat{\mathbf{x}}' + \left[\boldsymbol{\Psi}'\right]^T\mathbf{A}\left[\boldsymbol{\Psi}\hat{\mathbf{x}} + \boldsymbol{\Psi}'\hat{\mathbf{x}}'\right] - \left[\boldsymbol{\Psi}'\right]^T\mathbf{f} = \mathbf{0},$$

where $\hat{\mathbf{x}} : [0,T] \to \mathbb{R}^R$ are the coarse-scale generalized coordinates and $\hat{\mathbf{x}}' : [0,T] \to \mathbb{R}^{N-R}$ are the fine-scale generalized coordinates. The APG method proceeds to approximate the fine-scales via the Mori–Zwanzig formalism and a perturbation analysis, which here results in the quasi-static aproximation

$$\hat{\mathbf{x}}'(t) \approx -\tau\left[\boldsymbol{\Psi}'\right]^T\mathbf{A}\boldsymbol{\Psi}\hat{\mathbf{x}}(t),$$

where $\tau \in \mathbb{R}_{>0}$ is a stabilization constant. Injecting in the approximation to the fine-scale state into the coarse-scale equation results in

$$\boldsymbol{\Psi}^T\mathbf{M}\frac{d}{dt}\boldsymbol{\Psi}\hat{\mathbf{x}} + \boldsymbol{\Psi}^T\mathbf{A}\left[\boldsymbol{\Psi}\hat{\mathbf{x}} - \tau\boldsymbol{\Psi}'\left[\boldsymbol{\Psi}'\right]^T\mathbf{A}\boldsymbol{\Psi}\hat{\mathbf{x}}\right] - \boldsymbol{\Psi}^T\mathbf{f} = \mathbf{0}.$$

Next we use the property $\boldsymbol{\Psi}\boldsymbol{\Psi}^T\mathbf{M} + \boldsymbol{\Psi}'\left[\boldsymbol{\Psi}'\right]^T\mathbf{M} = \mathbf{I}$ to remove the dependence on the fine-scale basis functions and get

$$\boldsymbol{\Psi}^T\mathbf{M}\frac{d}{dt}\boldsymbol{\Psi}\hat{\mathbf{x}} + \boldsymbol{\Psi}^T\mathbf{A}\left[\boldsymbol{\Psi}\hat{\mathbf{x}} - \tau\mathbb{A}'\mathbf{A}\boldsymbol{\Psi}\hat{\mathbf{x}}\right] - \boldsymbol{\Psi}^T\mathbf{f} = \mathbf{0},$$

where $\mathbb{A}' = \mathbf{M}^{-1} - \boldsymbol{\Psi}\boldsymbol{\Psi}^T$. Next, assuming the forcing to be zero on the fine-scale space such that $\mathbb{A}'\mathbf{f} = \mathbf{0}$, we write the above in a Petrov–Galerkin form

$$\left[\left(\mathbf{I} - \tau\mathbb{A}'^T\mathbf{A}^T\right)\boldsymbol{\Psi}\right]^T\left[\mathbf{M}\frac{d}{dt}\boldsymbol{\Psi}\hat{\mathbf{x}} + \mathbf{A}\boldsymbol{\Psi}\hat{\mathbf{x}} - \mathbf{f}\right] = \mathbf{0},$$

where we have leveraged $\mathbb{A}'\mathbf{M}\boldsymbol{\Psi} = \mathbf{0}$. This Petrov–Galerkin projection is what we refer to as the Adjoint Petrov–Galerkin method.

Appendix 4: Proper Orthogonal Decomposition Algorithm

Algorithm 2 presents the algorithm for computing the trial basis via proper orthogonal decomposition.

Algorithm 2 Algorithm for generating POD basis.

Input: Snapshot matrix, $\mathbf{S}_{\mathbf{a}_\mathrm{h}} \in \mathbb{R}^{N\times N_s}$; cutoff energy tolerance, ϵ_c ; symmetric positive definite inner product matrix, $\mathbf{P}$
Output: POD Basis $\boldsymbol{\Psi} \in \mathbb{R}^{N\times R}$;
Steps:

1. Compute the "covariance matrix"
$$\mathbf{K} = \mathbf{S}_{\mathbf{a}_\mathrm{h}}^T\mathbf{P}\mathbf{S}_{\mathbf{a}_\mathrm{h}}.$$
2. Compute the eigenvalue decomposition
$$\mathbf{K} = \mathbf{E}_{\mathbf{a}_\mathrm{h}}\boldsymbol{\Lambda}_{\mathbf{a}_\mathrm{h}}[\mathbf{E}_{\mathbf{a}_\mathrm{h}}]^{-1}.$$
3. Compute the statistical energy
$$\epsilon_K = \frac{\sum_{i=1}^{K}\Lambda_i}{\sum_{i=1}^{N_s}\Lambda_i},$$
where $K \leq N_s$.
4. Determine basis dimension from cutoff criterion
$$R = \mathrm{Card}(\{\epsilon_i\}_{i=1}^{N_s} | \epsilon_i \leq \epsilon_\mathrm{c}).$$
5. Compute the ROM bases as
$$\boldsymbol{\Psi} = \mathbf{S}_{\mathbf{a}_\mathrm{h}}\mathbf{E}_{\mathbf{a}_\mathrm{h}}^R\sqrt{[\boldsymbol{\Lambda}_{\mathbf{a}_\mathrm{h}}^R]^{-1}},$$
where $\mathbf{E}_{\mathbf{a}_\mathrm{h}}^R$ and $\boldsymbol{\Lambda}_{\mathbf{a}_\mathrm{h}}^R$ comprise the first R columns of $\mathbf{E}_{\mathbf{a}_\mathrm{h}}$ and the first R columns and rows of $\boldsymbol{\Lambda}_{\mathbf{a}_\mathrm{h}}$, respectively.

Acknowledgements E. Parish acknowledges funding from the John von Neumann Postdoctoral Fellowship, ASC V &V 103723/05.30.02, and ASC V &V 131792/04.09.02. I. Tezaur acknowledges funding from her Presidential Early Career Award for Scientists and Engineers (PECASE), awarded by the U.S. Department of Energy (DOE), as well as support from the U.S. Office of Science, Office of Advanced Scientific Computing Research, Mathematical Multifaceted Integrated Capability Centers (MMICCS) program, under Field Work Proposal 22025291 and the Multifaceted Mathematics for Predictive Digital Twins (M2dt) project. T. Iliescu acknowledges funding from the NSF grants DMS-2012253 and CDS &E-MSS-1953113. This paper describes objective technical results and analysis. Any subjective views or opinions that might be expressed in the paper do not necessarily represent the views of the U.S. Department of Energy or the United States Government. Sandia National Laboratories is a multimission laboratory managed and operated by National Technology & Engineering Solutions of Sandia, LLC, a wholly owned subsidiary of Honeywell International Inc., for the U.S. Department of Energy's National Nuclear Security Administration under contract DE-NA0003525.

Author Contributions All authors wrote the main manuscript text. E.P. prepared all figures and performed numerical experiments. All authors reviewed manuscript. All authors contributed to numerical analysis.

Data Availability No datasets were generated or analysed during the current study.

Declarations

Competing interests The authors declare no competing interests.

References

1. Abgrall R, Crisovan R (2018) Model reduction using L1-norm minimization as an application to nonlinear hyperbolic problems. Int J Numer Methods Fluids 87:628–651
2. Afkham BM, Hesthaven JS (2017) Structure preserving model reduction of parametric Hamiltonian systems. SIAM J Sci Comput 39:A2616–A2644
3. Ahmed SE, Pawar S, San O, Rasheed A, Iliescu T, Noack BR (2021) On closures for reduced order models − a spectrum of first-principle to machine-learned avenues. Phys Fluids 33:091301
4. Ali S, Ballarin F, Rozza G (2020) Stabilized reduced basis methods for parametrized steady Stokes and Navier-Stokes equations, arXiv e-print
5. Alnæs MS, Blechta J, Hake J, Johansson A, Kehlet B, Logg A, Richardson C, Ring J, Rognes ME, Wells GN (2015) The FEniCS project version 1.5. Arch Numer Soft 3
6. Amsallem D, Farhat C (2012) On the stability of linearized reduced-order models: descriptor vs. non-descriptor form and application to fluid-structure interaction. In: 42nd AIAA fluid dynamics conference and exhibit
7. Amsallem D, Farhat C (2012) Stabilization of projection-based reduced-order models. Int J Numer Methods Eng 91:358–377
8. Azaïez M, Rebollo TC, Rubino S (2021) A cure for instabilities due to advection-dominance in POD solution to advection-diffusion-reaction equations. J Comput Phys 425:109916
9. Baiges J, Codina R, Idelsohn S (2013) Explicit reduced-order models for the stabilized finite element approximation of the incompressible Navier-Stokes equations. Int J Numer Methods Fluids 72:1219–1243
10. Baiges J, Codina R, Idelsohn S (2015) Reduced-order subscales for POD models. Comput Methods Appl Mech Eng 291:173–196
11. Balajewicz M, Dowell EH (2012) Stabilization of projection-based reduced order models of the Navier-Stokes. Nonlinear Dyn 70:1619–1632
12. Balajewicz M, Tezaur I, Dowell E (2016) Minimal subspace rotation on the Stiefel manifold for stabilization and enhancement of projection-based reduced order models for the compressible Navier-Stokes equations. J Comput Phys 321:224–241
13. Ballarin F, Manzoni A, Quarteroni A, Rozza G (2015) Supremizer stabilization of POD-Galerkin approximation of parametrized steady incompressible Navier-Stokes equations. Int J Numer Methods Eng 102:1136–1161
14. Barone MF, Kalashnikova I, Segalman DJ, Thornquist HK (2009) Stable Galerkin reduced order models for linearized compressible flow. J Comput Phys 228:1932–1946
15. Baumann M, Benner P, Heiland J (2018) Space-time Galerkin POD with application in optimal control of semilinear partial differential equations. SIAM J Sci Comput 40:A1611–A1641
16. Beattie C, Gugercin S (2011) Structure-preserving model reduction for nonlinear port-Hamiltonian systems. In: 2011 50th IEEE conference on decision and control and european control conference (CDC-ECC), pp 6564–6569. IEEE
17. Benner P, Gugercin S, Willcox K (2015) A survey of projection-based model reduction methods for parametric dynamical systems. SIAM Rev 57:483–531
18. Bergmann M, Bruneau CH, Iollo A (2009) Enablers for robust POD models. J Comput Phys 228:516–538
19. Berkooz G, Holmes P, Lumley JL (1993) The proper orthogonal decomposition in the analysis of turbulent flows. Annu Rev Fluid Mech 25:539–575
20. Bochev PB, Gunzburger MD, Shadid JN (2004) Stability of the SUPG finite element method for transient advection-diffusion problems. Comput Methods Appl Mech Eng 193:2301–2323
21. Borggaard J, Iliescu T, Wang Z (2011) Artificial viscosity proper orthogonal decomposition. Math Comput Modell 53:269–279
22. Brooks AN (1981) A Petrov-Galerkin finite element formulation for convection dominated flows, PhD thesis, California Institute of Technology
23. Brooks AN, Hughes TJ (1982) Streamline upwind/Petrov-Galerkin formulations for convection dominated flows with particular emphasis on the incompressible Navier-Stokes equations. Comput Methods Appl Mech Eng 32:199–259
24. Bui-Thanh T (2007) Model-constrained optimization methods for reduction of parameterized large-scale systems, PhD thesis, Massachusetts Institute of Technology
25. Bui-Thanh T, Willcox K, Ghattas O (2008) Model reduction for large-scale systems with high-dimensional parametric input space. SIAM J Sci Comput 30:3270–3288
26. Bui-Thanh T, Willcox K, Ghattas O (2008) Parametric reduced-order models for probabilistic analysis of unsteady aerodynamic applications. AIAA J 46:2520–2529
27. Caiazzo A, Iliescu T, John V, Schyschlowa S (2014) A numerical investigation of velocity-pressure reduced order models for incompressible flows. J Comput Phys 259:598–616
28. Carlberg K (2011) Model reduction of nonlinear mechanical systems via optimal projection and tensor approximation, PhD thesis, Stanford University
29. Carlberg K, Barone M, Antil H (2017) Galerkin v. least-squares Petrov-Galerkin projection in nonlinear model reduction. J Comput Phys 330:693–734
30. Carlberg K, Bou-Mosleh C, Farhat C (2011) Efficient non-linear model reduction via a least-squares Petrov-Galerkin projection and compressive tensor approximations. Int J Numer Methods Eng 86:155–181

31. Carlberg K, Choi Y, Sargsyan S (2018) Conservative model reduction for finite-volume models. J Comput Phys 371:280–314
32. Carlberg K, Farhat C, Cortial J, Amsallem D (2013) The GNAT method for nonlinear model reduction: effective implementation and application to computational fluid dynamics and turbulent flows. J Comput Phys 242:623–647
33. Carlberg K, Tuminaro R, Boggs P (2015) Preserving Lagrangian structure in nonlinear model reduction with application to structural dynamics. SIAM J Sci Comput 37:B153–B184
34. Chan J (2020) Entropy stable reduced order modeling of nonlinear conservation laws. J Comput Phys 423:109789
35. Chaturantabut S, Beattie C, Gugercin S (2016) Structure-preserving model reduction for nonlinear port-Hamiltonian systems. SIAM J Sci Comput 38:B837–B865
36. Chekroun MD, Liu H, McWilliams JC (2019) Variational approach to closure of nonlinear dynamical systems: autonomous case. J Stat Phys 1–88
37. Choi Y, Carlberg K (2019) Space-time least-squares Petrov-Galerkin projection for nonlinear model reduction. SIAM J Sci Comput
38. Chorin A, Hald O, Kupferman R (2002) Optimal prediction with memory. Phys D239–257
39. Codina R (1998) Comparison of some finite element methods for solving the diffusion-convection-reaction equation. Comput Methods Appl Mech Eng 156:185–210
40. Codina R (2000) Stabilization of incompressibility and convection through orthogonal sub-scales in finite element methods. Comput Methods Appl Mech Eng 190
41. Codina R, Principe J, Guasch O, Badia S (2007) Time dependent subscales in the stabilized finite element approximation of incompressible flow problems. Comput Methods Appl Mech Eng 196:2413–2430
42. Constantine PG, Wang Q (2012) Residual minimizing model interpolation for parameterized nonlinear dynamical systems. SIAM J Sci Comput
43. Couplet M, Sagaut P, Basdevant C (2003) Intermodal energy transfers in a proper orthogonal decomposition-Galerkin representation of a turbulent separated flow. J Fluid Mech 491:275–284
44. Dahmen W, Plesken C, Welper G (2014) Double greedy algorithms: reduced basis methods for transport dominated problems. ESAIM 48:623–663
45. DeCaria V, Iliescu T, Layton W, McLaughlin M, Schneier M (2020) An artificial compression reduced order model. SIAM J Numer Anal (accepted)
46. Eroglu FG, Kaya S, Rebholz LG (2017) A modular regularized variational multiscale proper orthogonal decomposition for incompressible flows. Comput Methods Appl Mech Eng 325:350–368
47. Farhat C, Avery P, Chapman T, Cortial J (2014) Dimensional reduction of nonlinear finite element dynamic models with finite rotations and energy-based mesh sampling and weighting for computational efficiency. Int J Numer Methods Eng 98:625–662
48. Franca L, Valentin F (2000) On an improved unusual stabilized finite element method for the advective-reactive-diffusive equation. Comput Methods Appl Mech Eng 190:1785–1800
49. Franca LP, Farhat C (1995) Bubble functions prompt unusual stabilized finite element methods. Comput Methods Appl Mech Eng 123:299–308
50. Franca LP, Frey SL, Hughes TJ (1992) Stabilized finite element methods: I. Application to the advective-diffusive model. Comput Methods Appl Mech Eng 95:253–276
51. Funaro D, Gottlieb D (1991) Convergence results for pseudospectral approximations of hyperbolic systems by a penalty-type boundary treatment. Math Comput 57
52. Giere S, Iliescu T, John V, Wells D (2015) SUPG reduced order models for convection-dominated convection-diffusion-reaction equations. Comput Methods Appl Mech Eng 289:454–474
53. Girfoglio M, Quaini A, Rozza G (2021) A POD-Galerkin reduced order model for a LES filtering approach. J Comput Phys 436:110260
54. Girfoglio M, Quaini A, Rozza G (2023) A linear filter regularization for POD-based reduced-order models of the quasi-geostrophic equations. C R Mech 351:1–21
55. Gong Y, Wang Q, Wang Z (2017) Structure-preserving Galerkin POD reduced-order modeling of Hamiltonian systems. Comput Methods Appl Mech Eng 315:780–798
56. Grepl MA, Maday Y, Nguyen NC, Patera AT (2007) Efficient reduced-basis treatment of nonaffine and nonlinear partial differential equations. ESAIM 41:575–605
57. Grepl MA, Patera AT (2005) A posteriori error bounds for reduced-basis approximations of parametrized parabolic partial differential equations. ESAIM 39:157–181
58. Grimberg S, Farhat C, Youkilis N (2020) On the stability of projection-based model order reduction for convection-dominated laminar and turbulent flows. J Comput Phys 419:109681
59. Gruber A, Gunzburger M, Ju L, Wang Z (2023) Energetically consistent model reduction for metriplectic systems. Comput Methods Appl Mech Eng 404:115709
60. Gruber A, Tezaur I (2023) Canonical and noncanonical Hamiltonian operator inference. Comput Methods Appl Mech Eng 416:116334
61. Gruber A, Tezaur I (2024) Variationally consistent Hamiltonian reduced order models. SIAM J Dyn Syst (under review)
62. Gunzburger M, Iliescu T, Mohebujjaman M, Schneier M (2019) An evolve-filter-relax stabilized reduced order stochastic collocation method for the time-dependent Navier-Stokes equations. SIAM-ASA J Uncertain 1162–1184
63. Haasdonk B (2013) Convergence rates of the POD-Greedy method. ESAIM 47:859–873
64. Haasdonk B, Ohlberger M (2008) Reduced basis method for finite volume approximations of parametrized linear evolution equations. Math Modell Numer Anal 42:277–302
65. Hald OH, Stinis P (2007) Optimal prediction and the rate of decay for solutions of the Euler equations in two and three dimensions. Proc Natl Acad Sci 104:6527–6532
66. Harari I (2004) Stability of semidiscrete formulations for parabolic problems at small time steps. Comput Methods Appl Mech Eng 193(2004):1491–1516
67. Hesthaven JS, Rozza G, Stamm B (2016) Certified reduced basis methods for parametrized partial differential equations. Springer, Cham
68. Hijazi S, Stabile G, Mola A, Rozza G (2019) Data-driven POD-Galerkin reduced order model for turbulent flows, arXiv preprint, arXiv:1907.09909
69. Holmes P, Lumley JL, Berkooz G (1996) Turbulence. Coherent structures, dynamical systems and symmetry. Cambridge University Press, Cambridge
70. Hsu M-C, Bazilevs Y, Calo V, Tezduyar T, Hughes T (2010) Improving stability of stabilized and multiscale formulations in flow simulations at small time steps. Comput Methods Appl Mech Eng 199:828–840
71. Huang C, Wentland CR, Duraisamy K, Merkle C (2022) Model reduction for multi-scale transport problems using model-form preserving least-squares projections with variable transformation. J Comput Phys 448:110742
72. Hughes T, Tezduyar T (1984) Finite element methods for first-order hyperbolic systems with particular emphasis on the compressible euler equations. Comput Methods Appl Mech Eng 45:217–284

73. Hughes TJ, Brooks AN (1979) A multidimensional upwind scheme with no crosswind diffusion. In: Finite element methods for convection dominated flows, ASME
74. Hughes TJ, Feijoo G, Mazzei L, Quincy J (1998) The variational multiscale method—a paradigm for computational mechanics. Comput Methods Appl Mech Eng 166:173–189
75. Hughes TJ, Franca LP, Hulbert GM (1989) A new finite element formulation for computational fluid dynamics: VIII. The Galerkin/least-squares method for advective-diffusive equations. Comput Methods Appl Mech Eng 73:173–189
76. Hughes TJ, Stewart JR (1996) A space-time formulation for multiscale phenomena. J Comput Appl Math 74:217–229
77. Iliescu T, Liu H, Xie X (2018) Regularized reduced order models for a stochastic Burgers equation. Int J Numer Anal Mod 15:594–607
78. Iliescu T, Wang Z (2013) Variational multiscale proper orthogonal decomposition: Convection-dominated convection-diffusion-reaction equations. Math Comput 82:1357–1378
79. Iliescu T, Wang Z (2014) Variational multiscale proper orthogonal decomposition: Navier-Stokes equations. Numer Methods PDEs 30:641–663
80. Ingimarson S, Rebholz LG, Iliescu T (2022) Full and reduced order model consistency of the nonlinearity discretization in incompressible flows. Comput Methods Appl Mech Eng 401:115620
81. Iollo A, Lanteri S, Désidéri JA (2000) Stability properties of POD-Galerkin approximations for the compressible Navier-Stokes equations. Theoret Comput Fluid Dyn 13:377–396
82. John V, Moreau B, Novo J (2022) Error analysis of a SUPG-stabilized POD-ROM method for convection-diffusion-reaction equations. Comput Math Appl 122:48–60
83. John V, Novo J (2011) Error analysis of the supg finite element discretization of evolutionary convection-diffusion-reaction equations. SIAM J Numer Anal 49:1149–1176
84. Johnson C, Nävert U, Pitkäranta J (1984) Finite element methods for linear hyperbolic problems. Comput Methods Appl Mech Eng 45:285–312
85. Kalashnikova I, Arunajatesan S, Barone MF, van Bloemen Waanders BG, Fike JA (2014) Reduced order modeling for prediction and control of large-scale systems, Sandia National Laboratories Report, SAND
86. Kalashnikova I, Barone M (2011) Stable and efficient Galerkin reduced order models for non-linear fluid flow. In: 6th AIAA theoretical fluid mechanics conference, AIAA-2011-3110, 6th AIAA theoretical fluid mechanics conference. Honolulu, Hawaii
87. Kalashnikova I, Barone MF (2010) On the stability and convergence of a Galerkin reduced order model ROM of compressible flow with solid wall and far-field boundary treatment. Int J Numer Methods Eng 83:1345–1375
88. Kalashnikova I, Barone MF, Arunajatesan S, van Bloemen Waanders BG (2014) Construction of energy-stable projection-based reduced order models. Appl Math Comput 249:569–596
89. Kalashnikova I, van Bloemen Waanders B, Arunajatesan S, Barone M (2014) Stabilization of projection-based reduced order models for linear time-invariant systems via optimization-based eigenvalue reassignment. Comput Methods Appl Mech Eng 272:251–270
90. Kaneko K, Tsai P-H, Fischer P (2020) Towards model order reduction for fluid-thermal analysis. Nucl Eng Des 370:110866
91. Kaptanoglu AA, Morgan KD, Hansen CJ, Brunton SL (2020) Physics-constrained, low-dimensional models for MHD: First-principles and data-driven approaches, arXiv preprint arXiv:2004.10389
92. Koc B, Rubino S, Schneier M, Singler JR, Iliescu T (2021) On optimal pointwise in time error bounds and difference quotients for the proper orthogonal decomposition. SIAM J Numer Anal 59:2163–2196
93. Kondrashov D, Chekroun MD, Ghil M (2015) Data-driven non-Markovian closure models. Phys D 297:33–55
94. Kragel B (2005) Streamline diffusion POD models in optimization, PhD thesis, Universität Trier
95. Kunisch K, Volkwein S (2001) Galerkin proper orthogonal decomposition methods for parabolic problems. Numer Math 90:117–148
96. Kragel B (2002) Galerkin proper orthogonal decomposition for a general equation in fluid dynamics. SIAM J Numer Anal 40:492–515
97. Lall S, Krysl P, Marsden JE (2003) Structure-preserving model reduction for mechanical systems. Physica D 184:304–318
98. Layton WJ, Rebholz LG (2012) Approximate deconvolution models of turbulence: analysis, phenomenology and numerical analysis, vol 2042. Springer, Berlin
99. LeGresley P, Alonso J (2000) Airfoil design optimization using reduced order models based on proper orthogonal decomposition. In: Fluids 2000 conference and exhibit
100. LeGresley P, Alonso J (2003) Dynamic domain decomposition and error correction for reduced order models. In: 41st Aerospace Sciences Meeting and Exhibit
101. LeGresley P, Alonso JJ (2001) Investigation of non-linear projection for POD based reduced order models for aerodynamics. In: 39th Aerospace Sciences Meeting and Exhibit
102. Lin KK, Lu F (2019) Data-driven model reduction, Wiener projections, and the Mori-Zwanzig formalism, arXiv preprint arXiv:1908.07725
103. Lindsay P, Fike J, Tezaur I, Carlberg K (2022) Preconditioned least-squares Petrov-Galerkin reduced order models. Int J Numer Methods Eng 123:4809–4843
104. Logg A, Mardal K-A, Wells GN et al (2012) Automated solution of differential equations by the finite element method. Springer, New York
105. Logg A, Wells GN (2010) DOLFIN: automated finite element computing. ACM Trans Math Softw 37
106. Logg A, Wells GN, Hake J (2012) DOLFIN: a C++/Python finite element library. In: Logg A, Mardal K-A, Wells GN (eds) Automated solution of differential equations by the finite element method, volume 84 of Lecture Notes in Computational Science and Engineering, ch. 10. Springer, New York
107. Loiseau J-C, Brunton SL (2018) Constrained sparse Galerkin regression. J Fluid Mech 838:42–67
108. Lorenzi S, Cammi A, Luzzi L, Rozza G (2016) POD-Galerkin method for finite volume approximation of Navier-Stokes and RANS equations. Comput Methods Appl Mech Eng 311:151–179
109. Maday Y, Patera AT, Rovas DV (2002) A blackbox reduced-basis output bound method for noncoercive linear problems. In: Nonlinear partial differential equations and their applications—Collège de France Seminar Volume XIV. Elsevier, Amsterdam, pp 533–569
110. Majda AJ, Chen N (2018) Model error, information barriers, state estimation and prediction in complex multiscale systems. Entropy 20:644
111. McLaughlin B, Peterson J, Ye M (2016) Stabilized reduced order models for the advection-diffusion-reaction equation using operator splitting. Comput Math Appl 71:2407–2420
112. Mohebujjaman M, Rebholz LG, Iliescu T (2019) Physically-constrained data-driven correction for reduced order modeling of fluid flows. Int J Numer Methods Fluids 89:103–122
113. Moore B (1981) Principal component analysis in linear systems: Controllability, observability, and model reduction. IEEE Trans Autom Control 26:17–32

114. Mou C, Koc B, San O, Rebholz LG, Iliescu T (2021) Data-driven variational multiscale reduced order models. Comput Methods Appl Mech Eng 373:113470
115. Mullis CT, Roberts RA (1976) Synthesis of minimum round-off noise fixed point digital filters. IEEE Trans Circ Syst 23:551–562
116. Novo J, Rubino S (2021) Error analysis of proper orthogonal decomposition stabilized methods for incompressible flows. SIAM J Numer Anal 59:334–369
117. Östh J, Noack BR, Krajnović S, Barros D, Borée J (2014) On the need for a nonlinear subscale turbulence term in POD models as exemplified for a high-Reynolds-number flow over an Ahmed body. J Fluid Mech 747:518–544
118. Pacciarini P, Rozza G (2014) Stabilized reduced basis method for parametrized advection-diffusion PDEs. Comput Methods Appl Mech Eng 274:1–18
119. Parish EJ, Carlberg KT (2021) Windowed least-squares model reduction for dynamical systems. J Comput Phys 426:109939
120. Parish EJ, Rizzi F (2023) On the impact of dimensionally-consistent and physics-based inner products for POD-Galerkin and least-squares model reduction of compressible flows. J Comput Phys 491:112387
121. Parish EJ, Wentland CR, Duraisamy K (2020) The Adjoint Petrov-Galerkin method for non-linear model reduction. Comput Methods Appl Mech Eng 365:112991
122. Patera AT, Rozza G (2007) Reduced basis approximation and a posteriori error estimation for parametrized partial differential equations. MIT Pappalardo Graduate Monographs in Mechanical Engineering, Massachusetts Institute of Technology, Department of Mechanical Engineering
123. Peng L, Mohseni K (2016) Symplectic model reduction of Hamiltonian systems. SIAM J Sci Comput 38:A1–A27
124. Pillage LT, Huang X, Rohrer RA (1989) Asymptotic waveform evaluation for timing analysis. In: Proceedings of the 26th ACM/IEEE design automation conference, DAC '89, New York, NY, USA, ACM, pp 634–637
125. Prud'homme C, Rovas DV, Veroy K, Machiels L, Maday Y, Patera AT, Turinici G (2001) Reliable real-time solution of parametrized partial differential equations: reduced-basis output bound methods. J Fluids Eng 124:70–80
126. Quarteroni A, Manzoni A, Negri F (2015) Reduced basis methods for partial differential equations: an introduction, vol 92. Springer, New York
127. Quarteroni A, Valli A (1997) Numerical approximation of partial differential equations. Springer, New York
128. Rathinam M, Petzold LR (2003) A new look at proper orthogonal decomposition. SIAM J Numer Anal 41:1893–1925
129. Rebollo TC, Ávila ED, Mármol MG, Ballarin F, Rozza G (2017) On a certified Smagorinsky reduced basis turbulence model. SIAM J Numer Anal 55:3047–3067
130. Reyes R, Codina R (2020) Projection-based reduced order models for flow problems: a variational multiscale approach. Comput Methods Appl Mech Eng 363:112844
131. Rezaian E, Duraisamy K (2023) Predictive modeling of complex flows using regularized conditionally parameterized graph neural networks. In: AIAA SCITECH 2023 Forum, p 1284
132. Rezaian E, Wei M (2020) Impact of symmetrization on the robustness of POD-Galerkin ROMs for compressible flows. In: AIAA Scitech. Orlando, Florida
133. Rezaian E, Wei M (2021) A global eigenvalue reassignment method for the stabilization of nonlinear reduced-order models. Int J Numer Methods Eng 122:2393–2416
134. Roop JP (2013) A proper-orthogonal decomposition variational multiscale approximation method for a generalized Oseen problem. Adv Numer Anal
135. Roos HG, Stynes M, Tobiska L (2008) Robust numerical methods for singularly perturbed differential equations: convection-diffusion-reaction and flow problems, 2nd ed, vol 24. Springer Series in Computational Mathematics, Springer, New York
136. Rovas DV (2003) Reduced-basis output bound methods for parametrized partial differential equations, PhD thesis, Massachusetts Institute of Technology
137. Rowley CW (2002) Modeling, simulation, and control of cavity flow oscillations, PhD thesis, California Institute of Technology
138. Rowley CW, Colonius T, Murray RM (2004) Model reduction for compressible flows using POD and Galerkin projection. Physica D 189:115–129
139. Rozza G, Huynh DBP, Patera AT (2008) Reduced basis approximation and a posteriori error estimation for affinely parametrized elliptic coercive partial differential equations. Arch Comput Methods Eng 15:229
140. Rozza G, Veroy K (2007) On the stability of the reduced basis method for Stokes equations in parametrized domains. Comput Methods Appl Mech Eng 196:1244–1260
141. Rubino S (2020) Numerical analysis of a projection-based stabilized POD-ROM for incompressible flows. SIAM J Numer Anal 58:2019–2058
142. Sabetghadam F, Jafarpour A (2012) α regularization of the POD-Galerkin dynamical systems of the Kuramoto-Sivashinsky equation. Appl Math Comput 218:6012–6026
143. Sagaut P (2006) Large eddy simulation for incompressible flows, scientific computation, 3rd edn. Springer, Berlin
144. San O, Maulik R (2018) Machine learning closures for model order reduction of thermal fluids. Appl Math Model 60:681–710
145. San O, Maulik R (2018) Neural network closures for nonlinear model order reduction. Adv Comput Math 44:1717–1750
146. Sanderse B, Stinis P, Maulik R, Ahmed SE (2024) Scientific machine learning for closure models in multiscale problems: a review, arXiv preprint arXiv:2403.02913
147. Sanfilippo A, Moore IR, Ballarin F, Iliescu T (2023) Approximate deconvolution Leray reduced order model. Finite Elem Anal Des 226:104021
148. Serre G, Lafon P, Gloerfelt X, Bailly C (2012) Reliable reduced-order models for time-dependent linearized Euler equations. J Comput Phys 231
149. Shakib F, Hughes TJ (1991) A new finite element formulation for computational fluid dynamics: Ix. Fourier analysis of space-time Galerkin/least-squares algorithms. Comput Methods Appl Mech Eng 87:35–58
150. Sharma H, Mu H, Buchfink P, Geelen R, Glas S, Kramer B (2023) Symplectic model reduction of Hamiltonian systems using data-driven quadratic manifolds. Comput Methods Appl Mech Eng 417:116402
151. Sharma H, Wang Z, Kramer B (2022) Hamiltonian operator inference: physics-preserving learning of reduced-order models for canonical Hamiltonian systems. Physica D 431:133122
152. Singler J (2014) New POD error expressions, error bounds, and asymptotic results for reduced order models of parabolic PDEs. SIAM J Numer Anal 52 (2014)
153. Sockwell K (2019) Mass conserving hamiltonian-structure-preserving reduced order modeling for the rotating shallow water equations discretized by a mimetic spatial scheme, PhD thesis, Florida State University
154. Sotomayor RR (2020) On approaching real-time simulations for fluid flows, PhD thesis, Universitat Politècnica de Catalunya
155. Stabile G, Ballarin F, Zuccarino G, Rozza G (2019) A reduced order variational multiscale approach for turbulent flows. Adv Comput Math 45:2349–2368
156. Stabile G, Hijazi S, Mola A, Lorenzi S, Rozza G (2017) POD-Galerkin reduced order methods for CFD using Finite Volume

Discretisation: vortex shedding around a circular cylinder, Commun. Appl. Ind Math 8:210–236
157. Stabile G, Rozza G (2018) Finite volume POD-Galerkin stabilised reduced order methods for the parametrised incompressible Navier-Stokes equations. Comput Fluids 173:273–284
158. Strazzullo M, Girfoglio M, Ballarin F, Iliescu T, Rozza G (2022) Consistency of the full and reduced order models for evolve-filter-relax regularization of convection-dominated, marginally-resolved flows. Int J Numer Methods Eng 123:3148–3178
159. Stynes M (2005) Steady-state convection-diffusion problems. Acta Numer 14:445–508
160. Tezduyar T (1991) Stabilized finite element formulations for incompressible flow computations. In: Hutchinson JW, Wu TY (eds) Advances in Applied Mechanics, vol 28. Elsevier, Amsterdam, pp 1–44
161. Thomée V (2006) Galerkin finite element methods for parabolic problems. Springer, New York
162. Tsai PH, Fischer P (2022) Parametric model-order-reduction development for unsteady convection. Front Phys 711
163. Urban K, Patera AT (2012) A new error bound for reduced basis approximation of parabolic partial differential equations. CR Math 350:203–207
164. Urban K, Patera AT (2014) An improved error bound for reduced basis approximation of linear parabolic problems. Math Comput 83:1599–1615
165. Veroy K, Patera AT (2005) Certified real-time solution of the parametrized steady incompressible Navier-Stokes equations: rigorous reduced-basis a posteriori error bounds. Int J Numer Methods Fluids 47:773–788
166. Veroy, K, Prud'homme C, Rovas D, Patera A (2003) A posteriori error bounds for reduced-basis approximation of parametrized noncoercive and nonlinear elliptic partial differential equations. In: 16th AIAA computational fluid dynamics conference
167. Volkwein S (2013) Proper orthogonal decomposition: Theory and reduced-order modelling, Lecture Notes, University of Konstanz. http://www.math.uni-konstanz.de/numerik/personen/volkwein/teaching/POD-Book.pdf
168. Wang Q, Ripamonti N, Hesthaven JS (2019) Recurrent neural network closure of parametric POD-Galerkin reduced-order models based on the Mori-Zwanzig formalism. J Comput Phys (2019)
169. Wang Z (2012) Reduced-order modeling of complex engineering and geophysical flows: analysis and computations, PhD thesis, Virginia Polytechnic Institute and State University
170. Wang Z, Akhtar I, Borggaard J, Iliescu T (2012) Proper orthogonal decomposition closure models for turbulent flows: a numerical comparison. Comput Methods Appl Mech Eng 237–240:10–26
171. Wells D, Wang Z, Xie X, Iliescu T (2017) An evolve-then-filter regularized reduced order model for convection-dominated flows. Int J Numer Methods Fluids 84:598–615
172. Wentland CR, Huang C, Duraisamy K (2019) Closure of reacting flow reduced-order models via the adjoint Petrov-Galerkin method. In: AIAA Aviation 2019 Forum
173. Xie X, Mohebujjaman M, Rebholz LG, Iliescu T (2018) Data-driven filtered reduced order modeling of fluid flows. SIAM J Sci Comput 40:B834–B857
174. Xie X, Nolan PJ, Ross SD, Mou C, Iliescu T (2020) Lagrangian data-driven reduced order modeling using finite time Lyapunov exponents. Fluids 5:189
175. Xie X, Wells D, Wang Z, Iliescu T (2017) Approximate deconvolution reduced order modeling. Comput Methods Appl Mech Eng 313:512–534
176. Xie X, Wells D, Wang Z, Iliescu T (2018) Numerical analysis of the Leray reduced order model. J Comput Appl Math 328:12–29
177. Yano M (2014) A space-time Petrov-Galerkin certified reduced basis method: application to the Boussinesq equations. SIAM J Sci Comput 36:A232–A266
178. Xie X, Wells D, Wang Z, Iliescu T (2019) Discontinuous Galerkin reduced basis empirical quadrature procedure for model reduction of parametrized nonlinear conservation laws. Adv Comput Math 45:2287–2320
179. Zoccolan F, Strazzullo M, Rozza G (2023) A streamline upwind Petrov-Galerkin reduced order method for advection-dominated partial differential equations under optimal control, arXiv preprint, arXiv:2301.01973
180. Zoccolan F, Strazzullo M, Rozza G (2023) Stabilized weighted reduced order methods for parametrized advection-dominated optimal control problems governed by partial differential equations with random inputs, arXiv preprint, arXiv:2301.01975